ADDIS ABABA UNIVERSITY

ADDIS ABABA INSTITUTE OF TECHNOLOGY

SCHOOL OF CIVIL AND ENVIRONMENTAL ENGINEERING

ESTIMATION OF SOIL SHEAR STRENGTH PARAMETERS FROM INDEX PROPERTIES USING ANN THE CASE OF ADDIS ABABA

By

Hanna Yoseph

May, 2022

Addis Ababa

A Thesis Submitted to School of Graduate Studies of Addis Ababa Institute of Technology in Partial Fulfillment of the Requirements for the Degree of Master of Science in Civil Engineering (Geotechnical Engineering)

ESTIMATION OF SOIL SHEAR STRENGTH PARAMETERS FROM INDEX PROPERTIES USING ANN THE CASE OF ADDIS ABABA

A Thesis Submitted to School of Graduate Studies of Addis Ababa Institute of Technology in Partial Fulfillment of the Requirements for the Degree of Master of Science in Civil Engineering (Geotechnical Engineering)

By

Hanna Yoseph

Advisor

Dr.-Ing. Tensay Gebremedhin

The undersigned have examined the thesis entitled '**Estimation of Soil Shear Strength Parameters from Index Properties Using ANN the Case of Addis Ababa**' presented by **Hanna Yoseph**, a candidate for the degree of **Master of Science** and hereby certify that it is worthy of acceptance.

Dr.-Ing. Tensay Gebremedhin		
Advisor	Signature	Date
Dr.-Ing. Henok Fikre		
Internal Examiner	Signature	Date
Dr. Tezera Firew		
External Examiner	Signature	Date
Chairperson	Signature	Date

UNDERTAKING

I certify that research work titled "**Estimation of Soil Shear Strength Parameters from Index Properties using ANN the Case of Addis Ababa**" is my own work. The work has not been presented elsewhere for assessment. Where material has been used from other sources it has been properly acknowledged / referred.

Signature of Student

Hanna Yoseph

ABSTRACT

Shear strength of a soil is perhaps the most important of its engineering properties, as stability analyses in the field of geotechnical engineering are dependent on it. This research work seeks to develop models for predicting the shear strength parameters (cohesion and angle of friction) of soils in Addis Ababa city using artificial neural network modeling technique; with a view to reducing time, effort and cost usually incurred in determining these shear strength parameters in the laboratory for future planning, design and construction projects in the study area. An attempt has been made to develop separate neural network models for c and ϕ from the index properties of soil consisting of Sand % (SP), Fines % (FP), Liquid limit (LL), Plasticity Index (PI), water content (ω), and Bulk density (BD) as input parameters. A multi-layer perceptron network with feed forward back propagation is used to model varying the number of hidden layers. For this purpose, 284 soil test result data was used. The geotechnical soil properties were determined in accordance with ASTM Standards. Direct shear box method was used to determine soil cohesion and soil internal friction angle. The developed models were found to be quite satisfactory in predicting shear strength parameters with correlation coefficients of about 0.98 and 0.92 for cohesion and angle of internal friction, respectively during the testing phase. The models are validated by primary soil test data and compared with some existing correlation methods. The result showed that the artificial neural network method gave better fit and accuracy than the selected empirical formulae in the prediction of shear strength parameters.

Key Words: ANN, Shear Strength, Cohesion, Friction Angle, Prediction, Index Property.

ACKNOWLEDGMENT

Great glory goes to the Almighty God, who is always standing at the right of my side in each and every step of my life.

I would like to pay my deepest respect to my Advisor Dr.-Ing. Tensay Gebremedhin, for his invaluable guidance, consistent encouragement, and advice right through the thesis work.

My special thanks also goes to MAFCON Engineering plc, G.I.A Engineering plc, Best consulting Engineers plc, Ethiopian Construction Design and Supervision Works Corporation (ECDSWC), for providing me the necessary data to my research.

My sincere thanks go to my precious husband, my family, and my friends for their encouragement and support throughout the research work.

TABLE OF CONTENTS

LIST OF TABLES

LIST OF FIGURES

ABBREVIATIONS AND SYMBOLS

AAiT	Addis Ababa Institute of Technology
AASHTO	American Association of State Highway and Transportation Officials
AI	Artificial Intelligence
ANN	Artificial Neural Network
ASTM	American Society for Testing and Materials
BD/ ρ_b	Soil Bulk Density
c	Cohesion
CC	Coarse-grained Content
Cc	Coefficient of Curvature
Cu	Coefficient of Uniformity
DD/ ρ_d	Soil Dry Density
ECDSWC	Ethiopian Construction Design and Supervision Works Corporation
FC/FP	Fine-grained Content (Percentage)
Gs	Specific Gravity
LGP	Linear Genetic Programming
LI	Liquidity Index
LL	Liquid Limit
MAE	Mean Absolute Error
MSE	Mean Squared Error
NMC/ ω	Natural Moisture Content
NN	Neural Network
NP	Non Plastic
PI	Plasticity Index

PL	Plastic Limit
R	Correlation Coefficient
R^2	Coefficient of Determination
RMSE	Root Mean Squared Error
SP	Sand Content (Percentage)
ϕ	Internal Friction Angle
γ	Soil Unit Weight
γ_d	Soil Dry Unit Weight.
τ	Shear (Tangential) Stress
σ_n	Normal Stress

CHAPTER 1 INTRODUCTION

1.1 Background of the Study

One of the most significant engineering properties of soil is its capability to resist sliding along internal surfaces within a mass. The shearing resistance of soil along probable slippage surfaces determines the stability of the structure built on the soil (Jain, Jain and Bhadauria, 2010). When the shearing stress caused in a burdened soil mass reaches a limiting value, the soil deforms and fails. Shear failure can take place in a number of ways, including the sinking of footing, the shifting of wedge soil behind a retaining wall, or the sliding of an earth embankment. An incorrect estimate will result in substantial property and life loss. As a result, determining the shear strength of soil is critical before planning a structure's foundation or a road embankment, retaining wall, or other structure. It is critical for an engineer to ensure that the structure is safe from shear catastrophe in the soil that supports it and that it does not settle excessively (Zumrawi & Mohammed, 2016).

The soil shear strength parameters can be determined either in the field or in the laboratory. In the laboratory, the most typical tests are the triaxial compression and direct shear tests. Measurements of shear strength properties both at field and laboratory conditions are cumbersome, expensive, time consuming and labor intensive. In addition, obtaining accurate undisturbed soil samples from the field is difficult; due to handling, transportation, release of overburden pressure and poor laboratory conditions. It needs careful supervision.

It has created a persistent demand and interest among researchers to study soil shear strength behavior, relating it to other characteristics and in-situ test results. Many authors proposed correlations on friction angle (ϕ) and cohesion (c) prediction also have then derived shear strength from simple index properties of soil; so difficulties and costs for undisturbed sampling could be diminished or even avoided for simple projects. Consequently there is now a tendency in countries all over the world towards building up correlation equations between the soil properties and index properties of soil (Obasi & Anyaegbunam, 2005). Many empirical and hyperbolic functions have already been employed for estimating shear strength parameters (Goktepe et al, 2008; Lee et al, 2003; Vanapalli et al, 1996). Although these methods to some extent are able to predict the soil

shear strength, but these have certain limitations though general practice shear strength parameters can be determined in the field as well as in the laboratory. Although the results obtained from existing correlations were proven to be consistent, these models were unable to predict both cohesion and friction angle simultaneously for soil mixtures in which it presents both shear resistance parts. For that matter, artificial neural networks (ANN) were proposed on shear resistance parameters prediction because of the generalization and capacity on modeling complex problems (Das & Basudhar, 2008; Shooshpasha, Amiri & Molaabasi, 2015). The advent of soft computing methods like ANN in developing robust models, where the data trends are allowed to evolve appropriate models is becoming widely accepted.

This study developed an artificial neural network models that helped to forecast the shear strength parameters (c and ϕ) from soils' index properties in order to give simple and accurate response for various soil types in Addis Ababa. Since index properties can be obtained simply with low-cost equipment when compared to strength properties equipment. Consequently, soft computing methods like artificial neural network (ANN) are a crucial method to predict soils' engineering properties, especially for developing countries like Ethiopia, where there is a financial limitation, lack of test equipment, and limited time, which is used for design purposes. Since the understanding of the shear strength of a soil is important in the assessment of bearing capacities of foundations, slope stability, retaining structures, embankment dams, tunnel linings, pavement and the resistance traction and tillage tools in agricultural applications.

1.2 Statement of the Problem

It is often necessary for the geotechnical engineer to quickly characterize the soil and determine its engineering properties to estimate the soil's appropriateness for any industrial practices. Most of the time, for the need to analyze and design engineering structures engineers follow some techniques apart from doing an applicable investigation of a subsoil incident, which may be the reason for the destruction of structures on it. Experimental determination of the strength parameters used for design purposes is widespread, challenging to perform, and costly compared to index properties of soils. In order to cope with the difficulty of experimental investigation, engineering design models are needed.

This research work seeks to develop a relationship between soils index property and shear strength parameters, which can be used to minimize cost, effort, and time for any geotechnical practice to analyze and design conditions of the study area.

1.3 Objective of the Study

1.3.1 General Objective

The general objective of this study is to develop a correlation between index soils properties and shear strength parameters using an artificial neural network which is used to predict shear strength parameters of soils from index properties of soils.

1.3.2 Specific Objective

In order to guide the research, the specific objectives are established as follows:

1. To gather a vast database of samples containing shear strength test results, Atterberge limit test results, bulk density and grain size distribution results, in order to build models that can be used to predict soil parameters for various soil types in Addis Ababa;
2. To evaluate the correlations among soil shear strength parameters and index properties of soils test results;
3. To investigate the importance level of the input variables in c and ϕ prediction;
4. To develop ANN model that can be used to obtain the desired output of c and ϕ;
5. To compare the results obtained by means of the proposed ANN with those obtained using existing methods.

1.4 Scope of the Study

A comprehensive set of experimental data were obtained from different construction projects done in Addis Ababa city in developing models of neural network based soil models. The input factors considered for shear strength parameters are the index properties of soils (consisting of Liquid Limit (LL), Plasticity Index (PI), Bulk Density (BD), Sand % (SP), Fine % (FP), and Natural Moisture Content (ω)). Separate neural network models are developed, to predict the internal friction angle ϕ and the cohesion c of soil from the

index properties. Cohesion c and angle of friction ϕ are the single output variables in the models.

1.5 Methodology

The first step of this work consisted in a literature review of soil shear strength, existing correlations for prediction of soil shear strength parameters, artificial neural networks and applications of ANN in geotechnical Engineering. Simultaneously, primary and secondary soil test results of index properties and shear strength tests performed on different soil samples of Addis Ababa city were gathered. So as data could be used during training, testing, validation and cross validation of ANN models. A total of 284 soil test result data, 20 primary and 264 secondary, were collected containing results for various soil types. The secondary data were then randomly divided into training, validation, testing. ANN models were trained and tested by software MATLAB 2020a, which performed adjustments in the networks by using correlation coefficient (R) and mean squared error (MSE). Later, the models cross validation was done by the 20 primary soil test result data performed in selected sites of Addis Ababa. The best model was chosen as being the one that obtained the greatest correlation between predicted and real values of c and ϕ. A schematic diagram of the research methodology that is used in this research work is shown in Figure 1-1.

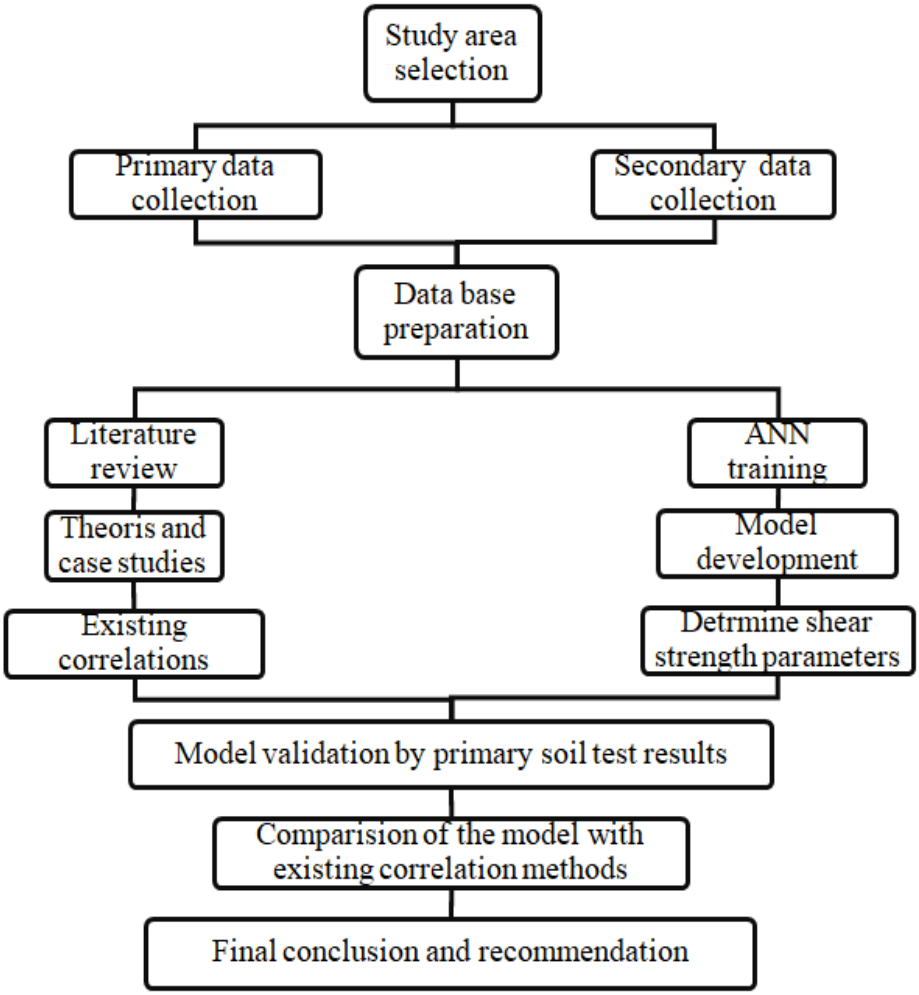

Figure 1-1: Schematic Diagram of the Research Methodology

1.6 Structure of the Study

This thesis manuscript is divided into five chapters, which will be described briefly in this section. The first chapter addresses the motivations of the study along with its objectives and a concise description of the methodology. The second chapter focuses on the literature review on soil shear strength, shear strength correlations, artificial neural networks and applications of ANN, in order to give a better understanding of the studied phenomena, and an overview of the artificial neural networks. In the third chapter, the methodology of this study is presented together with all its boundary conditions, which define the applicability of the proposed models. The presentation and analysis of the results are presented in the fourth chapter herein along with a discussion of the objectives and results. Finally, the fifth chapter shows the conclusions obtained from this research together with

the suggestions for other studies that can fill in gaps left when predicting soil shear strength parameters.

CHAPTER 2 LITERATURE REVIEW

The goal of this section is to describe the main concepts discussed herein. To begin, the shear strength of soils will be discussed as a result of particle interaction and index properties, because it is critical to understand this behavior in order to determine which soil properties have the greatest impact on its shear strength parameters. The concept of Artificial Neural Networks will be explained, how its computation and prediction processes function, as well as network training and validation. Thus, the models for prediction of shear strength parameters will be exposed and explained. Moreover, this will explain the working of these models so they can be compared to the results obtained by the ANN.

2.1 Soil Shear Strength

The internal resistance per unit area that a soil mass can supply to withstand failure and sliding along any plane inside it is known as its shear strength. Shearing strength refers to the highest shearing resistance that a material is capable of developing. The stability of a cut, the slope of an earth dam, the foundations of structures, the natural slopes of hillsides and other structures built on soil depend upon the shearing resistance offered by the soil along the probable surfaces of slippage. In the field of engineering, there is hardly an issue that does not involve the shear properties of the soil in some way (Murthy, 2008).

Understanding the mechanical behavior of soils is critical in Geotechnical engineering project designs, because it determines how structures will respond to loads imposed in the mass. Some constitutive models were proposed in this regard, with the Mohr-Coulomb criterion being the most widely employed in Geotechnics due to its precise and practical modeling theory. The soil shear strength, according to this theory, varies linearly with applied stress via two shear strength components known as cohesion intercept and angle of shearing resistance. The Mohr-Coulomb equation, as given in Equation (2.1), can be used to calculate the force acting on a failure surface in the soil body. If the cohesion intercept and angle of shearing resistance are determined using the total stresses, they are named as total or undrained cohesion intercept (c) and angle of shearing resistance (ϕ). The difference between the total stress and the excess pore water pressure is the effective stress. The effective circles can be plotted and the effective strength parameters (c' and ϕ')

can be derived if the pore water pressures are monitored during the test (Mollahasani et al, 2011). The Mohr circles and failure envelopes are shown in Figure 2-1 (a) and (b) in terms of total and effective stresses, respectively.

$$\tau = c + \sigma_n \tan\phi \qquad 2.1$$

Where, τ is the shear (tangential) stress, σ_n is the normal stress, c is the cohesion of soil, and ϕ is the internal friction angle of soil.

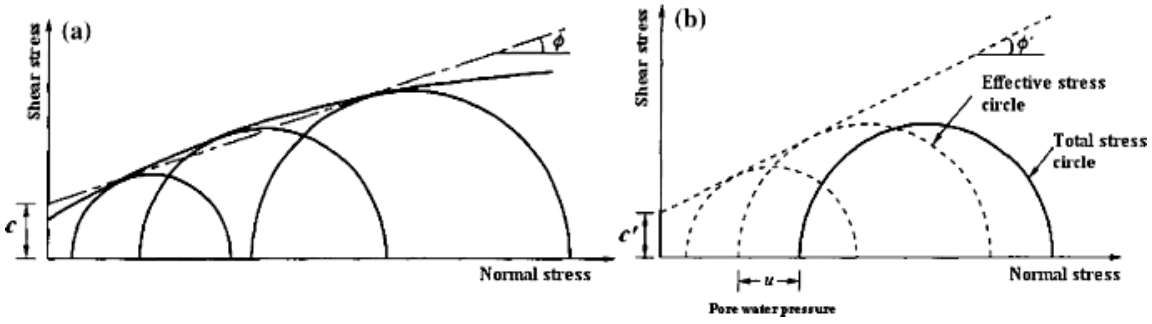

Figure 2-1: Mohr Circles and Failure Envelopes in Terms of Total Stresses and Effective Stresses (Murthy, 2008)

Cohesion (c): is the resistance of soil particles to displacement due to intermolecular attraction and surface tension of the held water. The soil cohesion is the intercept on the shear axis of the Mohr–Coulomb shear resistance line in the stress plane of the shear effect on normal stress (Mollahasani et al, 2011). Because of the size and polarity of grains, cohesion is extremely appropriate in fine-grained soils. True cohesion, on the other hand, can be seen in coarse-grained soils when particles stay in touch for long periods of time, resulting in contact cementing, as seen in the formation of sandstone from sand.

In soils, the factors responsible for true cohesion are electrostatic forces in stiff over consolidated clays (which may be lost through weathering), and cementing (by Fe_2O_3, $CaCO_3$, NaCl, etc). However, apparent cohesion can also occur, mainly caused due to negative capillary pressure (which generally disappears upon wetting), pore pressure response during undrained loading (which fades away with time), and root cohesion (which may be lost through logging or fire of the contributing plants, or through the solution).

Internal Friction Angle (ϕ): The shear resistance of a soil in the presence of normal effective stress at which shear failure occurs is described by its friction angle. The

mechanical behavior of coarse-grained soils is primarily determined by particle-to-particle contact, which implies that the frictional component of shear strength is more visible.

The values of these parameters for any soil depend on several factors; such as the soil textural properties, past history of the soil, initial state of the soil(i.e. whether it is saturated or unsaturated), permeability characteristics of the soil and the conditions of drainage allowed to take place during the test (Murthy, 2008).

2.2 Methods of Determining Shear Strength Parameters

The soil shear strength parameters c and ϕ can be determined either in the field or in the laboratory.

I. Laboratory methods
    a. Unconfined compression test
    b. Triaxial shear test
    c. Direct shear box test

II. Field (in-situ) tests
    a. Field vane shear test
    b. Standard penetration test
    c. Cone penetration test
    d. Piezo-cone test
    e. Pressure meter reading test.

The most typical laboratory tests are the triaxial shear and direct shear tests. When in-situ soil strength characteristics are required, laboratory tests can be used if undisturbed samples from the stratum can be extracted. Even though soil particles have cohesion, soils are prone to disturbance when sampling or extraction from sampling tubes in the laboratory. In cohesion less soils and highly pre-consolidated clay soils, it is practically impossible to get undisturbed samples. Soft sensitive clays are nearly always remolded during sampling (Murthy, 2008).

2.3 Effect of Index Properties on the Shear Strength Parameters

2.3.1 Related Studies

The soil shear strength characteristics are influenced by a variety of factors. The composition of particles in the soil, soil texture, and moisture all play a role in soil cohesion (Hosseini et al, 2018). Also Mineralogical composition, particle size and gradation, particle shape, compaction characteristics, confining pressure, roughness, moisture content, void ratio, and relative density all influence the friction angle (Jain, Jain and Bhadauria, 2010).

According to El-Maksoud (2006), Murthy (2008), Kayadelen et al (2009), c and ϕ were considered to be functions of the following parameters:

$$c, \phi = f\,(FC, CC, D_{10}, D_{30}, D_{60}, Cu, Cc, LL, \omega, \gamma, \gamma_d) \qquad 2.2$$

Where, c (kg/cm^2) is Cohesion, ϕ (°) is Friction angle, FC (%) is Fine-grained content, CC (%) is Coarse-grained content, D_{10} (mm) is Grain size for which 10% of the sample was finer, D_{30} (mm) is Grain size for which 30% of the sample was finer, D_{60} (mm) is Grain size for which 60% of the sample was finer, Cu is Coefficient of uniformity (D_{60}/D_{10}), Cc is Coefficient of curvature ($(D_{30})^2/(D_{60}\times D_{10})$), LL (%) is Liquid limit, ω (%) is Moisture content, γ (g/cm^3) is Soil unit weight, and γ_d (g/cm^3) is Soil dry unit weight.

The fabric characteristics, state and consolidation history of the soil are all known to influence soil shear strength parameters. The intrinsic soil properties are represented by FC, CC, D_{10}, D_{30}, D_{60}, Cu, Cc, and LL. γ, ω and γ_d provide information about the soil's condition and stress history. They are also void ratio indicators. The significant influence of these parameters in determining c and ϕ is well understood (Murthy, 2008).

According to a study by Mousavi et al (2012), soils with high plasticity have lower angle of shearing resistance and higher cohesion. This study was aimed at obtaining meaningful linear genetic programming (LGP) based relationships between the undrained cohesion intercept (c) and angle of shearing resistance (ϕ) and the soil physical properties. In contrast, when the size of the soil grains increases, the internal friction angle of the soil also increases, and its cohesion decreases. The soil unit weight and liquid limit were determined to have the greatest influence on c and ϕ. As a result, the study came to the

sensible conclusion that the soil type, soil plasticity, and soil density are the main factors that influence soil strength parameters.

A study by El-Maksoud (2006) showed that the value of soil cohesion varies depending on soil moisture content, grain size, and compaction. In the study, laboratory experiments were carried out with the help of a direct shear device. To determine the relation between soil strength parameters and both soil moisture content and soil bulk density linear regression equations were developed. The results indicate that both angle of internal friction and soil cohesion were inversely proportional to soil moisture content and were directly proportional to soil bulk density.

According to a study by Bekala et al (2021), undrained shear strength (C_u) was significantly correlated with liquid limit (LL), plastic limit (PL), bulk density (ρ_b), dry density (ρ_d), natural moisture content (NMC), and plasticity index (PI). While it was not significantly correlated with a specific gravity (Gs) and liquidity index (LI) of study area soil.

Jiang et al (2021), used soil physical parameters of paddy soils in the plastic stage to estimate soil shear strength indicators. Eight soil samples were gathered from eight paddy fields in Southeastern China for the study. Based on clay concentration, moisture content, and density, the soil samples were divided into five tiers. The effects of clay content, moisture content, and density on soil cohesion and internal friction angles of the soils were explored and assessed using the regression analysis approach after the direct shear tests were completed.

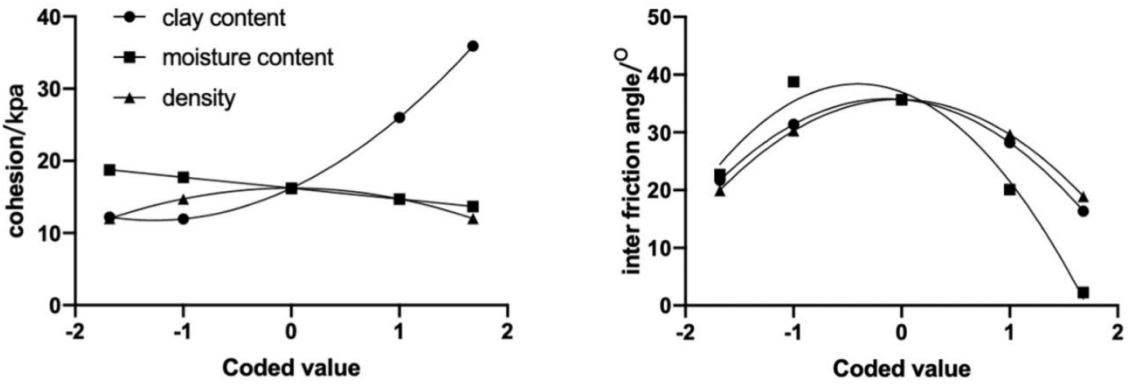

Figure 2-2: Single Factor and Response Value Curves for Cohesion and Internal Friction Angle (Jiang et al, 2021)

Figure 2-2 shows that soil cohesion reduced as soil moisture content increased and increased as clay content increased. However, it increased slightly at first but then decreased when wet bulk density reached 2.3 g/cm^3. Clay content had the greatest impact on cohesiveness among the three components, with the steepest regression line. Changes in clay content, moisture content, and wet bulk density all increased the internal friction angle until the three factors reached the middle level, then declined when the factors continued to increase. Among the three parameters, the soil moisture content had the greatest impact on the internal friction angle.

The soil friction angle and cohesion increases with increasing soil density, according to Dadkhah et al (2010). Also shear strength is affected by various factors, as studied by Lun (2011), including grain size distribution, density, and water content.

2.3.2 The Proposed Parameters

Liquid Limit: The moisture content above which a soil acts as a liquid is known as the liquid limit of the soil (Rogers, 2009). According to Roy and Dass(2014), shear strength parameters increase as the liquid limit increases. These results could be due to differences in soil properties (cohesionless and cohesive) at different locations. According to Mousavi et al (2012), cohesion increases as liquid limit increases; also angle of shearing resistance positively correlated up to 35% of liquid limit and thereafter the correlation became negative.

Plasticity Index: The plasticity index is the numerical difference between the liquid and plastic limits (Rogers, 2009). The flexibility of fine particles is determined by liquid and

plastic limits tests, which allows them to be classified as silts or clay soils(Guidelines, 2010). The shear strength parameters increased as the plasticity index increased. The plasticity index of soils increases linearly with the amount of clay present in the soil, as per Akayuli (2013). Clay content also increases the cohesion and decreases the friction angle. This is due to the fact that only the clay fraction provides plasticity, with the sand serving as inert filler with no physio-chemical interaction with the clay to impact its plasticity.

Bulk Density: Bulk density has a significant impact on soil shear strength. To give additional soil strength, engineers commonly pack soils tightly to achieve significant bulk densities. According to Garcia et al (2012), shear strength increases with increasing bulk density, showing that soil resistance is caused by a reduction in pore volume. Ojuri (2013) noticed an increase in bulk density with corresponding increase in undrained shear strength.

Natural Moisture Content: Cohesive and cohesionless properties of soils might cause variation in moisture content in the soils and hence variation in shear strength parameters. According to Dafalla (2013); Kumari (2009), cohesion and angle of shearing resistance depends on the presence of clay and moisture content in the soils. Most of the physical, chemical, and biological activities that occur in soil are influenced by water. . Water in soil works as a lubricant as well as a binding agent among soil particle components, affecting soil and geologic materials' structural stability and strength (Kristyna, Lenka and Pavla, 2013). Obasi and Anyaegbunam (2005) found that partially saturated soils exhibit undrained shear strength that is dependent on moisture content.

Fines Content: Ayodele (2009) investigated the effect of fines content on the performance of soil as a sub-base material for road construction and discovered that as fines content increased, the engineering properties of the soil samples analyzed decreased. Fines are defined as soil particles that pass through sieve No. 200 (75μm opening) according to USCS and AASHTO. The fines consist of clay and silt. The fines content in coarse grained soils are carefully considered because it affects key soil qualities like permeability, particle friction, and cohesion, as well as determines the composition and type of soil (Lade, Liggio and Yamamuro, 1998).

2.4 Artificial Neural Networks (ANNs)

2.4.1 Biological Neurons

The biological neurons were the inspiration for the Artificial Neural Network (ANN) idea (Kim, 2017). As a result, it's critical to know how these systems work. The neuron is the most basic component of neural networks. In biological systems, a neuron is a cell, like any other cell in the body that contains a DNA code and is produced in the same way as other cells. Despite the fact that each organism's DNA is different, the function is the same.

The neurons are commonly recognized as the biological nervous system's major functional elements, capable of receiving and transmitting electric pulses (spikes) through their cell bodies. The cell body (also known as Soma), dendrites, and axon are the three major components of a neuron (Akomalfe & Eluyode, 2013).

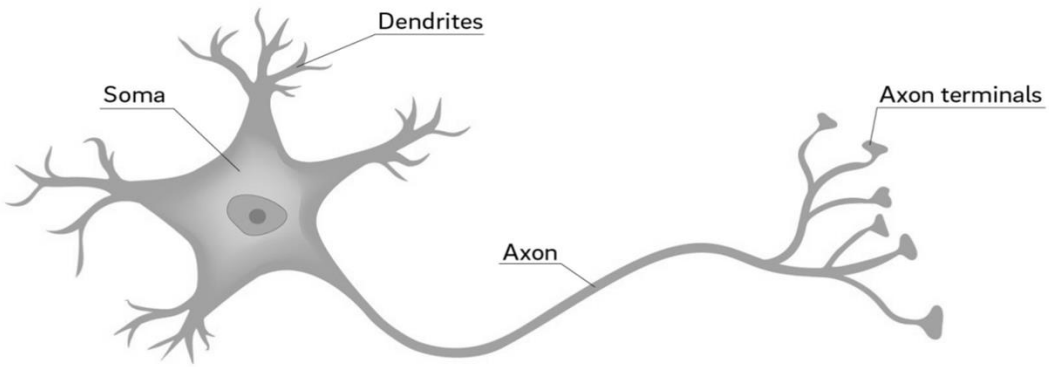

Figure 2-3: Anatomy of Biological Neuron

Figure 2-3 shows the anatomy of these cells as well as the spike propagation through them. Dendrites are like threads that branch out in different directions and connect to a large number of cells in a cluster. The axon receives signals from neighboring neurons and sends them to the other neurons through dendrites. A synapse connects the axon's terminating terminal to the dendrite. Axon is a long fiber that transfers the output signal along its length as electric impulses. Axons are the extensions of neurons. Each neuron has one axon. Axons act as a domino effect, passing impulses from one neuron to the next.

2.4.2 Artificial Neurons

On the basis of biological neurons, Warren MuCulloch (neuroscientist) and Walter Pitts (logician) presented the first computational model of a neuron in 1943, which led to the

development of ANNs (Haykin S. , 2009). The model was able to divide the data into two classes, which could be beneficial for simple data discrimination, but this configuration could not handle more sophisticated discrimination (Sagiroglu, Besdok, & Erler, 2003).

Table 2-1: Biological Nervous System with Similar Features of ANN (Sagiroglu, Besdok, & Erler, 2003)

Biological Nervous System	Artificial Neural Network
Dendrite	Artificial Neuron Input
Cell Body	Artificial Neuron Node (Processing Element)
Axon	Transfer Function
Terminal Axon	Artificial Neuron Output
Synapses	Weights

The artificial neuron was subsequently defined as a linear discriminator in order to employ it in more complicated applications. This discriminator, also known as the processing element, is separated into five sections, according to Haykin (2009). Inputs, weights, a summing function, a transfer function, and outputs are all included.

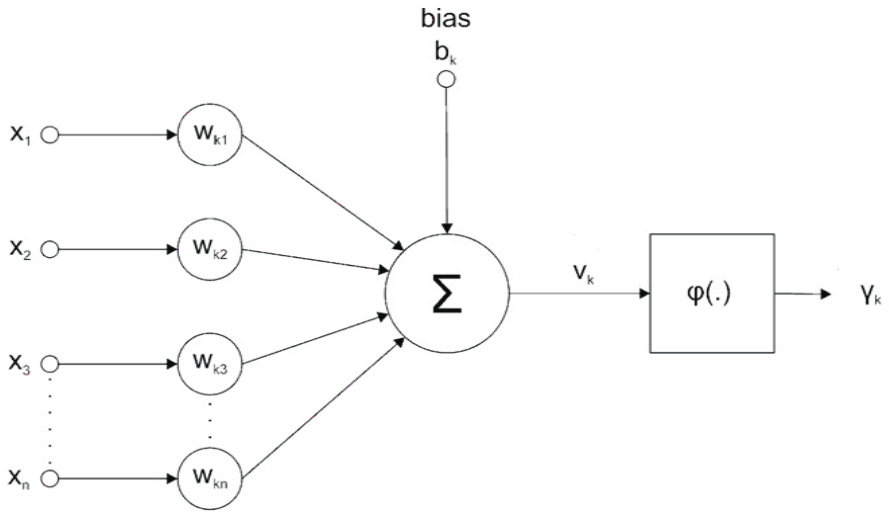

Figure 2-4: Model of an Artificial Neuron (Haykin, 2009)

Where, x_n is Entry (input) signal, w_{kn} is Synaptic weight, b_k is Bias or Threshold, v_k is Induced local field, or Activation potential, $\varphi(\cdot)$ is Activation function, y_k is Output signal.

2.4.2.1 Inputs

The inputs are defined as data from outside a neuron, which can come from an external neuron or the neuron itself. Input is the foundation of network training (Aslay & Ustun, 2013).

2.4.2.2 Weights

The weights are represented by w coefficients, which show how the neural nerve's input data affects the nerve cell. Each input has a weight. There is a weight assigned to each input. The input is important, and the effective rate is high, as indicated by the high weight value. Low weight levels imply that the input is unimportant. In the connection between input and output values, weights are used (Elmas, 2007).

2.4.2.3 Summing function

It estimates the net input from the neuron, and different functions to do so. The linear combiner is defined by the total of the entries weighted by each individual weight in this segment. Depending on the problem, the summing function may be chosen differently. The perfect summing function is determined using the trial and error method. (Hamzacebi, 2011)

2.4.2.4 Activation function

It's the function that keeps the neuron's output value in a specified range when compared to its net input value. It creates a link between the neuron's input and output values. It analyzes the cell's total input and creates the appropriate output (Haykin & Network, 2004). Depending on the function of the neuron, the activation function may be of different types. The most frequently used activation functions are sigmoid and hyperbolic tangent functions (Kakici, 2017).

i. Sigmoid Function (logsig): The sigmoid activation function is a continuous and derivative function. Because of its non-linearity, it is one of the most commonly employed functions in ANN applications. For each of the supplied input values, this function generates a value between zero and one.

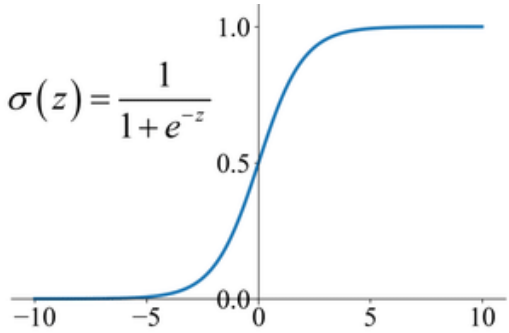

Figure 2-5: Sigmoid Activation Function

ii. Hyperbolic tangent sigmoid function (tansig): The function's dynamic change interval is [-1 1], and it shows a non-linear change in this range based on the neuron's total input neuron.

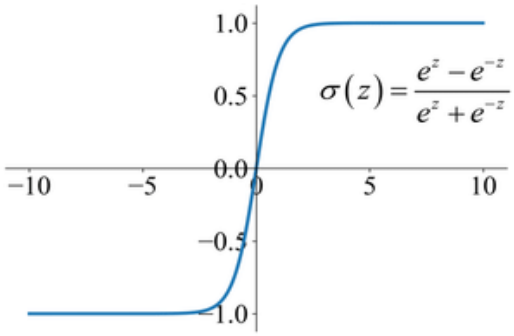

Figure 2-6: Hyperbolic Tangent Sigmoid Function

iii. Linear function (purelin): Neuron output changes linearly in response to changes in neuron inputs in this activation function. [-1 1] is the dynamic change interval. Figure 2-7 shows the function's input-output characteristic.

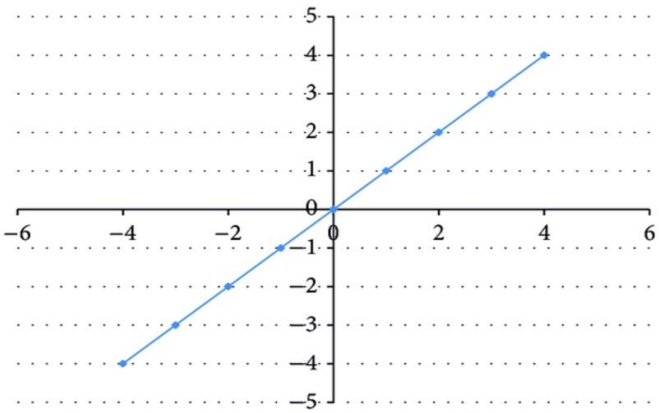

Figure 2-7: Linear (Purelin) Function

2.4.2.5 Outputs

The activation function generates the output value. This value can be communicated to another neuron or to the outside. The resulting output might be used as input by the cell (Oztemel, 2003).

2.4.3 Artificial Neural Network Architecture

ANN is a computational tool that is based on the underlying behavior of neural architecture in biological systems and is specifically designed to represent the human brain. The ability to build actual correlations between independent and dependent variables, as well as extract delicate information and complicated knowledge from representative data sets, is a distinguishing feature of ANN. Without making any assumptions regarding a formal representation of the events, the relationships between independent and dependent variables can be established. ANN models have several advantages over regression-based models, such as the ability to handle noisy data (Haykin, 2009).

A layer of input nodes and a layer of output nodes make up an ANN, which is connected by one or more layers of hidden nodes. By firing activation functions, input layer nodes send information to hidden layer nodes, while hidden layer nodes either fire or remain dormant depending on the evidence given. The evidence is weighted by the hidden layers, and when the value of a node or collection of nodes in the hidden layer hits a certain threshold, a value is passed to one or more nodes in the output layer. Because neurons are structured by layers that are mutually related by synaptic weights, the ANN exhibits tremendous parallelism (Kakici, 2017).

Initially, neural network pioneers had a very simple architecture with only input and output layers, which are called singlelayer neural networks. Inputs are connected to processing nodes with varying weights, resulting in a single output per node. A multi-layer neural network is created by adding hidden layers to a single-layer neural network. An input layer, hidden layer(s), and output layer make up the multi-layer neural network.

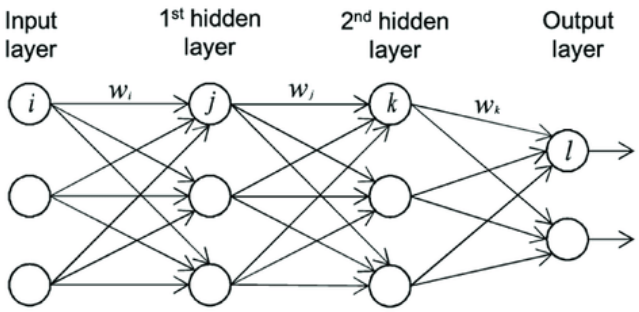

Figure 2-8:A Multi-Layer Feed-Forward Neural Network

2.4.3.1 ANN Basic Structures

The feed-forward model, the feed-back model, and the self-organizing competition model are the three core architectures of the ANN. Back-Propagation (BP) Networks, Hopfield Networks and Self-Organizing Map Networks (SOM) are the most representative networks for corresponding basic structures(Oztemel, 2003).

2.4.3.2 Back-Propagation (BP) Network

The feed-forward model's core is the Back-Propagation (BP) network, which is a multi-layer ANN based on the Back propagation Algorithm (Kukreja, Bharath, & Kuldeep, 2016). The BP networks' training process is under supervised learning, which means that the training data lacks label information. The BP network's training procedure is as follows: The training sample data is first entered into the network, then the data would transfer forward from the neural in the input layer by layer until the data reach the neural in the output layer and the outcome in the output layer is obtained. The deviation would be transferred reversely to the neural in the hidden layer when the gap between the input value and output value is bigger than expected value. The weight of each neural would then be modified depending on the deviation using the steepest descent approach, which involves computing the minimum (maximum) value of the loss function along the gradient descent (ascent) direction, and the deviation would then be passed to the input layer. In the next stage, the value would then proceed forward propagation once more, and the error would continue to decrease with each iteration (Haykin & Network, 2004). The training is complete when the difference between the input and output values is less than the predicted value.

2.4.3.3 Learning Data Sets

There are three learning Data Sets in Artificial Neural Networks:

i. *Training Data Set*: A set of samples used to learn how to fit the network's parameters [i.e. weights]. On the training set, one approach comprises one full training cycle. The training process is presented to the network during training, and the network is adjusted according to its error.

ii. *Validation data Set:* A set of examples used to tune the parameters [i.e. architecture] of the network. For example, to choose the number of hidden units in a Neural Network.On the other hand, once the weights have been corrected, the network is validated using an additional set of known samples that has not yet been used. This process is called validation and aims to verify the generalization capacity of the ANN from data not used in the training process.

iii. *Test data Set:* A set of examples is used only to assess the performance [generalization] of a fully specified network or apply successfully to predict output whose input is known. These have no effect on training and so provide an independent measure of network performance during and after training.

After providing the architecture, the model must be trained and validated. The weight vector is adjusted during the training phase by comparing the results acquired in a previous configuration with the desired outcome of previously known sample data. This comparison yields an error for each neuron. The weights are then adjusted and the training process continues as long as the error for all neurons is kept to a minimum (Hamzacebi, 2011).

2.5 Applications of ANNs in Geotechnical Engineering

Geotechnical engineering is the basis for the various engineering project construction which deals with materials like soil and rock. Traditional methods in geotechnical engineering cannot predict the non-linear and plastic properties of rock and soil accurately.

Machine learning techniques are able to deal with non-linear and plastic issues of rock and soil effectively and avoid the flaws that older methods might produce. ANN algorithm is a popular machine learning algorithm that is widely applied in geotechnical engineering.

Das (2013) and Juwaied (2018) have presented the state of art and the uses of ANN that have been applied in Geotechnical Engineering.

Table 2-2: Applications of ANN in Geotechnical Engineering (Juwaied, 2018)

Field of Applications	Researchers
Soil properties and behavior	Ghaboussi & Sidarta (1998) Goh (1995a; 1995c) Penumadu & Zhao (1999) Zhu, Zaman, & Anderson (1998a; 1998b) Najjar & Basheer (1996b) Cal (1995)
Site characterization	Najjar & Basheer (1996a) Rizzo & Dougherty (1994) Basheer, Reddi, & Najjar (1996) Rizzo, Lillys, & Dougherty (1996)
Earth retaining structures	Goh, Wong, & Broms (1995) Gordon et al (2007) Goh and Kulhawy (2005)
Slope stability	Ferentinou & Sakellariou (2007) Cho (2009) Gemitzi & Eskioglou (2011) Das et al (2011)
Settlement of foundations	Sivakugan, Eckersley, & Li (1998) Shahin, Jaksa, & Maier (2000;2003c) Shahin (2014a) Alkroosh & Nikraz (2011)
Liquefaction	Goh (1994b; 1996a) Najjar& Ali (1998) Baziar & Ghorbani (2005) Hanna, Ural, & Saygili (2007)
Design of tunnels and underground openings	Shi, Ortigao, & Bai (1998) Lee & Sterling (1992) Moon, Na, & Lee (1995) Hajihassani et al (2011)
Pile capacity Prediction	Lee & Lee (1996) Teh et al (1997) Shahin (2010) Wardani, Surjandari, & Jajaputra (2013) Maizir, Gofar, & Kassim (2015) Abu-Kiefa (1998)

2.6 Existing Prediction Models of Soil Shear Strength Parameters

In geotechnical engineering, empirical correlations are commonly employed to estimate the engineering parameters of soils. There are useful relationships between index parameters acquired from routine testing and soil strength properties. The findings of

routine index tests and correlations can be utilized as a first approximation of soil parameters in preliminary geotechnical structure design, and later as a means to validate the results of laboratory experiments. The most often utilized approaches for developing relationships between material properties are regression analysis and artificial neural networks (Harini & Naagesh, 2014).

2.6.1 Regression Approach for Predicting Shear Strength Parameters

Many approaches for predicting friction angle have been proposed over the years, mostly for sandy soil, considering only the frictional part of its mechanical behavior. However, analytical models were unable to give precise results on both cohesion and friction angle simultaneously.

Roy and Dass (2014) developed multiple regression models in Equation (2.3) and (2.4) for the prediction of shear strength parameters. They conducted a thorough investigation in Sirsa, India. The impact of geotechnical variables on shear strength parameters was investigated, including bulk density, dry density, natural moisture content, specific gravity, particle size, liquid limit, plastic limit, and plasticity index. The most influencing variables were chosen using a stepwise regression technique.

$$c = -0.525 + 0.241\ G_s \qquad 2.3$$

$$\phi = -29.604 + 34.220\ BD \qquad 2.4$$

Where c is cohesion (kPa), ϕ is internal friction angle (°), Gs is specific gravity, and BD is soil bulk density (g/cm^3).

Bekala et al (2021) conducted a study in Agaro town, Oromia Region, Ethiopia, to investigate a statistical analysis of the shear strength parameter based on the index properties of fine-grained soils. Single linear regression (SLR) and multiple linear regressions (MLR) methods were devised to estimate the undrained shear strength parameter (c_u) from Gs, NMC, ρ_b, ρ_d, LL, PL, and PI & LI. As a result, multiple linear regression (MLR) analysis yielded the best Model among all, with a higher coefficient of determination (R^2 = 0.806), a higher significance level, and lower standard error as mentioned in Equation (2.5).

$$c_u = 224.032 - 2.272\ PL - 2.485\ PI \quad (2.5)$$

Where, c_u is undrained shear strength in (kPa), PL is plastic limit (%) and PI is plasticity index (%).

Korayem et al. (1996) found regression equations, referred in Equation (2.6) and (2.7), linking soil strength parameters to both soil bulk density and moisture content in sandy loam soil.

$$c = 0.0865\ BD^{2.53}\omega^{-0.0277} \quad (2.6)$$

$$\phi = 0.761 - 0.0122\omega \quad (2.7)$$

Where, c is cohesion (kPa), ϕ is internal friction angle (°), BD is bulk density (g/cm^3), ω is moisture content (% d.b.).

Quantitative relationships between fines content and cohesion of the soil samples were developed by Adunoye (2013). Lateritic soil samples were obtained from three selected locations in Nigeria and the relationship between fines content and cohesion of soil was investigated. It was found that, when the fines content of the soil samples increased, the cohesion of the soil samples increased as well; the polynomial relationships in Equation (2.8) gave the best fitting between the fines content and cohesion of the soil samples.

$$c = -0.004FP^2 + 1.118\ FP - 7.383 \quad (2.8)$$

Where, c is cohesion (kPa) and FP is fines content (%).

In the study by Ersoy et al (2013), empirical equations were given utilizing statistical and multicriteria analysis based techniques for the prediction of strength parameters as a function of the index qualities of clayey soils (2013).According to the results of multiple regression analysis and analytical hierarchy process, the correlations characterized by the regression coefficient of 0.80 were determined among the friction angle, cohesion and plasticity properties. The study indicates that cohesion and the friction angle can be estimated from their plasticity properties with mathematical relations as shown in Equation (2.9) and (2.10).

$$c = 0.265(PI/LL)^{2.78} \quad 2.9$$

$$\phi = -204.5(PI/LL) + 56.3(PI/LL) + 31 \quad 2.10$$

Where, c is cohesion in (kPa), ϕ is internal friction angle (°), PI is plasticity index (%) and LL is liquid limit (%).

2.6.2 ANN Prediction Models of Shear Strength Parameters

In the last two decades, studies using neural networks to predict shear strength parameters have been issued, all with the goal of achieving better correlations between in-situ shear strength and soil properties than existing empirical models.

Using artificial neural network modeling, Iyeke et al (2016) develop models for predicting the shear strength parameters (cohesion and angle of friction) of lateritic soils in central and southern areas of Delta State. Eighty-three (83) soil samples were obtained in total. Plasticity indexes, percentage of particles passing sieve No.200, specific gravity, liquid limit, and plastic limit were all examined as input factors.

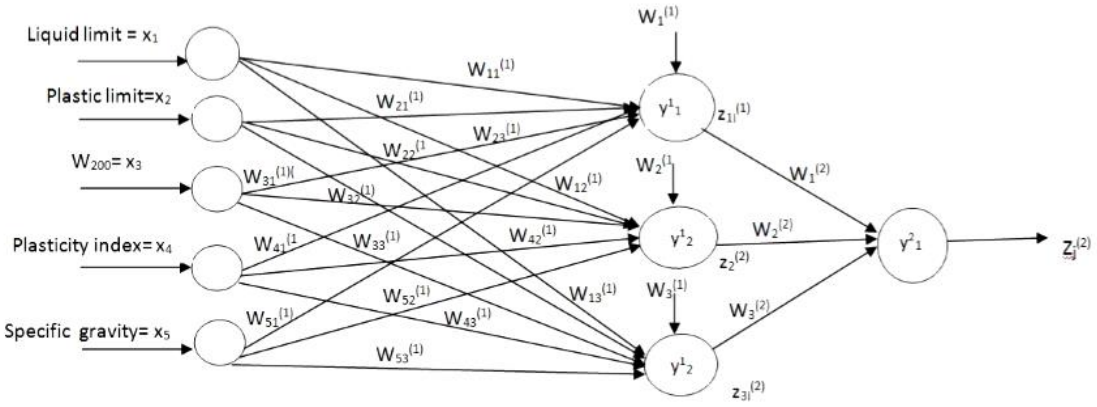

Figure 2-9: The Proposed Model Architecture by (Iyeke et al, 2016)

A one-hidden-layer MLP was employed in this study. The activation function for hidden and output layers was a logarithmic sigmoid transfer function. The number of hidden layer neurons was determined using a simple trial-and-error procedure with root mean square errors as the criterion (RMSE). The optimal network architecture obtained were 3-9-1 and 3-11-1 for cohesion and angle of friction respectively. Three standard approaches were used to compare the results of the anticipated and measured shear strength parameters

produced using ANNs. The results showed that the ANN method outperformed all of the empirical methods considered.

Das and Basudhar (2008) published a study on the residual shear strength of clays prediction with ANN. Since soil cohesion in a residual state is very low or inexistent, and its resistance is described in terms of residual friction angle (ϕ_r). In fact, an artificial neural network was built using 54 samples of volcanic ash clay (39 for training and 15 for testing), as well as triaxial and soil characterization test results. They developed four distinct MLP models based on LL, CF (clay fraction), PI and ΔPI, which represents the deviation from the A-line in classification chart and is given by:

$$\Delta PI = PI - 0.73(LL - 20) \qquad 2.11$$

Table 2-3: Statistical Performance of the Models Proposed by (Das and Basudhar, 2008)

Models	Input parameter	Coefficient of correlation	
		Training	Testing
Model 1	LL,CF	0.851	0.829
Model 2	LL,PI,CF	0.902	0.883
Model 3	LL,PI,CF, ΔPI	0.926	0.885
Model 4	CF, ΔPI	0.906	0.942

Table 2-3 shows the proposed models and their results, with Model 4 being chosen as the best for achieving the highest coefficients of correlation during both training (R= 0.906) and testing (R= 0.942).

Later, Shooshpasha, Amiri and MolaAbasi (2015) conducted a study on friction angle correlation using a GMDH (Group Method for Data Handling) artificial neural network. They collected 195 soil samples (120 for training, 50 for testing, and 25 for model validation).Then, using GMDH, several ANN were constructed one after the other, resulting in increasingly complicated networks at each level. The predicted to measured values adjustment was excellent, and the correlations achieved were high, with 0.998 for training and 0.997 for testing. The model was then validated by comparing the findings of regularly used correlations to the outcomes of unanticipated data.

2.7 Comparison between Regression and ANN Prediction Models

Goktepe et al (2008) proposed linear and non-linear regression, and artificial neural networks to estimate shear strength characteristics of clays from ω and PI. They performed

79 CU triaxial tests on normally consolidated plastic clays from the Antalya region in Turkey for the research. The results of the linear regression analysis are shown in Equations 2.11 and 2.12, where ε denotes the errors. The equations produced for predicting c' and ϕ' had coefficients of correlation of 0.72 and 0.87, respectively.

$$\phi' = -6.38 + 0.58\,\omega + 0.05\,PI + \varepsilon \qquad 2.12$$

$$c' = 1.61 - 0.03\,\omega - 0.01\,PI + \varepsilon \qquad 2.13$$

The results of non-linear multiple regression correlations were marginally better than those of linear regression analysis. Equations 2.13 and 2.14 for cohesion and friction angle presented R^2 equal to 0.73 and 0.90, respectively, which are already satisfactory.

$$\phi' = 0.0077\,\omega^2 + 0.1305\,\omega - 0.0125PI^2 + 0.4242\,PI - 0.0012\,\omega\,PI + \varepsilon \qquad 2.14$$

$$c' = 0.0006\,\omega^2 - 0.0737\,\omega - 0.0002\,PI^2 - 0.0282PI + 0.001\,\omega\,PI + \varepsilon \qquad 2.15$$

However, Goktepe et al (2008)used feed-forward multilayer perceptrons to achieve new results on estimating these parameters (MLP). To this goal, the authors provided models for two types of learning algorithms: gradient descent and the Lavenberg-Marquardt technique, both of which use the hyperbolic tangent as an activation function. In conclusion, the ANN model trained with the Lavenberg-Marquardt method achieved a significantly good performance in Antalya normally consolidated clays with architecture 2 x 30 x 2 and $R^2 = 0.99$.

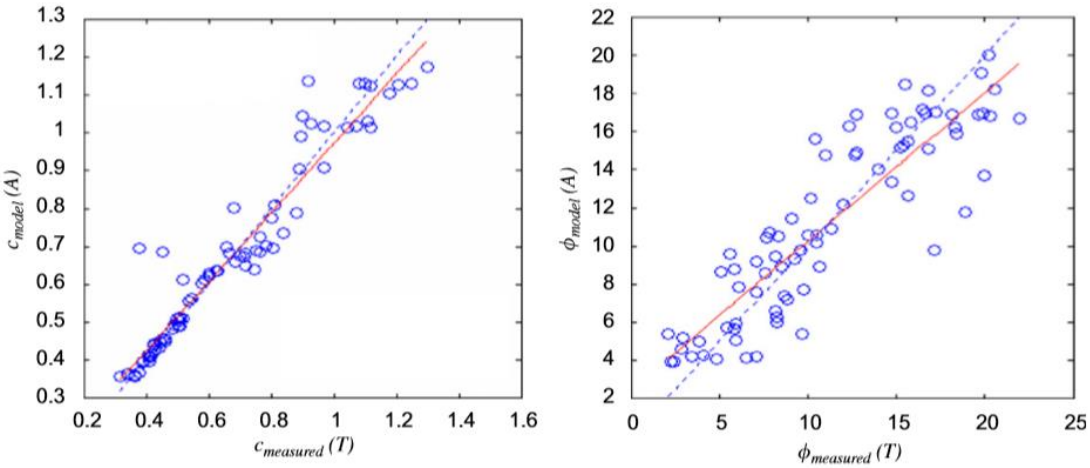

Figure 2-10: Scatter Graphs of ANN Models for C and Φ Using Gradient Descent Algorithm (Goktepe et al, 2008)

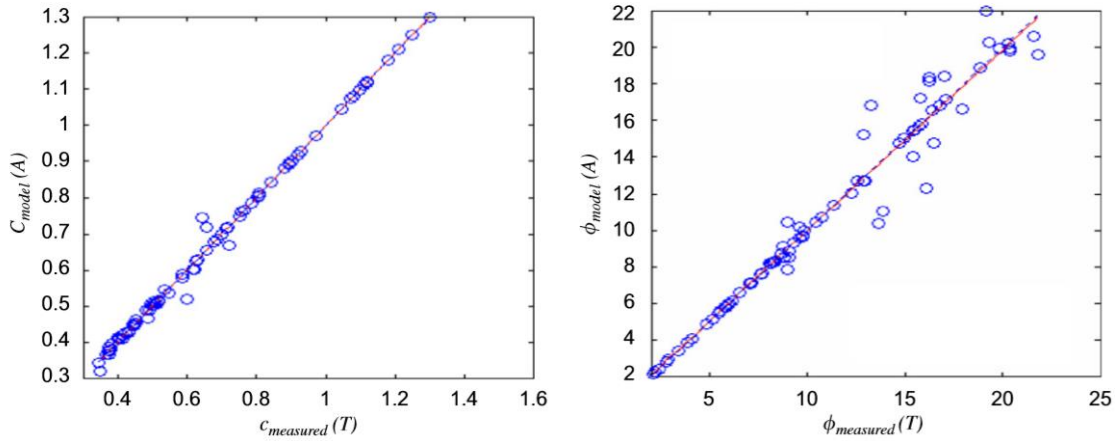

Figure 2-11: Scatter Graphs of ANN Models for C and Φ Using Lavenberg-Marquardt Algorithm (Goktepe et al, 2008)

Sushama and Bindhu (2016) developed an Artificial Neural Network as a prediction tool for determination of internal friction angle and cohesion. In this regard, an attempt was made to create a neural model using the index properties of soil as input parameters, which included water content (ω), Plasticity Index (PI), Bulk density (BD), Sand % (SP), Silt%(STP), and Clay % (CP). The development of neural network based soil models was based on a large set of experimental data collected in Bihar. According to this investigation, the most significant variables contributing to the estimation of the strength parameter c were clay percent (CP) and silt percent (STP). However, the plasticity index (PI) and dry density (DD) showed a significant impact on internal friction angle prediction.

Multivariable linear least square regression (LLSR) and non-linear least square regression were used in a regression analysis (NLSR).

The LLSR based equations used for formulation of c and ϕ are given as:

$$c = 0.216 - 0.00091\ PI - 0.0092\ SP - 0.008\ STP + 0.143\ CP - 2.14\ BD + 0.0347\ \omega + \varepsilon \quad 2.16$$

$$\phi = 5.481 + 0.057\ PI + 0.238\ SP + 0.1066\ STP - 0.489\ CP - 1.21\ BD + 0.079\ \omega + \varepsilon \quad 2.17$$

The NLSR based equations used for formulation of c and ϕ are as follows:

$$c = 0.0077\ PI^{1.58} - 0.005\ SP^{0.0076} + 0.008\ STP^{0.001} + 0.001\ CP^{0.0112} - 0.006\ BD^{0.89} \quad 2.18$$

$$\phi = 0.009\ PI^{0.008} + 0.9695\ SP^{0.7808} + 0.0055\ STP^{1.663} - 0.009\ CP^{0.0196} + 0.0014\ BD^{8.08} + 0.00078\ w^{0.243} + \varepsilon \quad 2.19$$

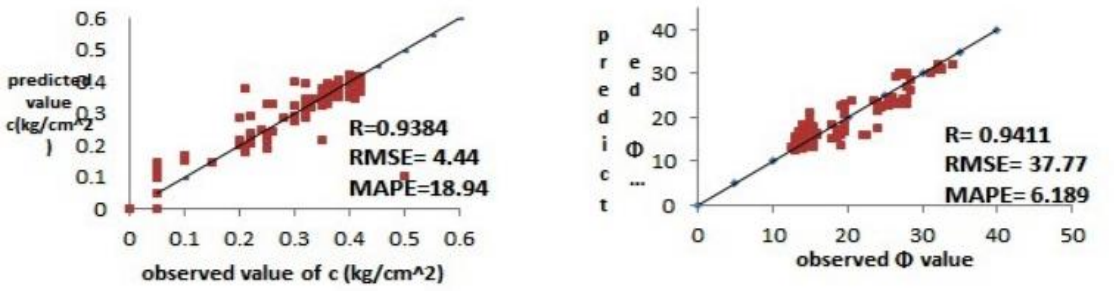

Figure 2-12: Comparison of observed vs predicted c and ϕvalues made by LLSR Model (Sushama and Bindhu, 2016)

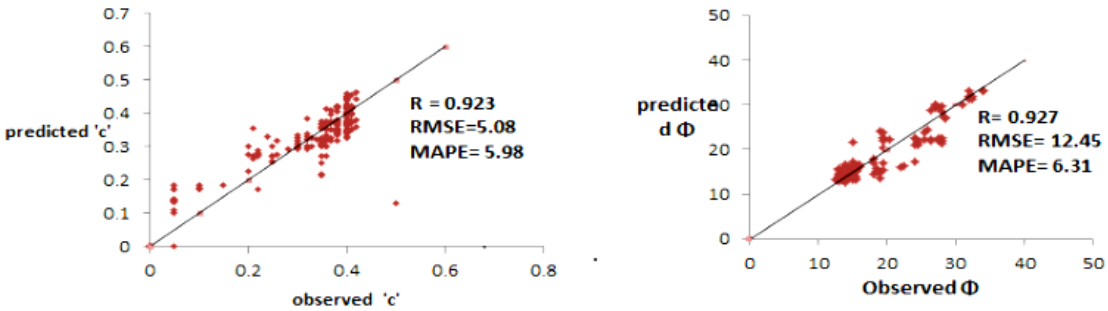

Figure 2-13: Comparison of observed vs predicted c and ϕ values made by NLSR Model (Sushama and Bindhu, 2016)

For the ANN MLP model 7-3-2 architecture gave the best result with the single hidden layer and 7-1-6-2 for the double hidden layers.

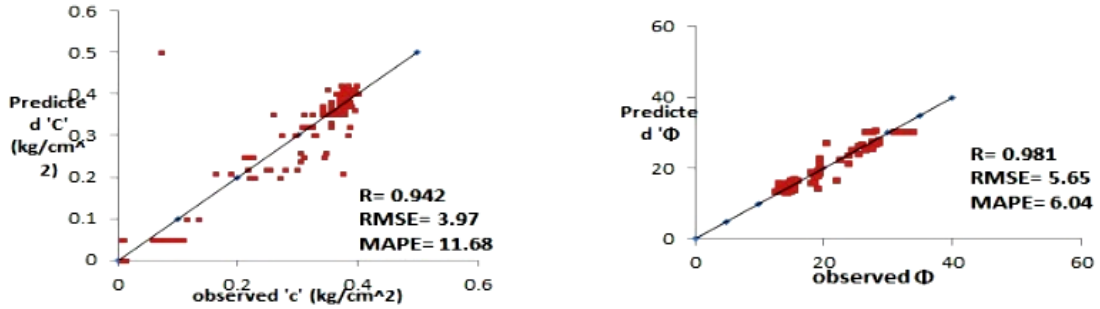

Figure 2-14: Comparison of Observed vs Predicted C and Φ Values Made by MLP Model (Sushama and Bindhu, 2016)

From the result the author concluded that developed ANN model using MLPs, the back-propagation training algorithm, and weight biases can be used with reasonable accuracy to model shear strength parameters. In ANN solution the equation results derived from weight and biases are closer to laboratory results with very less percentage of error.

Braga (2014) proposed a study utilizing ANN to predict cohesion and friction angle. The following inputs were used to develop multiple regression-based models (RLM) and artificial neural networks (ANN): clay, sand, and silt content, clay + silt content, limit of plasticity, liquid limit, plasticity index, relative density, and moisture content. Six models were created by grouping the input variables in different ways. The Lavenberg-Marquardt method was used to conduct the training. The RLM models performed reasonably well in the regression modeling, with a maximum R^2=0.58 for cohesiveness and for friction angle, R^2=0.64 is reached. The ANN models achieved correlations of up to 0.87 and 0.86 for c' and ϕ' prediction, respectively, outperforming regression modeling findings.

Finally, Braga (2014) compared the models' results using the statistical parameters previously discussed. According to Braga (2014), the RLM's performance was insufficient, whereas the ANN's findings were superior. The RLM findings ranged from regular to poor performances, implying that regression-based models may not be suitable for predicting shear strength parameters due to data behavior. Modeling utilizing artificial neural networks, on the other hand, produced results that were far more consistent with soil behavior and had a better generalization capacity.

CHAPTER 3 METHODOLOGY

The following section will explain the steps taken in this study, revealing the difficulties encountered throughout the research. Also the stages of the work done, which were designed to obtain soil strength parameters cohesion and friction angle by creating and validating an artificial neural network based on the primary and secondary data of the index property results and direct shear test results obtained, are discussed.

3.1 Description of Study Area

This study was conducted in Addis Ababa city, the capital city of Ethiopia. Addis Ababa lies at an estimated latitude of 9° 0' 19.4436" **N** and longitude of 38° 45' 48.9996" E and has an average altitude of 2,355 meters above sea level. From its lowest point, around Bole International Airport, at 2,326 meters (7,631 ft) above sea level in the southern periphery, Addis Ababa rises to over 3,000 meters (9,800 ft) in the Entoto Mountains to the north. Addis Ababa has a subtropical highland climate with precipitation varying considerably by the month. The city is divided into 10 sub cities.

3.2 Soils of Addis Ababa

Regarding the soil types, residual soils ranging from red to dark gray (black cotton soils) are found covering extensive areas in the city. Red clays are mainly found around Kolfe Keranyo and Asko areas. The black cotton soils cover relatively flat areas starting from Bole Medhanealem through Megenagna to the entire CMC and Kality in the east and southeastern part. In the western and southwestern Addis Ababa, black cotton soils coverthe entire Mekanisa and Lebu areas. On the other hand, the colluvial and alluvial deposits in the city and its surroundings are commonly observed at the foot of hills and river banks.

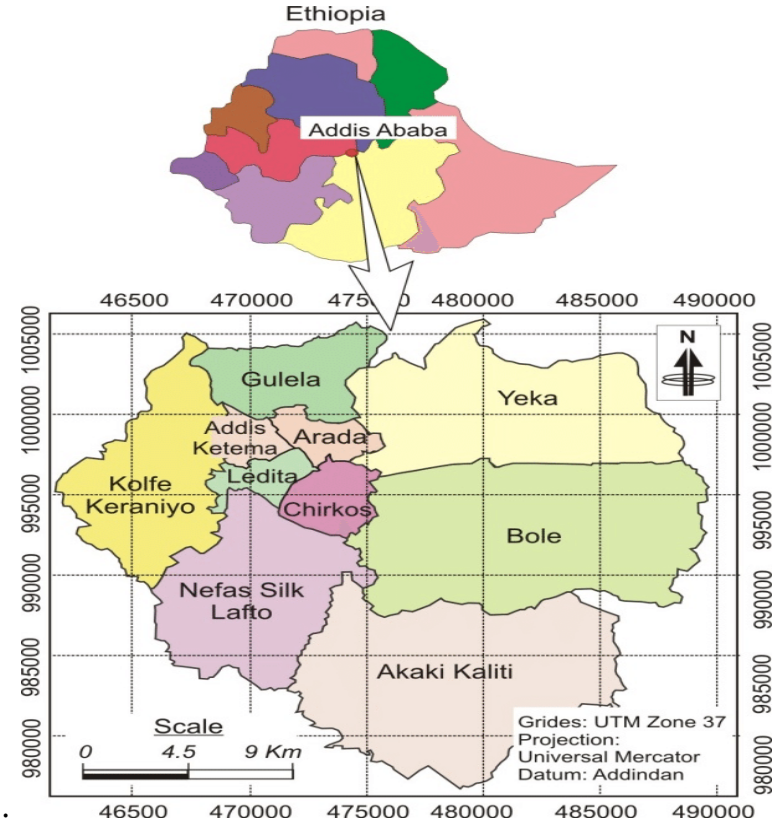

Figure 3-1: Location Map of the Study Area

3.3 Input Parameters Selection

At an early stage the collection and review of previous publications about the study were accomplished. In these previous studies, shear strength parameters were correlated with index properties of soils. bulk density, dry density, natural moisture content, specific gravity, liquid limit, plastic limit, plasticity index were significantly correlated with shear strength parameters(Roy & and Dass, 2014). The most important factors representing the behavior of c and φ were detected on the basis of literature review discussed in chapter two. Based on these literatures different combinations of the input parameters were proposed; finally, Liquid Limit (LL), Plasticity Index (PI), Bulk Density (BD), Sand % (SP), Fine % (FP), and Natural Moisture Content (ω), are selected to be the optimal input parameters of this study.

3.4 Database Collection and Preparation

A total of 284 laboratory test results, 20 primary data soil samples and 264 secondary data soil samples, were used in order to determine soil shear strength parameters from index properties. Grain size distribution, Atterberg limits, and soil shear strength parameters are included in each soil test result.

3.4.1 Primary Data Collection

Before selecting primary data sample locations, visual site investigation was accomplished and necessary information was gathered regarding soil type and distribution throughout the city. Field identification of soils was carried out according to the ASTM D 2488 (Standard Practice for Description and Identification of Soil). Then the sample locations were selected in order to characterize the soil types over the city. The soil laboratory tests were done in AAiT (Addis Ababa Institute of Technology) and MAFCON Engineering plc geotechnical laboratories. All the tests were done according to the ASTM manual.

3.4.1.1 Sampling Area

The location of test pits was selected to characterize the soil types found in the study area. Eleven sites were selected from six sub cities as illustrated in Figure 3-2. The soil samples depth with respect to the sample locations is described in Table 3-1.

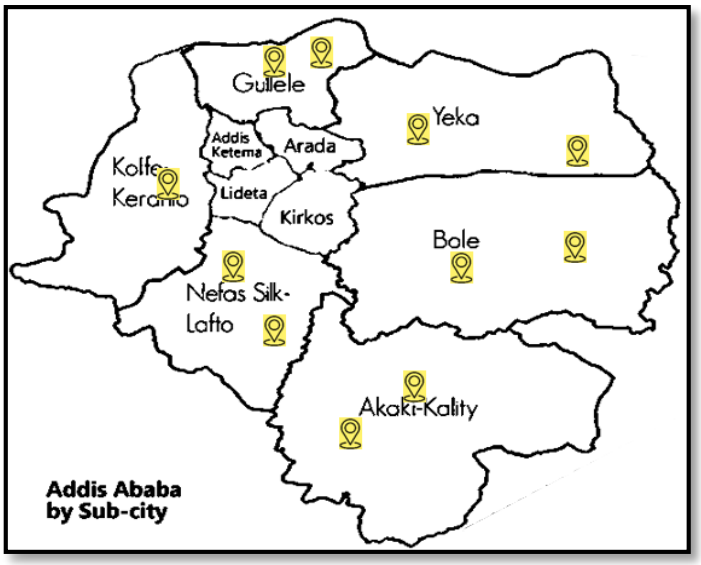

Figure 3-2: Primary Data Soil Samples Location

Table 3-1: Sample Location and Depth of Primary Data Soil Samples

No	Test pit	Sample location	Sampling depth
	TP1-1	Shiromeda	1.50
	TP1-2		3.00
	TP2-1	Ferensay	2.00
	TP2-2		3.50
	TP3-1	Shola-megenagna	1.50
	TP3-2		3.00
	TP4-1	Kechene	1.50
	TP4-2		3.50
	TP5-1	Bole Michael	2.00
	TP5-2		3.50
	TP6-1	Wollosefer	1.50
	TP6-2		3.00
	TP7-1	Kadisco	2.00
	TP7-2		3.50
	TP8	Lafto	3.00
	TP9-1	Kolfe	1.50
	TP9-2		3.00
	TP10	KalityGebre'el	1.50
	TP11-1	Gelan	1.50
	TP11-2	Condominium	3.00

3.4.1.2 Soil Sampling and Preparation

For the study, a total of twenty representative disturbed and undisturbed soil samples were taken from eleven test pits of eleven selected sites. The samples were obtained at depths ranging from 1.5 to 3.5 m below the ground surface. All samples were collected from pits excavated for construction. The samples were selected by the standard sampling methods and techniques. The preserving and transporting of the samples were done according to ASTM D-4220-95 (standard Practice for Preserving and Transporting of Soil samples).

For determination of natural moisture content, shear strength parameters, and density tests, undisturbed samples were used. In contrast, disturbed samples were used to determine liquid limit, plastic limit, plasticity index, and grain size analysis.

3.4.1.3 Laboratory Soil Test Standards

ASTM manual of standard test methods were used for the laboratory soil tests of this study as presented in Table 3-2.

Table 3-2: ASTM Manual of Standard Test Methods

Test Type	ASTM standard manual	Sample type
Atterberg limits	D 4318-00	Disturbed
Grain size analysis	D 1140-14	Disturbed
Moisture content	D 4643-00	Undisturbed
Bulk density	D 7263-21	Undisturbed
Direct shear test	D 3080-04	Undisturbed
Field identification of soils	D 2488-00	Disturbed and Undisturbed
Sample preserving and transporting	D 4220-95	Disturbed and Undisturbed

3.4.2 Secondary Data Collection

For this research, three hundred three (303) soil test results were gathered from different soil investigation consulting firms found in Addis Ababa. The data comprises soil test results of different areas in Addis Ababa. Therefore, the database was prepared to obtain a wide variety of soil types that represent Addis Ababa's soil. Then, the data analysis and treatment step took place by removing unreliable and unrealistic test result data and analyzing the remaining data in order to verify the input and output range so that the models' interval of confidence could be understood. Nineteen (19) Unreliable data was removed by analyzing test results and verifying if the soil classification and strength parameters were consistent with each other. Also twenty (20) coarse grained soil result data were removed due to small sample size. Finally, two hundred sixty four (264) soil sample data were selected as secondary data for the study.

3.5 ANN Modeling Procedure

In this Study, the Multilayer Perceptron Network (MLP) technique has been utilized to obtain a precise model relating Shear strength parameters (c and φ) to Index properties of soils. (MLPs) are classes of ANNs using feed forward architecture. MLPs are usually applied to perform supervised learning tasks, which involve iterative training methods to adjust the connection weights within the network. They are usually trained with Back Propagation (BP) algorithm. The number of nodes at the input layer is equal to the input parameters and the number of nodes at the output layer is equal to the output parameter.

3.5.1 Data Preprocessing

Some of the input variables were fundamentally interdependent. The first step in the analysis of interdependency of the data was to make a careful study of what it is that these variables are measuring, and eliminate any highly correlated pairs. High positive or negative correlation coefficients between the pairs may lead to poor performance of the models and difficulty in interpreting the effects of the explanatory variables on the response. This interdependency can cause problems in analysis as it will tend to exaggerate the strength of relationships between variables.

The data sets were randomly divided into training, validation and testing subsets. Training data were used for learning. The testing data were used to measure the performance of the models on data that played no role in building the models. In order to obtain a consistent data division, several combinations of the training, validation and testing sets were considered. Finally, for the neural network validation evaluation test 20 primary soils data were used.

3.5.2 Model Development

Separate ANN models were proposed to predict c and ϕ. The input layer consists of 6 neurons while the output layer has one neuron for each. The feed forward back propagation training network models have been coded into a MATLAB program using a neural network toolbox. The MATLAB software enables training with different convergence criteria, tolerance level, activation functions and number of epochs. The performance of an ANN model mainly depends on the network architecture and parameter settings. Choosing the number of the hidden layers, hidden nodes, learning rate, epochs, and activation function type plays an important role in the model construction. Hence, several MLP network models with different settings for the mentioned characters were trained to reach the optimal configurations with the desired precision.

Several works have shown that a single hidden layer is sufficient for an ANN to approximate any complex nonlinear function. In addition, using too many neurons will increase the training time and may cause the over fitting problem (memorizing the training pattern rather than generalizing the prediction). On the other hand, using fewer hidden neurons often increases the likelihood of learning algorithms becoming trapped in a local. Based on this one and two hidden layers with different numbers of neurons were used for

the model development. For obtaining an optimized structure of neural network no. of neurons in the hidden layer(s) are changed in steps. The numbers of hidden layer neurons were found using a simple trial-and-error method adjudged by the mean squared errors (MSE).

For nonlinear problems, sigmoid functions (Hyperbolic tangent sigmoid or log-sigmoid) are usually adopted as the activation function. Hyperbolic tangent sigmoid (tansig) was adopted as the activation function between the input and hidden layer. The transfer function between the hidden layer and output layer was a linear transfer function (purelin).

Levenberg–Marquardt (trainlm) training algorithm was implemented for the training of the network. This algorithm typically requires more memory but less time. Training automatically stops when generalization stops improving, as indicated by an increase in the mean square error of the validation samples. Training multiple times will generate different results due to different initial conditions and samples.

3.5.3 Performance Measures

Correlation coefficient (R), mean squared error (MSE), Root mean squared error (RMSE) and error histograms were used to evaluate the performance of the proposed models. Mean squared error (MSE) is the average squared difference between outputs and targets. Lower values are better and zero means no error. Regression (R) values measure the correlation between outputs and targets. An R value of 1 means a close relationship of the actual and the predicted data, 0 values means a random relationship.

R, MSE and RMSE are given in the form of equations as follows:

$$R = \frac{\sum_{i=1}^{n}(h_i-\overline{h_i})(t_i-\overline{t_i})}{\sqrt{\sum_{i=1}^{n}(h_i-\overline{h_i})^2 \sum_{i=1}^{n}(t_i-\overline{t_i})^2}} \quad 3.1$$

$$MSE = \frac{\sum_{i=1}^{n}(h_i-t_i)^2}{n} \quad 3.2$$

$$RMSE = \sqrt{\frac{\sum_{i=1}^{n}(h_i-t_i)^2}{n}} \quad 3.3$$

Where, h_i and t_i are the actual and predicted output values for the i^{th} output respectively, $\overline{h_i}$ is the average of the actual outputs, and n is the number of samples.

The R value alone is not a good indicator of prediction accuracy of a model, because R value will not change by equally shifting the values predicted by a model. MSE is one of the most popular measures of error. It has the advantage that large errors receive much greater attention than small errors. Higher R values and lower MSE and RMSE values indicate a more precise model.

CHAPTER 4 RESULT DISCUSSION

4.1 Laboratory Test Results

Typical test result of the Grain size analysis, Atterberg limits and direct shear tests of soil sample TP6-1 is shown in Figures 4.1 to 4.3 and Table 4.2 to 4.5. The details of the 20 primary soil sample test results, and graphs, have been summarized and reported in Appendix A of this paper.

4.1.1 Grain Size Analysis

For grain size analysis, the disturbed soil samples were wet sieved through 75 μm (No. 200) Sieve to determine the amount of material finer than the sieve in the soils. Particles with a size greater than 75 μm were then oven dried and Sieved through a set of sieves ranging from number 3″ to 200 (75 mm to 75 μm) sieves. Percent finer for different sizes of the particles retained on different sieves were calculated. The percentage finer (summation passing) was plotted as ordinate (on arithmetic scale) and the particle size (aperture size) as abscissa (on log scale). Finally the soils were classified according to the Unified Soil Classification System (USCS) as shown in Table 4-1.

Table 4-1: USCS Soil Classification

Class	Grain size
Gravel	4.75 mm to 75 mm
Sand	0.075 mm to 4.75 mm
Fines	<0.075 mm

Table 4-2: Typical Grain Size Analysis of TP6-1

Total dry mass = 1502 g				
Sieve size		Mass of soil retained (g)	Percent of soil retained (%)	Percent Passing (%)
No.	(mm)			
3"	75	0	0	100.00
21/2"	63	0	0	100.00
2"	50	0	0	100.00
11/2"	37.5	0	0	100.00
1"	25	0	0	100.00
3/4"	19	0	0	100.00
1/2"	12.5	0	0	100.00

3/8"	9.5	23	1.53	98.47
No.4	4.75	44	2.93	95.54
No.10	2	52	3.46	92.08
No.16	1.18	29.74	1.98	90.10
No.30	0.6	33.80	2.25	87.85
No.40	0.425	17.60	1.17	86.68
No.50	0.3	67.44	4.49	83.36
No.100	0.15	76.00	5.06	78.30
No.200	0.075	44.61	2.97	75.33
Sum		370.58	24.67	
Pan		1131.42	75.33	
Total		1502	100	
		Gravel = 8%	Sand = 17%	Fine = 75%

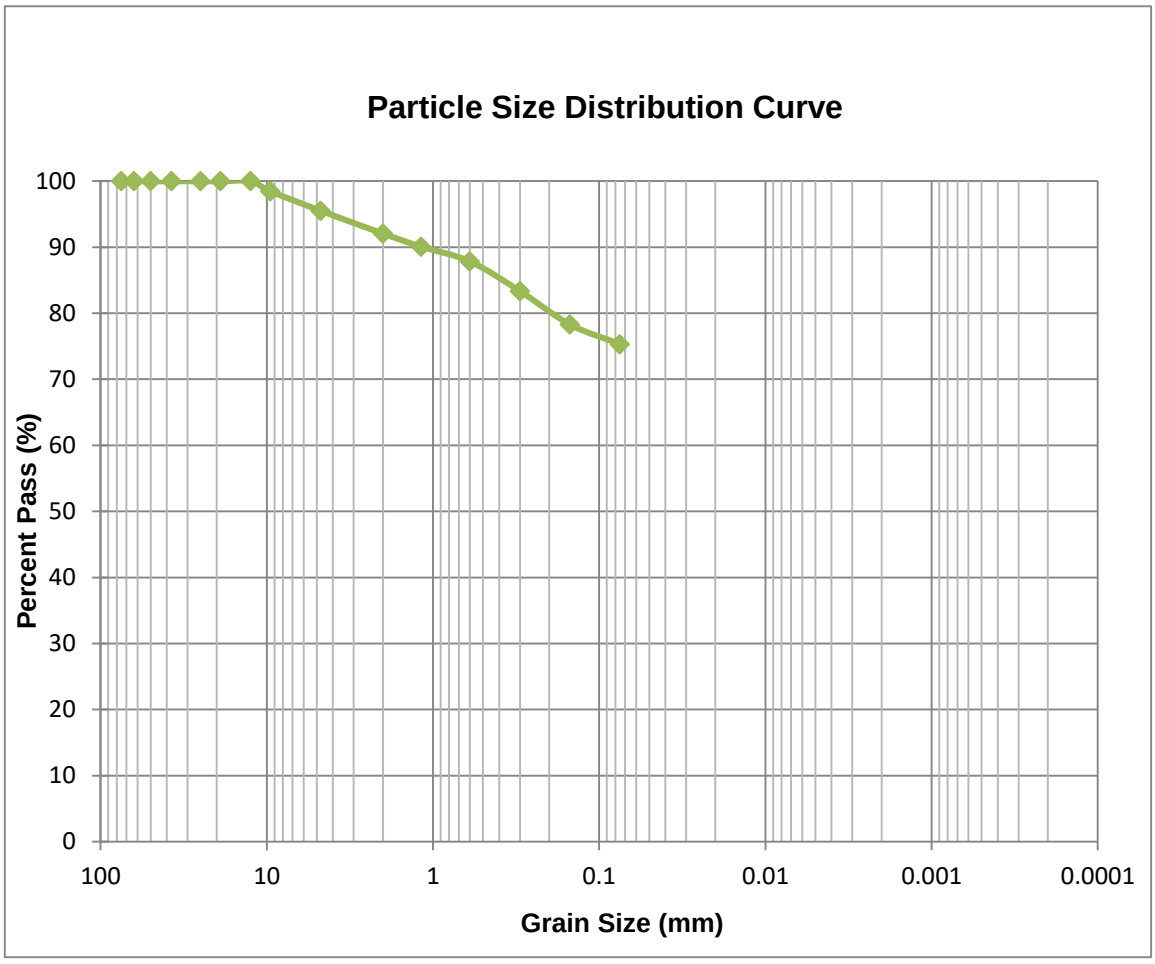

Figure 4-1: Typical Particle Size Distribution Curve of TP6-1

4.1.1.1 Bulk Density

Bulk density is the ratio of the mass of the soil to the total volume of soil including water. The density was determined using the direct measure method according to the ASTM

standard. Soil samples were taken using sampling tubes. The core samples were immediately weighed, and also the height and the diameters were measured to calculate the volume.

Table 4-3: Typical Density and Moisture Content Analysis of TP6-1

		Sample Data
Sample condition		Undisturbed
Sampling depth	m	2.50
Initial Volume	cm^3	72.00
Initial mass	g	134.40
Final dry mass	g	115.49
Bulk density	gm/cm^3	1.867
Dry density	gm/cm^3	1.604
Moisture Content	%	16.38

4.1.2 Natural Moisture Content

The moisture content is the ratio of the mass of water to the dry mass of soil, it is expressed in percentage, as shown in the above table. It was determined by the oven drying method. Samples were weighed, and then they were dried at 105 ^oC up to 24 hours by an electric oven.

4.1.3 Atterberg Limits

This test was used to determine the plastic limit, liquid limit, and the plasticity index of the soil. The test was done according to ASTM D 4318 standard test method. Soil that passes through a sieve diameter of 0.425mm was used to perform the tests. Greater the difference between liquid and plastic limits, greater is the plasticity of the soil. A cohesionless soil has zero plasticity index. Hence it is called non-plastic (Murthy, 2002).

Table 4-4: Typical Atterberg Limits Analysis for TP6-1

				Atterberg Limits	
	Liquid Limit			Plastic Limit	
No. of blows	34	26	18		
Mass of cont. + wet soil (g)	49.07	49.49	49.68	16.20	15.94
Mass of cont. + dry soil (g)	39.85	39.99	39.88	15.63	15.29
Mass of water (g)	9.21	9.50	9.80	0.57	0.65
Mass of container (g)	21.66	21.84	21.97	14.11	13.52
Mass of dry soil (g)	18.20	18.15	17.92	1.52	1.77
Water Content (%)	50.64	52.36	54.71	37.50	36.72
	LL=53%			PL =	37%

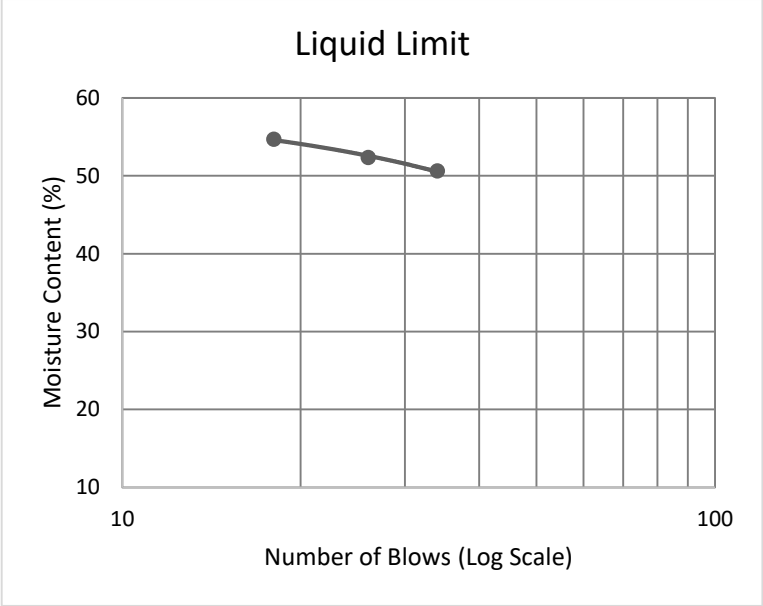

Figure 4-2: Typical Liquid Limit Chart of TP6-1

4.1.4 Direct Shear Test

The direct shear test is a very popular test for determining shear strength of soils. This test was conducted to determine the shear strength parameters of soil. The test was performed in accordance with ASTM. The Undisturbed sample is placed in to a metal square shear box of 60 mm x 60 mm x 20 mm undergoes a horizontal force. The soil fails by shearing along a plane when the force is applied. The applied shear force and horizontal displacements were recorded for further analyses. Three levels of normal load were used. Normal stress was calculated by dividing the normal load by the cross-section area of the soil sample. Shearing stress was obtained from the dial of proving ring readings.

Table 4-5: Typical Direct Shear Test Sample Data of TP6-1

	Sample Data
Depth, m	2.50
Initial Height, mm	20.00
Initial area, cm^2	36.00
Sample condition	Undisturbed
Sample size, mm	60x60x20
c, kN/m^2	21
ϕ, Degrees	19

(a) **(b)**

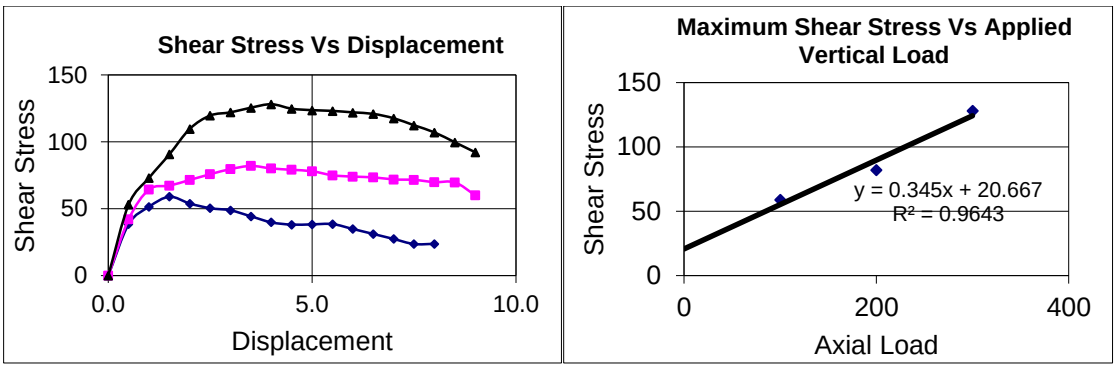

Figure 4-3: Typical Direct Shear Test Output Value Charts of TP6-1 (A) Shear Stress vs Displacement (B) Maximum Shear Stress vs Applied Vertical Load

4.1.5 Summary of Primary Data Soil Test Results

The primary data soil test results are summarized, as required for further analysis, below in Table 4-6.

Table 4-6: Summary of the Primary Data Soil Test Results

No	Test pits	Grain size		Atterberg limits		ω	BD	Shear strength parameters	
		% Sand	% Fine	LL	PI			C	Φ
	TP1-1	13.0	72.0	52.4	13.6	19.0	1.834	18.0	20.0
	TP1-2	15.0	75.0	43.6	7.3	18.0	1.879	20.0	20.0
	TP2-1	11.0	70.0	50.4	14.2	16.6	1.824	15.0	19.0
	TP2-2	14.0	68.0	48.7	10.3	18.4	1.858	19.0	21.0
	TP3-1	14.0	73.0	51.0	13.1	23.6	1.821	18.0	20.0
	TP3-2	11.0	89.0	52.7	16.2	19.4	1.824	21.0	18.0
	TP4-1	16.0	79.0	55.6	18.0	21.7	1.882	22.0	20.0
	TP4-2	14.0	66.0	51.5	14.0	18.2	1.892	18.0	21.0
	TP5-1	17.0	75.0	53.7	16.5	16.4	1.867	21.0	19.0
	TP5-2	15.0	85.0	48.7	12.5	18.4	1.864	26.0	18.0
	TP6-1	11.0	89.0	54.2	15.6	18.6	1.854	23.0	19.0
	TP6-2	12.0	88.0	56.2	17.8	12.6	1.872	10.0	28.0
	TP7-1	9.0	66.0	42.9	11.6	18.4	1.861	10.0	22.0
	TP7-2	11.0	69.0	40.3	4.5	16.4	1.872	12.0	22.0
	TP8	23.0	77.0	57.9	19.5	16.5	1.902	7.0	24.0
	TP9-1	18.0	64.0	52.7	15.1	15.6	1.855	17.0	19.0
	TP9-2	14.0	44.0	51.7	13.7	21.0	1.862	21.0	19.0
	TP10	10.0	36.0	56.2	17.8	9.5	1.872	6.0	30.0
	TP11-1	20.0	56.0	42.4	7.2	16.2	1.802	14.0	22.0
	TP11-2	12.0	88.0	59.0	19.6	22.4	1.872	21.0	19.0

4.2 Database Analysis

It is important to have a vast database for the proper working of an Artificial Neural Network, since a higher number of training subjects results in a better generalization and helps to prevent overtraining (Haykin S. , 2009).

4.2.1 Secondary Data Analysis

Statistical descriptions of examined soils parameters are given below in Table 4-7. It can be seen from the table that the distributions of the median and average values of the soil properties are close together. This shows that soil experimental data are approximately normally distributed. This is further collaborated by the value of the skewness (-2.55 to 4.96). Also the standard deviation tells, on average, how far each value lies from the mean; this low standard deviation indicates that values are clustered close to the mean.

Table 4-7: Descriptive Statistics of the Secondary Data Soil Test Results

Parameters	Sand %	Fine %	LL	PI	ω	BD	C	Φ
Average	15.43	77.99	53.80	17.69	21.65	1.84	20.87	19.09
Median	15.00	80.00	53.55	16.46	19.39	1.85	20.00	19.00
Standard Deviation	5.89	11.21	6.90	6.66	9.07	0.06	11.64	3.74
Minimum	1.12	51.00	36.40	3.17	12.36	1.43	6.00	6.30
Maximum	34.00	98.88	84.00	49.00	63.90	2.15	124.70	41.10
Skewness	0.34	-0.59	0.61	1.17	2.68	-2.55	4.96	-0.19
N	264	264	264	264	264	264	264	264

The cohesion values had a mean of 20.87 kPa and standard deviation of 11.64 kPa. Also the values are in the range of 6 kPa to 124.7 kPa. Meanwhile, friction angle statistics presented in the table show a mean value of 19.09° and distribution of gathered values in a range of 6.3° to 41.10°. That might represent a limitation on the prediction of values outside this range.

Scatter plot of the variables distribution throughout the sample depth, illustrated in Figure 4-4 showed that great amplitude of Sand percent value between 10% and 20%. Besides Fine percent values are concentrated between 80% and 90%. Intensity of Liquid Limit values are showed between 50% and 55%, also Plasticity Index values are concentrated between 12% and 18%. Natural Moisture Content values have great amplitude between 15% and 20%. Bulk Density values have showed intensity between 1.8 g/cm^3 and 1.9 g/cm^3.

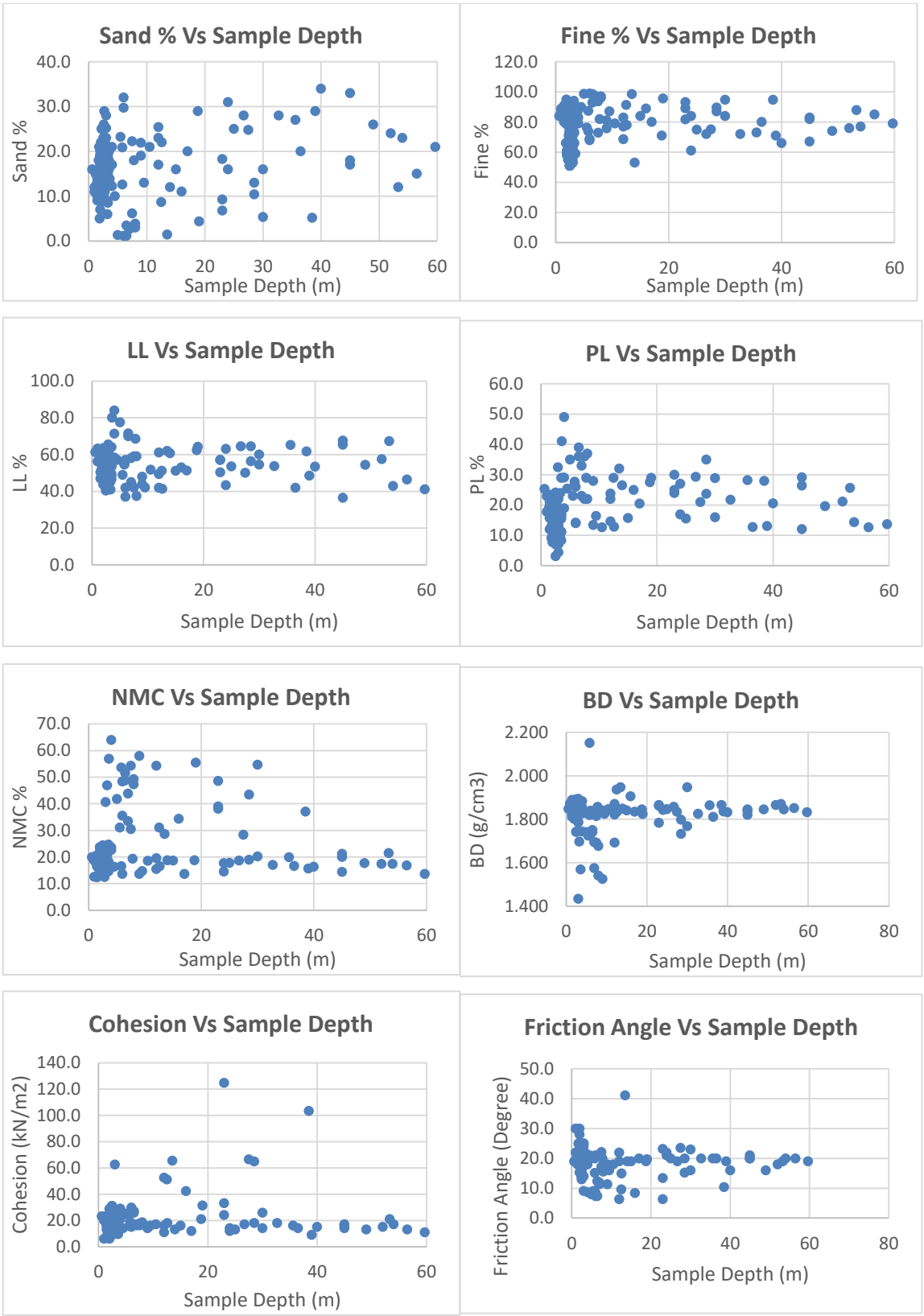

Figure 4-4: Scatter Plots of the Variables Vs Sample Depth

Cohesion values showed concentration between 19 kPa and 25 kPa, meanwhile Internal Friction Angle values are concentrated between 18° and 22°.

A correlation matrix was carried out on the soil parameters using Pearson's correlation. The correlation matrix is given in Table 4-8. The matrix indicated a high correlation between liquid limit and plasticity index. Except that there is no high positive or negative correlation between the variables; since high correlation coefficient between the pairs may lead to poor performance of the models and difficulty in interpreting the effects of the explanatory variables on the response. In the selection process of input parameters, it was tried to avoid multicollinearity. Also the correlation of cohesion and angle of internal with the other soil parameters did not give a high relationship, hence using regression analysis is likely to produce inappropriate models, but not for ANNs.

Table 4-8: Pearson's Correlation Matrix of the Variables

Soil Parameters	Sand %	Fine %	LL	PI	w	B.D	c	Φ
Sand %	1.000							
Fine %	-0.362	1.000						
LL	-0.103	0.352	1.000					
PI	-0.130	0.458	0.783	1.000				
ω	-0.272	0.320	0.280	0.596	1.000			
B.D	0.033	-0.173	-0.068	-0.337	-0.470	1.000		
C	-0.151	0.289	0.189	0.299	0.382	-0.077	1.000	
Φ	0.066	-0.307	-0.143	-0.340	-0.454	0.425	-0.378	1.000

Figures 4-5 and 4-6, show the scatter diagram plots for between cohesion and the other soil parameters, also angle of friction and the other soil parameters, respectively. As can be seen from the Figures 4-5 and 4-6, there are extremely nonlinear relationships among the selected parameters, and several uphill and downhill points which exist on the graphs. In all the graphs, the points are not very useful at explaining the relationship with reference to the dependent variables although a direct correlation between the variables cannot be assured for the data spreads as the independent variables rises. Hence, from those graphs it may be stated that each input variable alone is not enough to predict c and ϕ; also the input parameters have completely unrecognized correlation with the output parameters (c and ϕ).

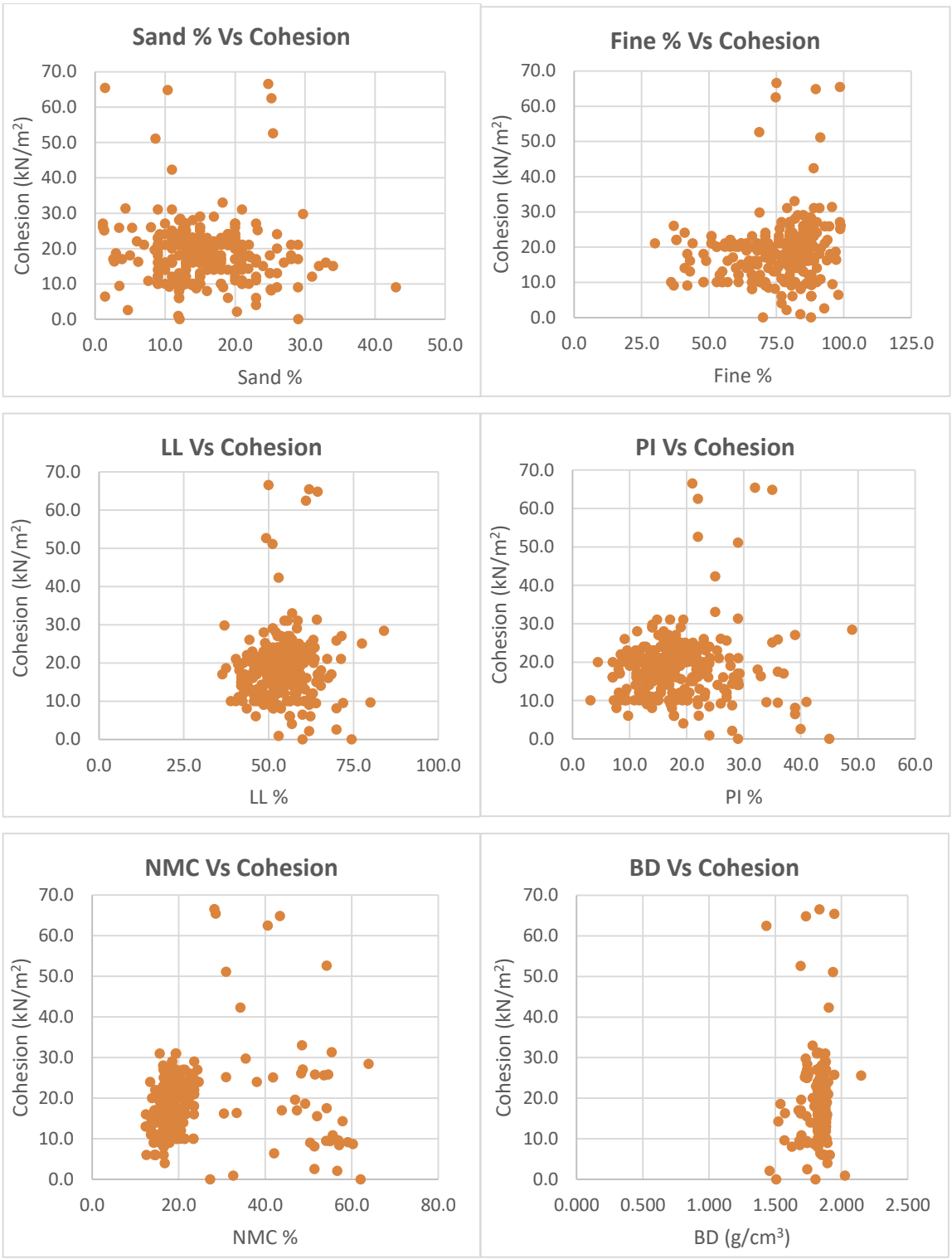

Figure 4-5: Scatter Plots of Cohesion vs Index Properties of Soils

Figure 4-6: Scatter Plots of Internal Friction Angle vs Index Properties of Soils

4.2.2 Primary Data Analysis

The statistical analysis of the laboratory test results of the primary data is summarized below in Table 4-9. The cohesion values are ranged from 6 kPa to 26 kPa. Also as shown in the table the value of the friction angle ranges from 18° to 30°.

Table 4-9: Descriptive Statistics of the Primary Data Set

Parameters	Sand %	Fine %	LL	PI	ω	B.D	C	Φ
Average	14.00	71.45	51.08	13.89	17.84	1.86	16.95	20.90
Median	14.00	72.50	52.04	14.10	18.30	1.86	18.50	20.00
Standard Deviation	3.51	14.23	5.30	4.13	3.21	0.02	5.48	2.83
Minimum	9.00	36.00	40.26	4.48	9.54	1.80	6.00	18.00
Maximum	23.00	89.00	58.96	19.55	23.56	1.90	26.00	30.00
Skewness	0.99	-0.95	-0.66	-0.75	-0.66	-0.68	-0.64	1.99
N	20	20	20	20	20	20	20	20

4.3 Prediction Models

After input and output data gathered and structured; training and test sets were established. A total of 264 secondary data were used to develop the models in this study, 70% used for the training, 15% for validation and 15% for test. After the models developed the 20 primary data used for cross validation of the selected best model. The general characteristic of the developed models is presented in Table 4-10.

Table 4-10: Summary of the Developed Neural Network Models Characteristics

Parameters	Description
Input parameters	Sand %, Fine %, LL, PI, ω, BD
Output parameters	C, Φ
Number of hidden layer	1
Number of hidden neurons	Trial and Error (from 6 up to 20)
Learning method	Supervised Learning
Network type	Feed Forward Back Propagation
Architecture	Multilayer Perceptron (MLP)
Data division	Random (dividerand)
Hidden layer activation function	Hyperbolic Tangent Sigmoid Function (tansig)
Output layer activation function	Linear Function (purelin)
Training Function	Levenberg-Marquardt (trainlm)
Performance function	MSE

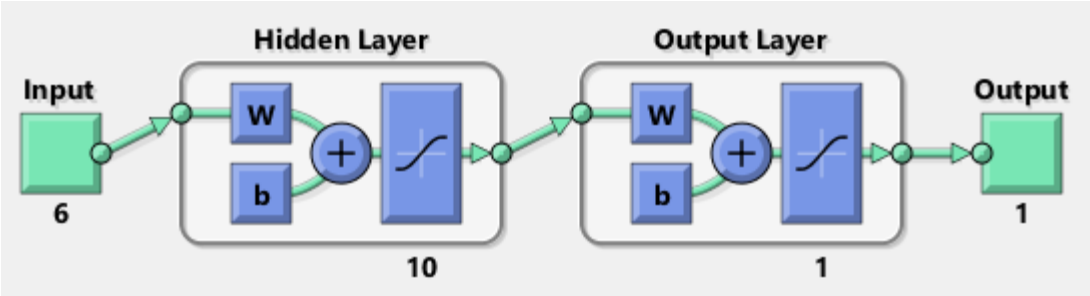

Figure 4-7: Neural Network Architecture Sample of the Models

4.3.1 Prediction to Cohesion

For prediction of Cohesion values 20 models were developed. In the present case different architectures were developed for single hidden layer neurons. First the neuron was fixed as 6 in three layer architecture (input layer-hidden layer-output layer), then neurons were increased consecutively so as to study each architecture with increase in the neurons in hidden layer. Table 4-11summarizes the different neural architectures and their accuracies in terms of correlation coefficient (R), mean squared error (MSE)and root mean squared error (RMSE)values.

Table 4-11: Prediction Models Developed for c

		Correlation Coefficient, R					
Model No.	Network	Training	Validation	Test	All	MSE	RMSE
1	6-6-1	0.76278	0.92013	0.81905	0.81029	46.03	6.88
2	6-7-1	0.84224	0.86968	0.86819	0.84484	40.51	6.46
3	6-8-1	0.9139	0.69946	0.71311	0.84343	42.57	6.62
4	6-9-1	0.82703	0.72909	0.87574	0.80098	52.72	7.35
5	6-9-1	0.87756	0.89237	0.93388	0.89066	31.38	5.69
6	6-10-1	0.91356	0.85595	0.32541	0.84396	43.13	6.66
7	6-10-1	0.88818	0.93314	0.9835	0.92429	23.46	4.93
8	6-10-1	0.79222	0.87294	0.96689	0.84039	20.43	4.52
9	6-10-1	0.86009	0.90596	0.96279	0.88929	17.55	4.19
10	6-11-1	**0.87939**	**0.87982**	**0.98141**	**0.91507**	**14.59**	**3.82**
11	6-11-1	0.86009	0.9844	0.92354	0.91507	14.59	3.82
12	6-12-1	0.91729	0.86335	0.74643	0.86307	40.09	6.42
13	6-13-1	0.9301	0.82018	0.70565	0.84275	43.57	6.69
14	6-14-1	0.95069	0.94397	0.13295	0.92205	23.59	4.95
15	6-15-1	0.91311	0.8944	0.73465	0.8888	31.9	5.74
16	6-16-1	0.95504	0.7973	0.5882	0.86985	41.21	6.51
17	6-17-1	0.85026	0.87906	0.92821	0.8787	38.14	6.27
18	6-18-1	0.94481	0.85441	0.20154	0.8487	41.32	6.52
19	6-19-1	0.86357	0.99188	0.9027	0.90209	30.19	5.59
20	6-20-1	0.81437	0.79679	0.58814	0.77587	71.53	8.55

The training, validation and testing accuracies in terms of R values observed across different models are as follows: 0.76 to 0.95 for training, 0.69 to 0.99 for validation and 0.13 to 0.98 for testing. R value close to 1 and MSE value near zero indicates a predicting capability. So a stable architecture can be reported among these architectures. Accordingly, a robust model selected among 20 architectures developed is model 10 of network 6-11-1.

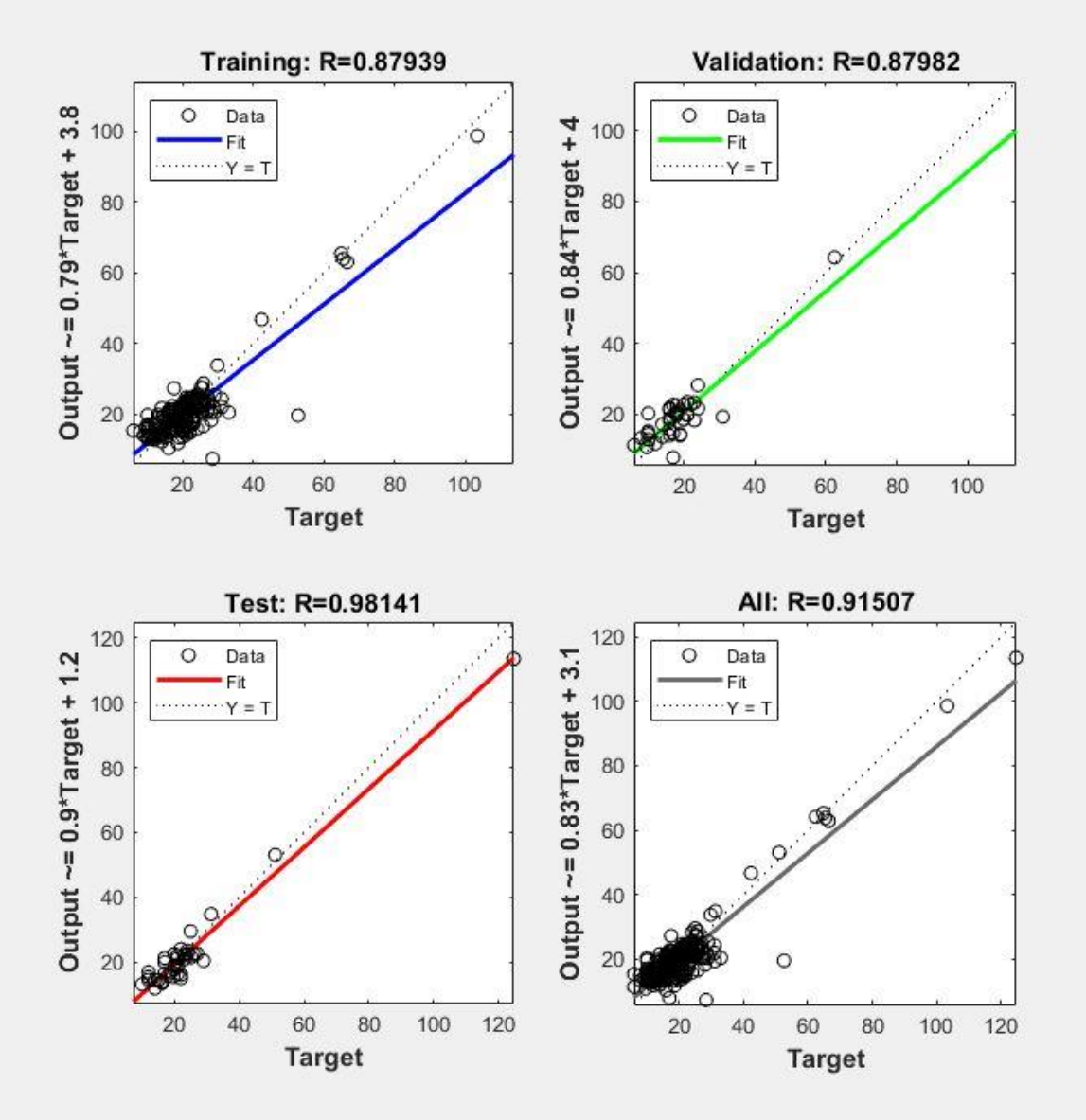

Figure 4-8: Regression Plot of Model 10

The regression plot describes the relationship between the response (output) variable, and the predictor (input) variables; also relationship between the actual (target) value and the predicted (output) value. As shown in Table 4-11 and Figure 4-8, Model 10 was determined to be the best structure to solve this problem. In order to examine the relationship between the values obtained as a result of the network and the actual values, the regression plot generated at the end of the process is looked at. In this study, R values were calculated as 0.88 for the training, 0.88 for the validation, 0.98 for the test, and 0.92 for all data as shown in Figure 4-8.

4.3.2 Prediction to Internal Friction Angle

For prediction of Internal friction angle values 28 models were developed. In the present case different architectures were developed for single hidden layer neurons. First the neuron was fixed as 6 in three layer architecture (input layer-hidden layer-output layer), then neurons were increased consecutively up to 18, so as to study each architecture with increase in the neurons in hidden layer. Table 4-12 summarizes the different neural architectures and their accuracies in terms of correlation coefficient (R), mean squared error (MSE) and root mean squared error (RMSE) values.

Table 4-12: Prediction Models Developed for ϕ

		Correlation Coefficient R					
Model No.	Network	Training	Validation	Test	All	MSE	RMSE
1	6-6-1	0.72384	0.73447	0.71907	0.72151	12.26	3.50
2	6-6-1	0.81273	0.73505	0.69762	0.78911	9.14	3.02
3	6-7-1	0.87221	0.76437	0.77835	0.83326	7.42	2.72
4	6-7-1	0.88685	0.77976	0.74575	0.85776	6.25	2.50
5	6-8-1	0.85774	0.72972	0.67169	0.7984	12.25	3.50
6	6-8-1	0.792	0.72212	0.66147	0.76651	13.28	3.64
7	6-9-1	0.84505	0.82431	0.60781	0.81061	9.54	3.09
8	6-9-1	0.78614	0.61346	0.76912	0.755	10.83	3.29
9	6-9-1	0.80816	0.72977	0.90103	0.8061	8.25	2.87
10	6-11-1	0.78394	0.86062	0.85616	0.8061	8.25	2.87
11	6-11-1	0.78094	0.82841	0.89695	0.8061	8.25	2.87
12	6-12-1	0.77087	0.91829	0.89659	0.81276	8.00	2.83
13	6-12-1	0.81972	0.81361	0.85907	0.82178	7.89	2.81
14	6-10-1	0.91224	0.76727	0.68936	0.86599	6.12	2.47
15	6-10-1	0.89131	0.71169	0.67388	0.85685	6.08	2.47
16	6-10-1	**0.81968**	**0.88693**	**0.92423**	**0.84097**	**6.01**	**2.45**
17	6-13-1	0.73071	0.88725	0.7779	0.74384	10.51	3.24
18	6-13-1	0.81545	0.74764	0.98086	0.85065	7.15	2.67
19	6-15-1	0.87146	0.86785	0.87764	0.87311	6.53	2.56
20	6-15-1	0.85973	0.87899	0.91985	0.87311	6.53	2.56
21	6-17-1	0.74719	0.83297	0.87307	0.78417	10.06	3.17
22	6-16-1	0.80124	0.77284	0.93383	0.8274	7.65	2.77
23	6-16-1	0.82829	0.80166	0.87067	0.8274	7.65	2.77
24	6-16-1	0.81362	0.82414	0.88041	0.8274	7.65	2.77
25	6-18-1	0.68194	0.71541	0.75861	0.7064	15.18	3.90

The training and testing accuracies in terms of R values observed across different models are as follows: 0.68 to 0.91 for training, 0.71 to 0.91 for validation and 0.60 to 0.98 for testing. R value close to 1 and MSE value near zero indicates a predicting capability. So

a stable architecture can be reported among these architectures. Accordingly, a robust model selected among 28 architectures developed is model 16 of network 6-10-1 (six input neurons, ten hidden neurons and one output neuron).

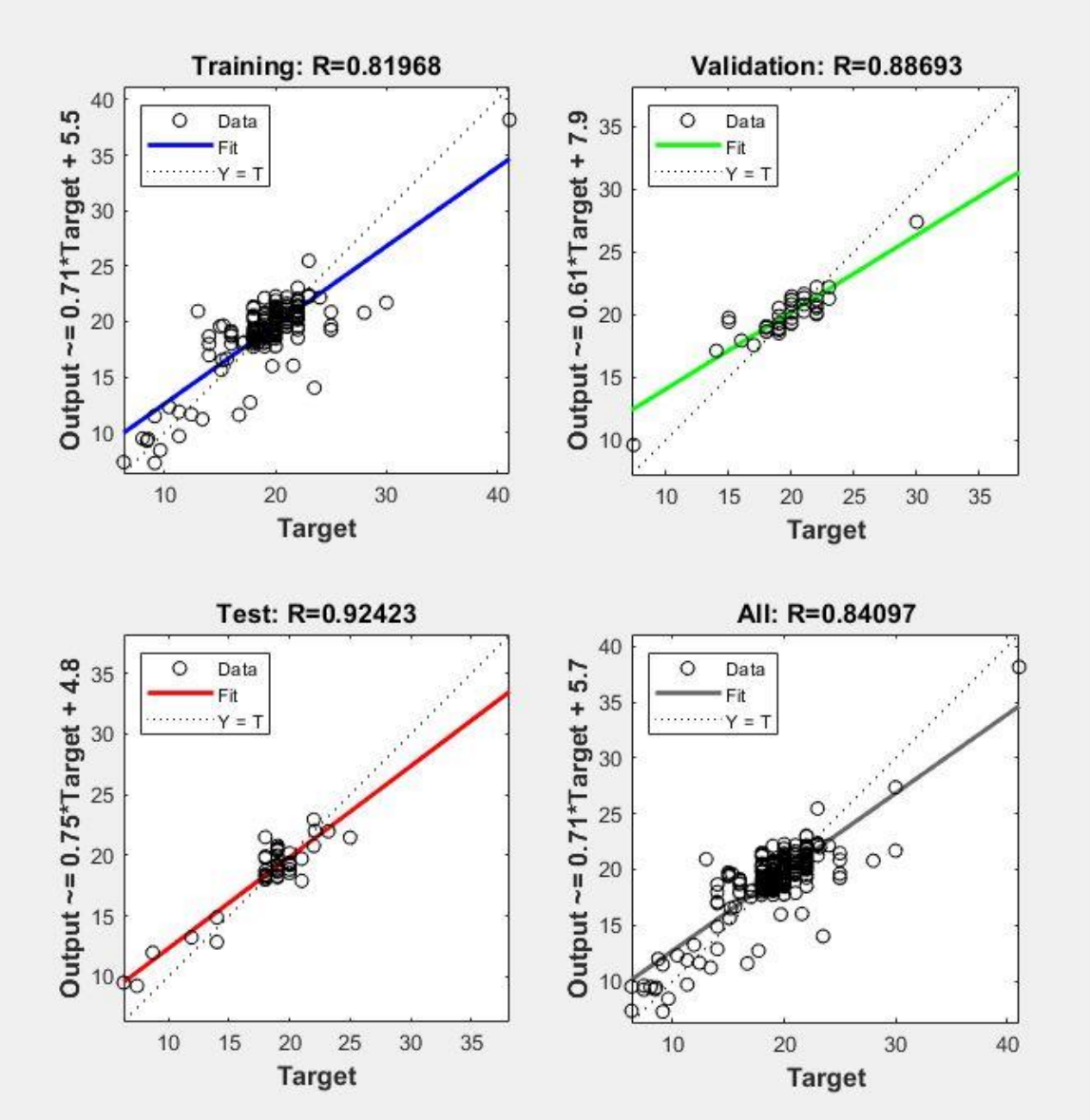

Figure 4-9: Regression plot of Model 16

As shown in Table 4.12 and Figure 4.9, Model 16 was determined the best structure to solve this problem. In order to examine the relationship between the values obtained as a result of the network and the actual values, the regression graph generated at the end of the process is looked at. In this study, adjusted R values were calculated as 0.81 for the training, 0.88 for the validation, 0.92 for the test, and 0.84 for all data as shown in Figure 4.9.

4.4 Model Performance Evaluation

4.4.1 Model Performance evaluation for c prediction

The model performance was evaluated by the coefficient of correlation (R) values of the test data and the combined data, Error histogram of the combined data and also MSE & RMSE values. The selected model, Model 10 (network 6-11-1) showed R value of 0.98 and 0.92 for testing and combined data sets respectively; also minimum values of MSE and RMSE, 14.59 and 3.82 respectively. The correlation coefficient R= 0.92 of the combined data indicates very good correlation between the actual and the predicted values of the entire data. R = 0.98 of the test data also indicates the performance of the model on new data sets. The comparison between the actual and predicted value of c using model 10, is plotted on Figure 4-10. The plot indicates good fitting and accuracy between experimental and predicted c values.

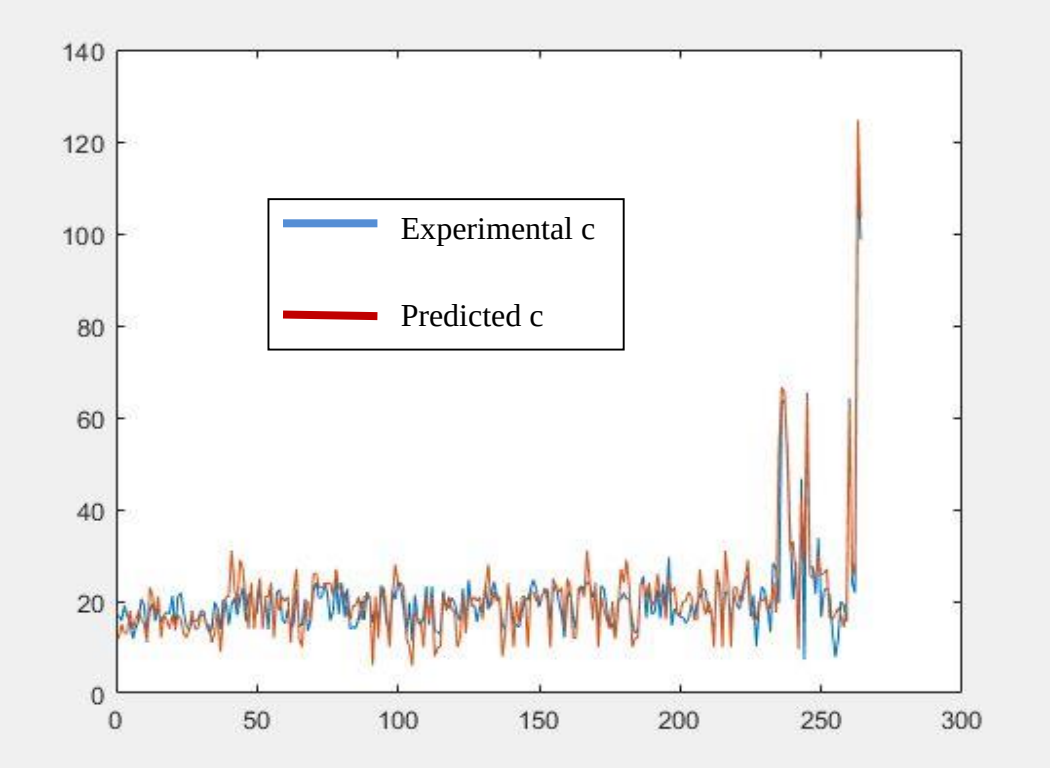

Figure 4-10: Comparison of Measured and Predicted c Value of Model 10

Error histogram indicates the errors between target values and predicted values of the model. As these error values indicates how predicted values are differing from the target values, hence these can be negative.

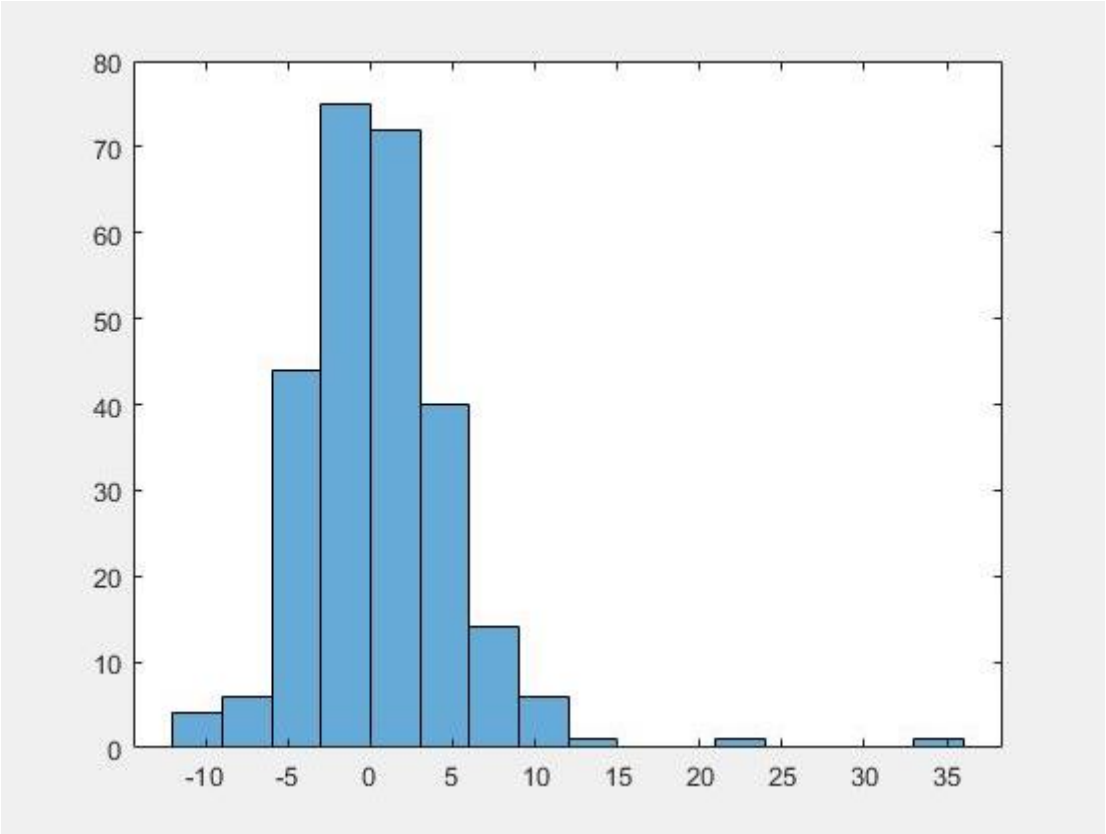

Figure 4-11: Error Histogram of Model 10 for Prediction of c

Error distribution of the entire data using model 10 is plotted on an error histogram graph of Figure 4-11. A significant concentration of error is seen at 0. The error histogram also shows that instances near zero error are higher than the rest indicating a minimum difference between actual and predicted values.

4.4.2 Model Performance Evaluation for ϕ Prediction

The model performance was evaluated by the coefficient of correlation (R) values of the test data and the combined data, Error histogram of the combined data and also MSE & RMSE values. The selected model, Model 16 (network 6-10-1) showed R value of 0.92 and 0.84 for testing and combined data sets respectively; also minimum values of MSE and RMSE, 6.01 and 2.45 respectively. The correlation coefficient R= 0.84 of the combined data indicates very good correlation between the actual and the predicted values of the entire data. R = 0.92 of the test data also indicates the performance of the model on

new data sets. The comparison between the actual and predicted value of c using model 16, is plotted on Figure 4-12 and it showed good fitting and accuracy between experimental and predicted c values.

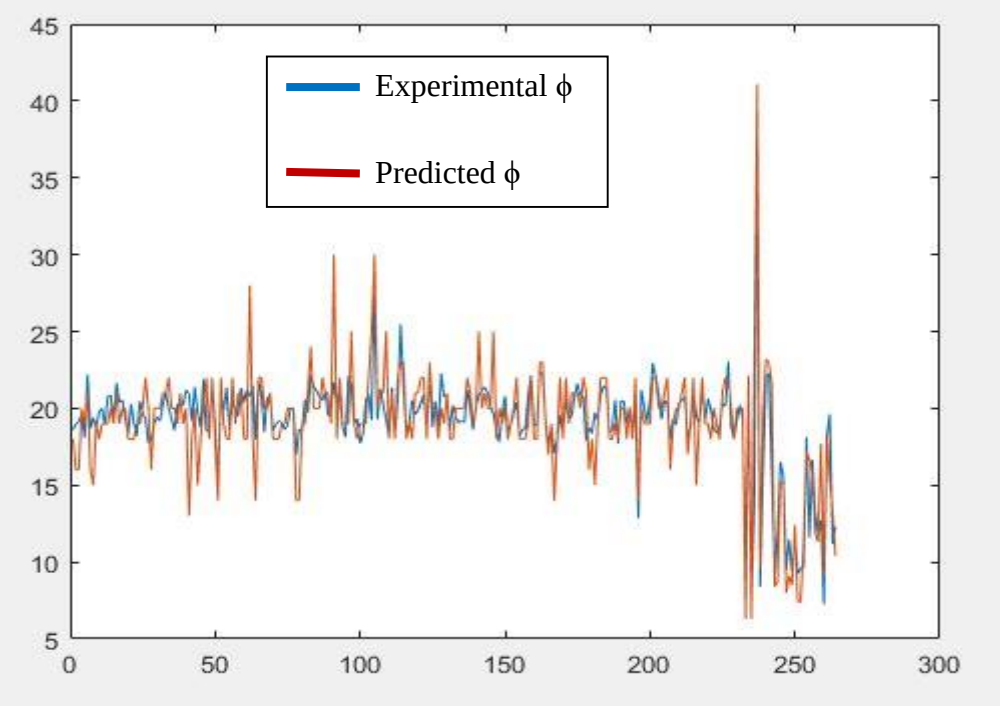

Figure 4-12: Comparison of measured and predicted ϕ value of model 16

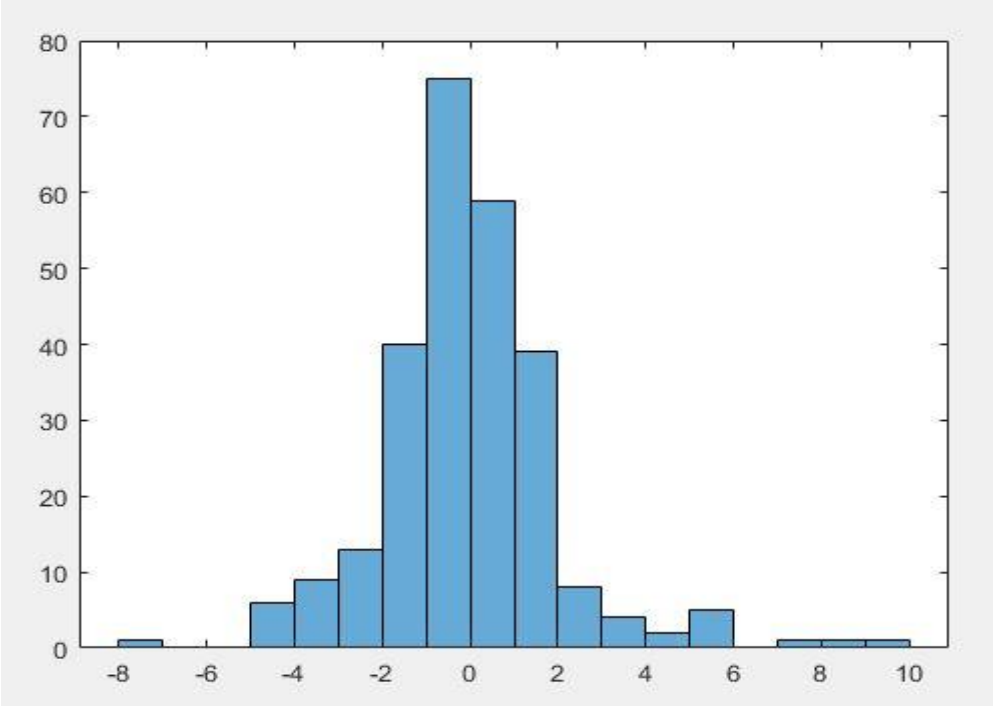

Figure 4-13: Error histogram of model 16 for ϕ prediction

Error distribution of the entire data using model 16 is plotted on an error histogram graph of Figure 4-13. A significant concentration of error is seen at 0, indicating a minimum difference between actual and predicted values.

4.5 Cross Validation of the Model

4.5.1 Model Validation for c Prediction

The model was validated on primary soil test result data. The result indicates a very good prediction of cohesion (c) of the model with average difference value of 1.3, R value of 0.97 and RMSE value of 1.68, between experimental c and Predicted c values. Table 4-13 shows experimental and predicted values and of c for primary data set.

Table 4-13: Experimental and Predicted Values of c for Primary Data Set

Experimental c (kPa)	Predicted c (kPa)	Difference (kPa)
18.0	18.6	0.6
20.0	17.6	-2.4
15.0	14.1	-0.9
19.0	17.7	-1.3
18.0	17.4	-0.6
21.0	21.2	0.2
22.0	21.8	-0.2
18.0	14.7	-3.3
21.0	17.6	-3.4
26.0	25.5	-0.5
23.0	22.4	-0.6
10.0	11.4	1.4
10.0	11.5	1.5
12.0	14.0	2.0
7.0	6.6	-0.4
17.0	14.9	-2.1
21.0	20.4	-0.6
6.0	6.2	0.2
14.0	13.6	-0.4
21.0	24.3	3.3
	Average Difference	= 1.3

The maximum difference showed between the experimental c and predicted c value was 3.4 kPa and the average difference was 1.3 kPa. The model showed very good prediction capacity on primary data set of the research.

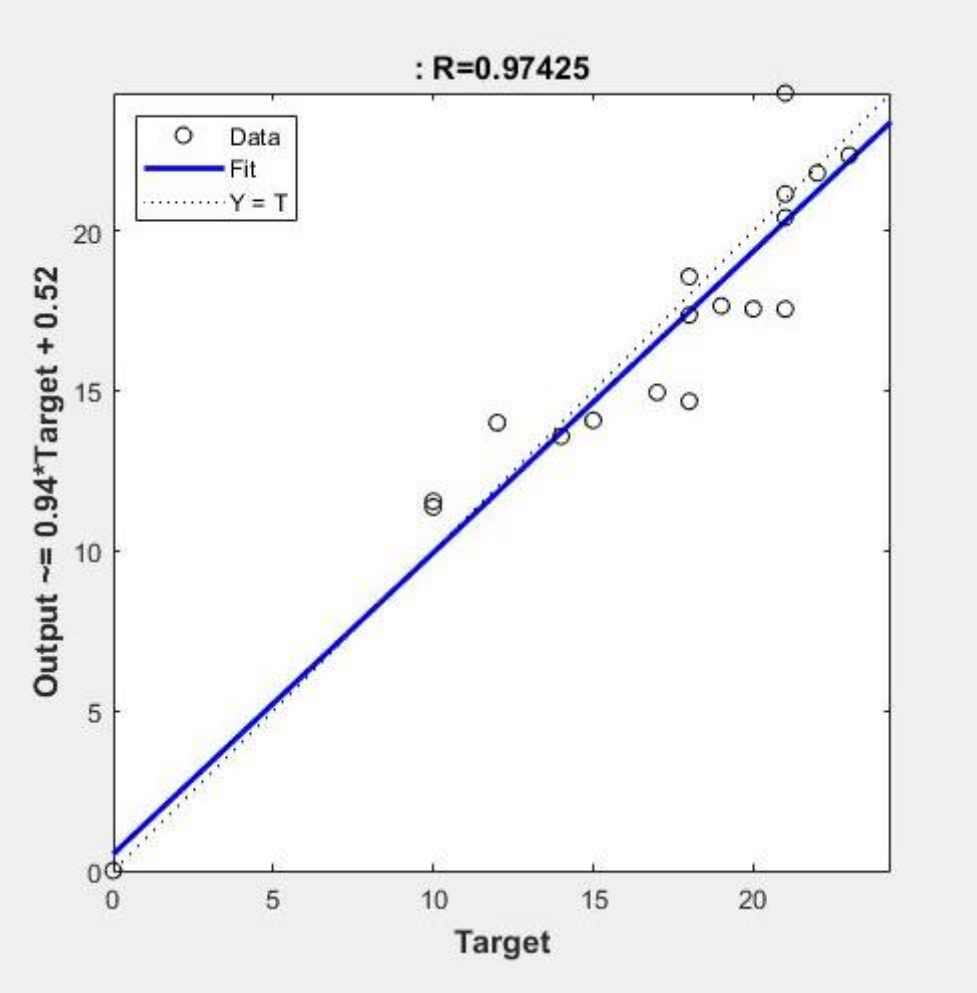

Figure 4-14: Regression Plot of Prediction of c Value for Primary Data Set

As can be seen from the regression graph in Figure 4-14, the data points are scattered near the line Y=T. the correlation coefficient R= 0.97425 indicates very good correlation between the actual and the predicted values of the primary data set.

4.5.2 Model Validation for ϕ Prediction

The model validation on primary soil test result data indicates an average difference value of 1.0, R value of 0.97 and RMSE value of 1.31, between experimental c and Predicted c values. The result shows a very good prediction of friction angle (ϕ) of the model. Table 4-14 shows the experimental and predicted values of ϕ for primary data set.

Table 4-14: Experimental and Predicted Values of Φ for Primary Data Set

Experimental ϕ (°)	Predicted ϕ (°)	Difference(°)
20	20.7	-0.7
20	20.6	-0.6
19	21.0	-2.0
21	20.8	0.2
20	20.4	-0.4
18	18.1	-0.1
20	19.2	0.8
21	21.2	-0.2
19	20.9	-1.9
18	19.5	-1.5
19	19.2	-0.2
31	27.4	0.6
22	20.4	1.6
22	20.7	1.3
24	21.4	2.6
19	22.0	-3.0
19	18.7	0.3
30	29.5	0.5
22	20.6	1.4
19	18.6	0.4
	Average Difference	= 1.0

The maximum difference showed between the experimental ϕ and predicted ϕ value was 3.0° and the average difference was 1.0°. Generally the model showed very good prediction capacity on primary data set of the research. Also the regression graph in Figure 4-15 shows that, the data points are scattered near the line Y=T. the correlation coefficient R= 0.96517 indicates very good correlation between the actual and the predicted values of the primary data set of ϕ values.

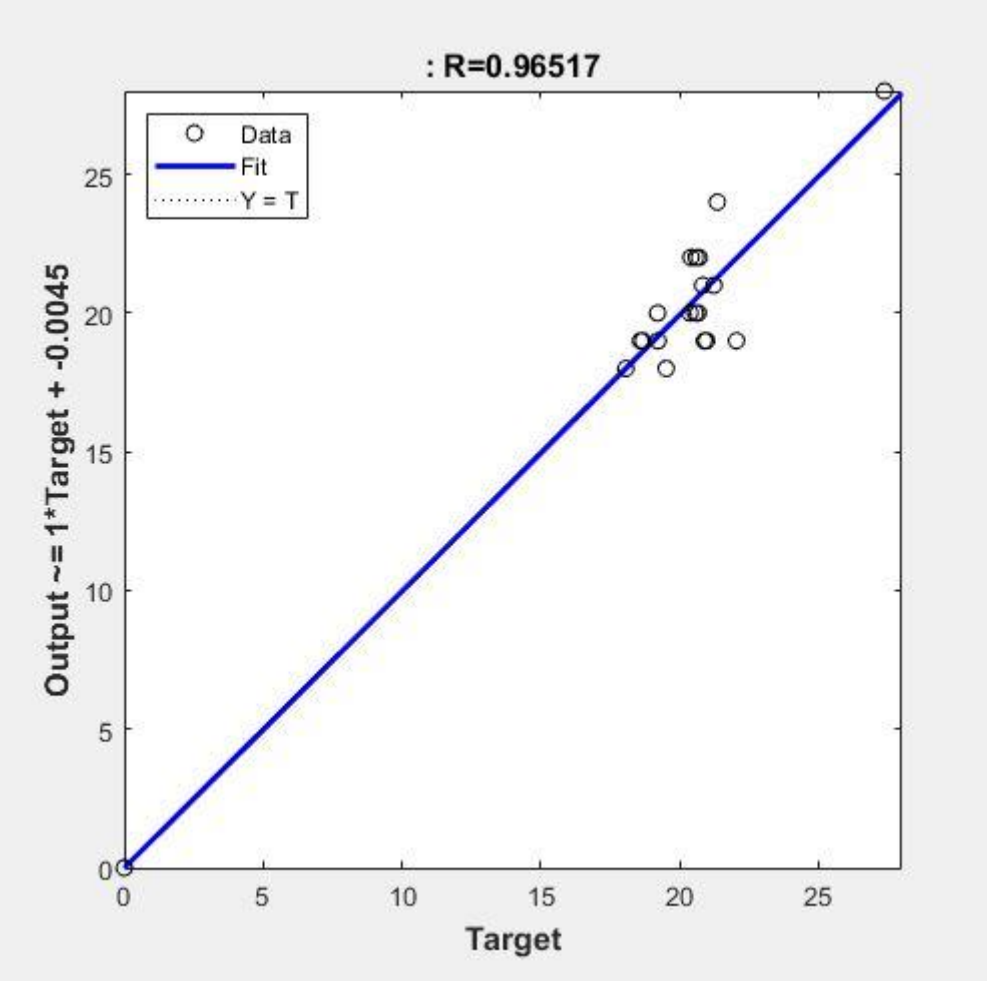

Figure 4-15: Regression Plot of Prediction of Φ Value for Primary Data Set

4.6 ANN Model Equations

Various differentiable nonlinear functions can be used as a transfer function; however, a sigmoid function is commonly used. These functions were incorporated for mapping desired nonlinear input output relation. In this research hyperbolic tangent sigmoid function (tansig) was selected as the transfer function in the hidden neurons, given by Equation 4.1.

$$F_{tansig} = f(x) = \frac{2}{1+e^{-2x}} - 1 \qquad 4.1$$

Equation 4.2 was derived by putting the general characteristics used to develop the models into the mathematical representation of the ANN model.

$$c, \phi = \sum_{h=1}^{n}\{v_h * F_{tansig}(b_h + \sum_{i=1}^{p}(w_{ih} * x_i))\} + b_0 \quad 4.2$$

Where, w_{ih} is connection weight between the input and hidden neurons; v_h is connection weight between h^{th} hidden layer and output layer; b_h is Bias at the h^{th} neuron of hidden layer; b_0 is Bias at output layer; n is number of neurons in hidden layer; x_i is normalized input variables; and p is no. of input variables.

4.6.1 Model Equation for c

Model 10 of network 6-11-1 architecture gave the best result for cohesion value prediction. A model equation can be formulated from the model equation in terms of weight and biases between input-hidden and hidden-output neurons. The matrix of weight and biases of the model is tabulated in Table 4-15.

Table 4-15: Weights and Biases of Model 10 (Network 6-11-1) for c Prediction

	Connection Weights (w_{ih})							Biases	
h	Sand % (x_1)	Fine % (x_2)	LL (x_3)	PI (x_4)	ω (x_5)	BD (x_6)	v_h	b_h	b_0
1	-3.161	0.255	-1.601	1.973	0.303	2.222	0.027	0.015	-2.007
2	-1.086	-1.292	0.344	-0.836	1.431	-2.260	2.337	2.432	
3	-0.325	0.506	0.309	-3.819	0.340	0.084	0.177	1.041	
4	3.074	-0.688	2.308	-2.554	-1.463	-0.800	0.120	-3.239	
5	-2.021	5.796	-0.127	-1.193	-2.802	-0.841	0.056	1.829	
6	1.239	-0.720	1.470	-1.430	-3.157	-1.357	-0.318	0.181	
7	0.833	1.647	-0.765	1.594	-0.546	3.196	1.193	-1.152	
8	-1.437	1.739	-0.180	2.696	0.008	0.676	-0.811	-0.614	
9	-0.243	-1.520	0.676	-0.582	0.827	-1.585	0.208	-0.619	
10	8.253	1.005	0.377	-0.876	-2.704	3.426	0.013	-0.090	
11	-1.597	1.452	1.161	1.588	-1.340	-2.454	0.481	-1.237	

w_{ih} is a 11 by 6 connection weight between the input and hidden neurons; since i represents the input variables which is equal to 6, and 11 represents the number of hidden neurons that is equal to 11. v_h is a 11 by 1 connection weight between h^{th} hidden layer and output layer of h equal to 11 hidden neurons, and 1 represents the number of output layer. b_h is bias at the h^{th} neuron of hidden layer and b_0 is a bias at output layer with one output c. The weighted sum, w_h for each hidden neurons is calculated as:

$$w_h = b_h + \sum_{i=1}^{p}(w_{ih} * x_i) \quad 4.3$$

x_i represents the normalized value of the input variables. minmax normalization was used in this research, given by:

$$x_i = \left(\frac{x_{norm,max} - x_{norm,min}}{x_{max} - x_{min}}\right)(x - x_{min}) + x_{norm,min} \quad 4.4$$

Where, x_{min} is the minimum value of each input variables of the entire data set; x_{max} is the maximum value of each input variables of the entire data set; $x_{norm,min}$ is the minimum value of the normalized data range; and $x_{norm,max}$ is the maximum value of the normalized data range. The values used for normalizing each input variables are tabulated below in Table 4-16.

Table 4-16: Normalizing Values for Input Variables

x_{min}	$\frac{(x_{norm,max} - x_{norm,min})}{(x_{max} - x_{min})}$	$x_{norm,min}$
1.1	0.0608	-1
51	0.0417	
36.4	0.0420	
3.2	0.0436	
12.4	0.0388	
1.434	2.7894	

The resulted value of a 11 by 1 weighted sum (w_h), calculated by using Equation 4.3 was then inserted into the hyperbolic tangent sigmoid transfer function in Equation 4.5.

$$T_h = F_{tansig}(w_h) = \frac{2}{1+e^{-2w_h}} - 1 \quad 4.5$$

The summation of the resulted a 11 by 1 matrix value of T_h multiplied with corresponding values of v_h 11 by 1 matrix was then added with b_0 value as shown in Equation 4.6 resulting normalized c value.

$$c_{norm} = b_0 + \sum_{h=1}^{n}(v_h * T_h) \quad 4.6$$

Finally, the real values of c then can be obtained by denormalizing the normalized c values with respect to the values given in Table 4-17 and by using Equation 4.7.

$$c = \frac{c_{norm} - y_{norm,min}}{\left(\frac{y_{norm,max} - y_{norm,min}}{y_{max} - y_{min}}\right)} + y_{min} \quad 4.7$$

Table 4-17: Normalizing Values for Output Variable c

$y_{norm,min}$	$\left(\frac{y_{norm,max} - y_{norm,min}}{y_{max} - y_{min}}\right)$	y_{min}
-1	0.0168	6

The formulation of c, based on the ANN result is as given in Equation 4.3 to 4.7. Using these mathematical equations output can be derived from input variables.

4.6.2 Model Equation for ϕ

Model 16 of network 6-10-1 architecture gave the best result for prediction of ϕ values. A model equation can be formulated from the model equation in terms of weight and biases between input-hidden and hidden-output neurons.

Table 4-18: Weights and Biases of Model 16 (Network 6-10-1) for Φ Prediction

	Connection weights							Biases	
h	Sand % (w_{1h})	Fine % (w_{2h})	LL (w_{3h})	PI (w_{4h})	ω (w_{5h})	BD (w_{6h})	v_h	b_h	b_0
1	0.663	-1.849	-1.526	2.598	-0.478	1.546	-0.450	0.684	1.5843
2	-2.371	-0.292	1.220	1.346	0.121	1.647	0.316	2.196	
3	1.973	-0.684	-0.085	-0.917	2.288	-3.533	-2.539	5.322	
4	-0.198	1.053	-0.231	0.726	0.975	-1.603	-0.619	0.591	
5	1.785	-0.613	0.491	-3.159	2.468	-1.719	0.336	-0.132	
6	-0.192	1.956	1.885	-3.930	1.142	1.123	-0.554	-0.341	
7	-1.419	-0.412	-1.628	-0.102	-1.370	0.317	-0.730	0.030	
8	-1.750	0.907	0.462	0.850	0.512	0.793	-0.453	-2.991	
9	-0.328	2.029	-0.420	-0.587	0.262	1.591	0.464	0.160	
10	-2.294	-1.071	-1.735	-0.259	-0.809	3.140	0.684	0.583	

Following the same procedure for deriving model equation for c, by using Equations 4.3 to 4.6 and weight and bias values tabulated in Table 4-18, normalized ϕ shown in Equation 4.8 was obtained.

$$\phi_{norm} = b_0 + \sum_{h=1}^{n} (v_h * T_h) \quad 4.8$$

Finally, the real values of ϕ then can be obtained by denormalizing the normalized ϕ values with respect to the values given in Table 4-19 and by using Equation 4.9.

$$\phi = \frac{\phi_{norm} - y_{norm,min}}{\left(\frac{y_{norm,max} - y_{norm,min}}{y_{max} - y_{min}}\right)} + y_{min} \quad 4.9$$

Table 4-19: Normalizing Values for Output Variable Φ

$y_{norm,min}$	$\left(\frac{y_{norm,max} - y_{norm,min}}{y_{max} - y_{min}}\right)$	y_{min}
-1	0.0575	6.3

4.7 Comparison of Current ANN Model with Existing Correlations

There is no specific equation developed to determine shear strength parameters from index properties for Addis Ababa city. But many empirical methods for shear strength parameters prediction of soils are presented in literature. Among these, four have been chosen for the purpose of assessing the relative performance of the ANN model. These include the methods proposed by Goktepe et al (2008); Ersoy et al (2013); Korayem, Ismail & Sehari (1996); Roy & Dass (2014). These methods are chosen as the database used in this work contains most parameters required to calculate shear strength parameters by these methods and also the models are developed for fine grained soils. The performance of the existing correlation methods and the ANN model on the validation set are given in Tables 4-20 and 4-21 for cohesion and internal friction angle respectively; also the graphical comparison of the models are shown in Figure 4-16 and 4-17.

Table 4-20: Comparison of ANN Model and Existing Correlations for c Prediction

No	Existing Models	Equation for c	R	MSE	RMSE
1	Goktepe et al (2008)	c= 1.61- 0.03 ω- 0.01PI	0.596	94.17	9.70
2	Ersoy et al (2013)	$c= 0.265(PI/LL)^{2.78}$	0.108	134.50	11.60
3	Roy & Dass (2014)	c= 224.032- 2.272 PL- 2.485 PI	0.036	72.65	8.52
4	Korayem et al (1996)	$c= 0.0865\ BD^{2.53}\omega^{-0.0277}$	0.274	201.35	14.19
5	Current Study	ANN	0.974	2.82	1.68

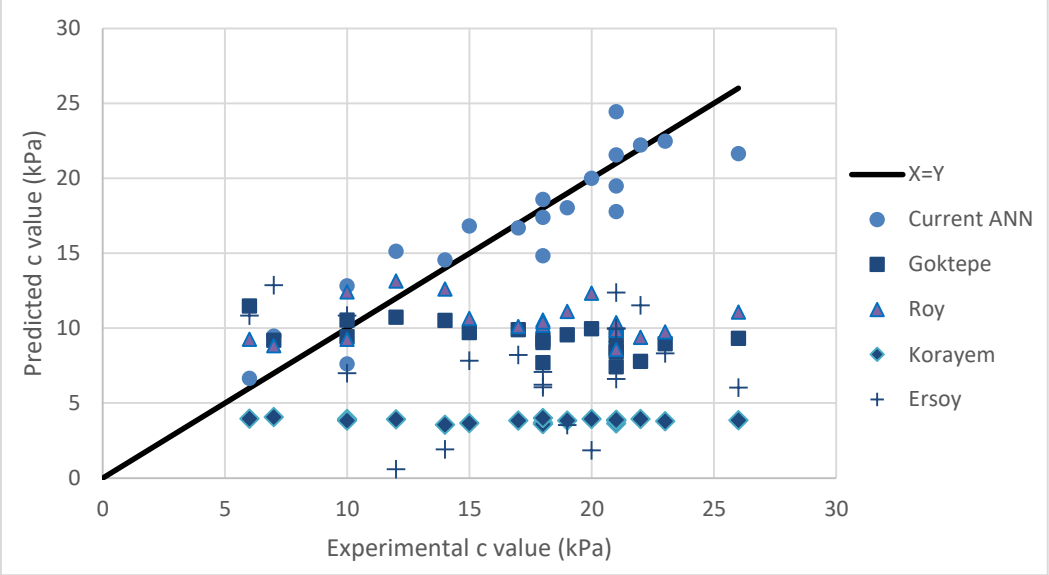

Figure 4-16: Graphical Comparison of ANN Model and Existing Correlations for c Prediction

For cohesion prediction the ANN model out performs the existing empirical equations with a very good precision and prediction capacity.

Table 4-21: Comparison of ANN Model and Existing Correlations for Φ Prediction

No	Existing Models	Equation for ϕ	R	MSE	RMSE
1	Goktepe et al (2008)	ϕ= -6.38 + 0.58 ω + 0.05 PI	0.503	295.93	17.20
2	Ersoy et al (2013)	ϕ= -204.5(PI/LL) + 56.3(PI/LL) + 31	0.309	123.52	11.11
3	Roy & Dass (2014)	ϕ= -29.604 + 34.220 BD	0.296	175.92	13.26
4	Korayem et al (1996)	ϕ= 0.761 - 0.0122ω	0.535	257.17	16.04
5	Current Study	ANN	0.965	1.72	1.31

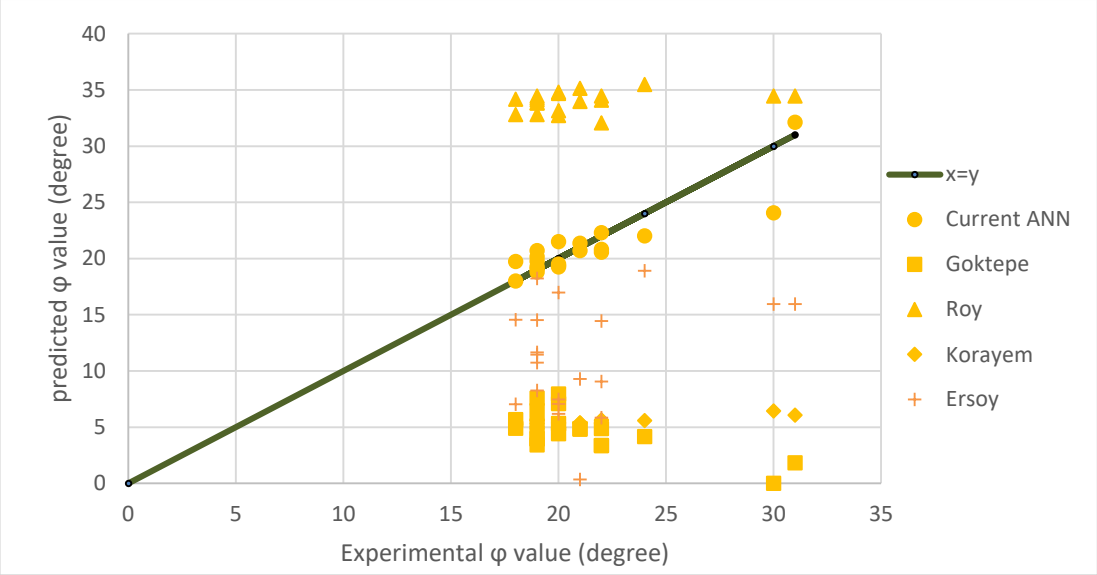

Figure 4-17: Graphical Comparison of ANN Model and Existing Correlations for ϕ Prediction

Also for the Internal Friction Angle as Cohesion prediction, the ANN model out performs the existing empirical equations with a very good precision and prediction capacity.

From tables and figures above, one can see that there is much variation of prediction values between the models. This indicates that correlation developed for a certain soil is not applicable for other soil. The reason for this variation may be due to the difference in test procedures and also the unique properties of the geological material where this correlation was developed.

CHAPTER 5 CONCLUSIONS AND RECOMMENDATIONS

5.1 Conclusions

The research was conducted to develop ANN models to predict the value of soil shear strength parameters (cohesion and angle of internal friction) from soil index properties. A total of two hundred eighty four soil test result (20 primary and 264 secondary) data were used for the study. Using these test results, artificial neural network models for c and ϕ were developed and validated separately. Multilayer perceptron (MLP) feed-forward network architecture with back propagation algorithm was used. From the results of this study the following conclusions are drawn:

- The optimum input parameters selected on the basis of previous literatures for this study are Sand Percent, Fines Percent, Liquid Limit, Plasticity Index, Water Content, and Bulk Density. The parameters have less interdependency between them.
- The optimum architecture for the ANN network for cohesion and angle of friction was found to be 6-11-1 (six inputs nodes, eleven hidden layer nodes, and one output node) and 6-10-1 (six inputs nodes, ten hidden layer nodes, and one output node) with a correlation coefficient of R=0.98 and R=0.92 for testing data and entire data sets of cohesion respectively. While the angle of friction had a correlation coefficient of R=0.92 and R=0.84 for testing data and entire data sets of angle of friction respectively.
- The selected best models were validated with primary data. The results between the experimental and predicted shear strength parameters obtained by the models showed a very good performance with a regression value of R=0.97 and R=0.96 for cohesion and angle of friction respectively.
- The results between the predicted and measured shear strength parameters obtained by utilizing ANNs were compared with five traditional methods. The results obtained demonstrated that the ANN method gave close prediction than the empirical methods considered.
- Based on the results, it is concluded that the proposed ANN models achieve the best performance in terms of predictive power and generalization ability. This proves the proposed models are reliable and robust models to shear strength

parameters of soil with the input ranges considered in this study. Therefore, the developed ANN models can be used to predict the values of shear strength parameters from soil index properties for Addis Ababa soil.

5.2 Recommendations

Based on the findings of the study, the following points are recommended.

1. The present study should be extended by gathering more quality soil test data and further detailed laboratory analysis carried out on a number of additional disturbed and undisturbed samples from different locations of the city, with a focus on considering various soil types ranging from fine to coarse grained soils. Since non plastic (NP) soils were not considered in the present study.
2. This study was carried out only on Addis Ababa soils. Work areas and parameters can be expanded during future work. It is advisable to conduct frequent researches in the soil, due to the fact that soil property varies from place to place and seasonally.

5.3 Limitation of the Study

This study is limited to fine-grained soils within the specified soil properties range used in this work. Also it only considers the direct shear test results, which is more suitable for cohesionless soils.

REFERENCES

AASHTO, A. A. (1986). *Standard specification for transportation materials and methods of sampling and testing, 14th ed.* Washinton, D.C.

Abu-Kiefa, M. A. (1998). General regression neural networks for driven piles in cohesionless soils. *J. Geotech. Geoenv. Engrg. ASCE, Vol. 123* .

Adunoye, G. O. (2013). Study of Relationship between Fines Content and Cohesion of Soil. *British Journal of Applied Science & Technology 4(4)* , 682-692.

Akayuli, C., Ofosu, B., Nyako, S. O., & and Opuni, K. O. (2013). The Influence of Observed Clay Content on Shear Strength and Compressibility of Residual Sandy Soils,. *International Journal of Engineering Research and Applications (IJERA), 3 (4)* , 2538-2542.

Akomalfe, D., & Eluyode, O. (2013). Comparative study of the biological and artificial neural networks. *European Journal of Applied Engineering and Scientific Research* , 36-46,.

Alkroosh, I., & Nikraz, H. (2011). Simulating pile load settlement behavior from CPT data using intelligent computing. *Central European Journal of Engineering* .

Al-Shayea, N. A. (2001). The combined effect of clay and moisture content on the behavior of remolded unsaturated soils. *Eng. Geol., Vol. 62, No. 4* , 319-342.

Arora, K. R. (1988). *Introductory Soil Engineering: Text Book,.* Delhi: Nem Chand Jane (Prop), Standard Publishers Distributors, Nai Sarak,.

Aslay, F., & Ustun, O. (2013). Estimating Soil Temperature With Artificial Neural Networks Using Meteorological Parameters. *Politeknik Dergisi, 16(4)* , 139-145.

Ayodele, L. (2009). Effect of fines content on some engineering properties of lateritic soil in Ile-Ife, . *Nigeria Journal of Engineering Research.* , 9(32).

B Zhang, Q. Z. (2001). Shear strength of surface soil as affected by soil bulk density and soil water content. *Soil and Tillage Research Volume 59, Issues 3-4* , 97-106.

Bakala, T., Quezon, E., & Yasin, M. (2021). Statistical Analysis on Shear Strength Parameter from Index Properties of Fine-grained Soils. *Journal of Engineering Research and Reports 20(4)* , 15-28.

Barends F B J, L. J. (1999). *Geotechnical Engineering for Transportation Infrastructure: Theory and Practice, Planning and Design, Construction and Maintenance.* Netherlands: Balkema Publishers.

Basheer, I. A., Reddi, L. N., & Najjar, Y. M. (1996). Site characterisation by neuronets: An application to the landfill siting problem. *Ground Water, 34* , 610-617.

Baziar, M., & Ghorbani, A. (2005). Evaluation of lateral spreading using artificial neural networks. *Soil Dynamics and Earthquake Engineering* .

Bolton, M. (1986). The strength and dilatancy of sands. *Geotechnique 36* , 65-78.

Cal, Y. (1995). Soil classification by neural-network. *Advances in Engineering Software*.

Cho, S. (2009). Probabilistic stability analyses of slopes using the ANN-based response surface. *Computers and Geotechnics. Vol. 36* .

Dadkhah, R., Mohammad, G., Rassoul, A., & and Gholam, R. (2010). The Effect of Scale Direct Shear Test on the Strength Parameters of Clayey Sand in Isfahan City, Iran. *Journal of Applied Sciences 10(18)* .

Dafalla, M. A. (2013). Effects of clay and moisture content on direct shear tests for clay-sand mixtures,. *Advances in Materials Sience and Engineering* .

Das, S. K. (2013). Artificial Neural Networks in Geotechnical Engineering. *Metaheuristics in Water, Geotechnical and Transport Engineering* , p.231-270.

Das, S. K., & Basudhar, P. K. (2008). Prediction of residual friction angle of clays using artificial neural network. *Engineering Geology, [s.l.], v. 100, n. 3-4* , 142-145.

El-Maksoud, M. A. (2006). Laboratory determining of soil strength parameters in calcareous soils and their effect on chiseling draft prediction. *Proc. Energy Efficiency and Agricultural Engineering Int. Conf.* Rousse, Bulgaria.

Elmas, C. (2007). *Artificial intelligence applications.* Ankara.

Ersoy, H., Karsli, M. B., Cellek, S., Kul, B., Baykan, I., & Parsons, R. L. (2013). Estimation of the soil strength parameters in Tertiary volcanic regolith (NE Turkey) using analytical hierarchy process. *J. Earth Syst. Sci. 122, No. 6* , 1545–1555.

Faramarzi, L. R. (2016). An experimental study of the effect of cement and chemical grouting on the improvement of the mechanical and hydraulic properties of alluvial formations. . *Construction and Building Materials, 126,* , 23–43.

Ferentinou, M., & Sakellariou, M. (2007). Computational intelligence tools for the prediction of slope performance. *Computers and Geotechnics* .

Garcia, A. J., Jaime, Y. N., Contreras, A. M., Bastardo, L. D., & and Llovera, F. A. (2012). Savanna soil water content effect on its shear strength-compaction relationship,. *Revista Científica UDO Agrícola, 12 (2)* , 324-337.

Gemitzi, F., & Eskioglou, P. (2011). Evaluating Landslide Susceptibility Using Environmental Factors, Fuzzy Membership Functions and Gis. *Global Nest Journal* .

Ghaboussi, J., & Sidarta, D. E. (1998). New nested adaptive neural networks (NANN) for constitutive modeling. *Jornal of Computers and Geotechnics, 22(1)* , 29-52.

Goh, A. T. (1995a). Back-propagation neural networks for modeling complex systems. *Artificial Intelligence in Engineering, 9* , 143-151.

Goh, A. T. (1995c). Modeling soil correlations using neural networks. *J. Computing in Civil Engrg., ASCE, 9(4)* , 275-278.

Goh, A. T. (1996a). Neural-network modeling of CPT seismic liquefaction data. *J. Geotech. Engrg., ASCE* .

Goh, A. T. (1994b). Seismic liquefaction potential assessed by neural network. *J. Geotech. & Geoenv. Eng., 120* .

Goh, A. T., Wong, K. S., & Broms, B. B. (1995). Estimation of lateral wall movements in braced excavation using neural networks. *Canadian Geotech. J., 32* , 1059-1064.

Goh, A., Kulhawy, F., & Chua, C. (2005). Bayesian neural network analysis of undrained side resistance of drilled shafts. *J. Geotech. Geoenviron. Eng* .

Goktepe, A. B., Altun, S., Altintas, G., & and Tan, O. (2008). Shear strength estimation of plastic clays with statistical and neural approaches. *Building and Environment, 43* , 849-860.

Gordon, T. K., Evan, C. H., Matt, S., & C. Hsein, J. (2007). A neural network approach to estimating deflection of diaphragm walls caused by excavation in clays. *Computers and Geotechnics* .

Graf F, F. M. (2009). Effects of vegetation on the angle of internal friction of a moraine. *Forest, Snow and Landscape Research, 82(1)* , 61–77.

Guidelines. (2010). Geotechnical Site Investigation Guidelines for Building Foundations in Permafrost January. *I. Holubec Consulting Inc.,* .

Hajihassani, M., Marto, A., Nazmi, E., Abad, S., & Shahrbabaki, M. (2011). Prediction of surface settlements induced by NATM tunneling based on artificial neural networks. *Electro. J. Geotech. Eng* .

Hamzacebi, C. (2011). *Artificial neural networks: predictive use of MATLAB and Neurosolutions applied.*

Hanna, A., Ural, D., & Saygili, G. (2007). Evaluation of liquefaction potential of soil deposits using artificial neural networks. Engineering Computations. *International Journal for Computer-Aided Engineering and Software. Vol. 24* .

Harini, H., & Naagesh, S. (2014). Fine grained soils CBR prediction by Multiple Linear Regression and Artificial Neural Networks. *Volume 5, Issue 2* , 119-126.

Haykin, S. (2009). *Neural networks and learning machines 3rd ed.* Upper Saddle River, New Jersey: Pearson Education, Inc.,.

Haykin, S., & Network, N. (2004). *A comprehensive foundation. Neural Networks 2.*

Hosseini, M., MovahediNaeini, S., & Dehghani, A. (2018). Modeling of soil mechanical resistance using intelligent methods. *Journal of SoilScience andPlant Nutrition,vol.18, no. ahead* , 939–951.

Huat, B. B. (2009). Experimental investigation on geomechanical properties of tropical organic soils and peat. *American Journal of Engineering and Applied Science, 2(1),* , 184–188.

Jain, R., Jain, P. K., & and Bhadauria, S. S. (2010). Computational approach to predict soil shear strength. *International Journal of Engineering Science and Technology, 2(8)* , 3874-3885.

Jiang, Q., Cao, M., Wang, Y., Wang, J., & He, Z. (2021). Estimation of Soil Shear Strength Indicators Using Soil Physical Properties of Paddy Soils in the Plastic State. *Appl. Sci.*

Juwaied, N. S. (2018). Applications of artificial intelligence in geotechnical engineering. *ARPN Journal of Engineering and Applied Sciences* , 2764-2785.

Kakici, A. (2017). *Artificial Neural Networks Architecture and Structure Elements #2.*

Kayadelen, C., Gunaydın, O., Fener, M., Demir, A., & Ozvan, A. (2009). A modeling of the angle of shearing resistance of soils using soft computing systems;. *Expert. Syst. Appl. 36* , 11,814–11,826.

Kim, P. (2017). *MATLAB Deep Learning: With Machine Learning, Neural Networks and Artificial Intelligence.* Seoul, Korea (Republic of).

Korayem, A., Ismail, K., & Sehari, S. (1996). Prediction of soil shear strength and penetration resistance using some soil properties. *Misr J. Agr. Res., 13 (4)* , 119-140.

Kristyna, B., Lenka, S., & and Pavla, P. (2013). Influence of water content on the shear strength parameters of clayey soil in relation to stability analysis of a hillside in Brno region. *Acta Universitatis Agriculturae et Silviculturae Mendelianae Brunensi LXI No. 6*, 1583–1588.

Kukreja, H., Bharath, N., & Kuldeep, S. (2016). An Introduction to Artificial Neural Network. *International Journal Of Advance Research And Innovative Ideas In Education, vol. 1, no. 5* , 27-30.

Kumari, D. (2009). A study on the effect of moisture on strength characteristics of river sand. *UG Dissertation, NIT Rourkela, India* .

Lade, P., Liggio, J. C., & and Yamamuro, J. (1998). Effects of non-plastic fines on minimum and maximum void ratios of sand. *Geotechnical Testing Journal. 21(4)* , 336–347.

Lal, S. K. (2016). Modelling of Soil Shear Strength Using Neural Network Approach. *EJGE Vol. 21, Bund. 10* , 3751-3771.

Lee, C., & Sterling, R. (1992). Identifying probable failure modes for underground openings using a neural network. *Int. J. Rock Mechanics and Mining Science & Geomechanics Abstracts, 29(1)* , 49-67.

Lee, I. M., & Lee, J. H. (1996). Prediction of pile bearing capacity using artificial neural networks. *Computers and Geotechnics18* , 189-200.

Lee, S., Lee, S., & and Kim, Y. (2003). An approach to estimate unsaturated shear strength using artificial neural network and hyperbolic formulation. *Computers and Geotechnics 30* , 489-503.

Maizir, H., Gofar, N., & Kassim, K. (2015). Artificial Neural Network Model for Prediction of Bearing Capacity of Driven Pile. *Jurnal Teoretis dan Terapan Bidang Rekayasa Sipil* .

Mardookhpour, A. &. (2011). Advantages of utilizing geotextiles in fixing sandy soils and increasing shear strength in water conveyance trenches., . *American Journal of Geoscienced, 2(1)* , 1–3.

Mollahasani, A., Alavi, A., Gandomi, A., & and Rashed, A. (2011). Nonlinear neural-based modeling of soil cohesion intercept. *KSCE J. Civil. Eng. 15(5)* , 831–840.

Moon, H. K., Na, S. M., & Lee, C. W. (1995). Artificial neural-network integrated with expert-system for preliminary design of tunnels and slopes. *Proc., 8th Int. Congress on Rock Mechanics* (pp. 901-905). Balkema: T. Fujii, ed., Rotterdam.

Mousavi, S. M., Alavi, A. H., Gandomi, A. H., & Mollahasani, A. (2012). Nonlinear genetic-based simulation of soil shear strength parameters. *Journal of Earth System Science, 120 (6)* , 1001–1022.

Murthy, S. (2008). *Geotechnical Engineering: Principles and Practices of Soil Mechanics, 2nd edn;*. UK: Taylor & Francis, CRC Press.

Najjar, Y. M., & Ali, H. E. (1998). CPT-based liquefaction potential assessment: A neuronet approach. *Geotechnical Special Publication, ASCE* .

Najjar, Y. M., & Basheer, I. A. (1996a). Neural network approach for site characterization and uncertainty prediction. *Geotechnical Special Publication, ASCE, 58(1)* , 134-148.

Najjar, Y. M., & Basheer, I. A. (1996b). Utilizing computational neural networks for evaluating the permeability of compacted clay liners. *Geotechnical and Geological Engineering, 14* , 193-221.

Obasi, N. L., & Anyaegbunam, A. J. (2005). Correlation of the Undrained Shear Strength and Plasticity Index of Tropical clays;. *Nigerian Journal of Technology, Vol. 24, No. 2* , 1-11.

Ojuri, O. O. (2013). Predictive shear strength models for tropical lateritic soils. *Journal of Engineering, Volume 2013, Article ID 595626,* , 1-8.

Oyediran, A. a. (2011). Variability in the geotechnical properties of some residual clay soils from southwestern Nigeria. *International Journal of Scientific & Engineering Research, 2 (9)* , 1-6.

Oztemel, E. (2003). *Artificial Neural Network.* Istanbul.

Penumadu, D., & Zhao, R. (1999). Triaxial compression behavior of sand and gravel using artificial neural networks (ANN). *Journal of Computers and Geotechnics, 24* , 207-230.

Prakash, S. a. (2002). Engineering Soil Testing. *Nem Chand & Bros, Roorkee,* .

R. E. Sojka, W. J. (2001). In Situ Strength, Bulk Density, and Water Content Relationships of A Durinodic Xeric Haplocalcid Soil. *soil sience Vol. 166, No. 8* , 0038-075C/01/16608-520-529.

Rajeev Jain, P. S. (2013). Unconsolidated Undrained Shear Strength of Remolded Clays by Anns Technique. *International Journal of Engineering Research and Technology (IJERT)* , 2827-2832.

Ranjkesh Adarmanabadi, H. R. (2020). Thermal image analysis of a cement kiln dust treated slope. . *International Journal of Science and Engineering Investigations, 9(107),* , 29–36.

Rizzo, D. M., & Dougherty, D. E. (1994). Application of artificial neural networks for site characterization using hard and soft information. *Proc., 10th Int. Conf. Computational Methods in Water Resources* .

Rizzo, D. M., Lillys, T. P., & Dougherty, D. E. (1996). Comparisons of site characterization methods using mixed data. *Geotechnical Special Publication, ASCE, 58(1)* , 157-179.

Rogers, J. D. (2009). Correlations Between Soil Plasticity and Strength Parameters,. *GE 441 - Engineering Geology and Geotechnics,* .

Roy, S., & and Dass, G. (2014). Statistical models for the prediction of shear strength parameters at Sirsa, India. *International Journal of Civil and Structural Engineering Volume 4 Issue 4* , 483-498.

S. D Iyeke, E. O. (2016). Estimation of shear strength parameters of lateritic soils using artificial neural network . *Nigerian Journal of Technology Vol. 35, No. 2, April*, 260–269.

Sagiroglu, S., Besdok, E., & Erler, M. (2003). *Artificial intelligence applications in engineering-1: Artificial neural networks.*

Shahin, M. A. (2010). Intelligent computing for modeling axial capacity of pile foundations. *Canadian Geotechnical Journal* .

Shahin, M. A., Jaksa, M. B., & Maier, H. R. (2001). Artificial Neural Network Applications in Geotechnical Engineering. *Australian Geomechanics Journal* .

Shahin, M. A., Jaksa, M. B., & Maier, H. R. (2000). *Predicting the settlement of shallow foundations on cohesionless soils using back-propagation neural networks. Research Report No. R 167.* Adelaide: The University of Adelaide .

Shahin, M. A., Maier, H. R., & Jaksa, M. B. (2003c). Neural and neurofuzzy techniques applied to modelling settlement of shallow foundations on granular soils. *Int. Congress on Modelling and Simulation* .

Shahin, M. (2014a). Load-settlement modelling of axially loaded drilled shafts using CPT-based recurrent neural networks. *International Journal of Geomechanics* .

Shi, J., Ortigao, J. A., & Bai, J. (1998). Modular neural networks for predicting settlement during tunneling. *J. Geotech. & Geoenv. Engrg., ASCE, 124(5)* , 389-395.

Shooshpasha, I., Amiri, I., & and Molaabasi, H. (2015). An Investigation of Friction Angle Correlation with Geotechnical Properties for Granular Soils Using GMDH Type Neural Networks. *Scientia Iranica, Tehran, v. 22, n. 1* , 157-164.

Sivakugan, N., Eckersley, J. D., & Li, H. (1998). Settlement predictions using neural networks. *Australian Civil Engineering Transactions, CE40* , 49-52.

Teh, C. I., Wong, K. S., Goh, A. T., & Jaritngam, S. (1997). Prediction of pile capacity using neural networks. *J. Computing in Civil Eng* .

Tuncer, E. R. (1977). An engineering classification for basalt-derived lateritic soils. *Engineering Geology, 4* , 319– 339.

USCS, U. S. (2006). *Standard practice for classification of soils for engineering purposes.*

Vanapalli, S., Fredlund, D., Pufahl, D., & and Clifton, A. (1996). Model for the prediction of shear strength with respect to soil suction. *Canadian Geotechnical Journal 33* , 379-392.

Wardani, S., Surjandari, N., & Jajaputra, A. (2013). Analysis of Ultimate Bearing Capacity of Single Pile Using the Artificial Neural. *Proceedings of the 18th International Conference on Soil Mechanics and Geotechnical Engineering.* Paris.

Zhu, J. H., Zaman, M. M., & and Anderson, S. A. (1998b). Modelling of shearing behaviour of a residual soil with recurrent neural network. *International Journal of Numerical and Analytical Methods in Geomechanics, 22(8)* , 671-687.

Zhu, J. H., Zaman, M. M., & Anderson, S. A. (1998a). Modeling of soil behavior with a recurrent neural network. *Canadian Geotechnical Journal 35(5)* , 858-872.

Zumrawi, M. M., & Mohammed, L. A. (2016). Correlation of Placement Conditions and Soil Intrinsic Properties with Shear Strength of Cohesive Soils. *7th Annual Conference for*

Postgraduate Studies and Scientific Research - Basic Sciences and Engineering Studies. Khartoum .

APPENDIX A: PARTICLE SIZE DISTRIBUTION CURVES

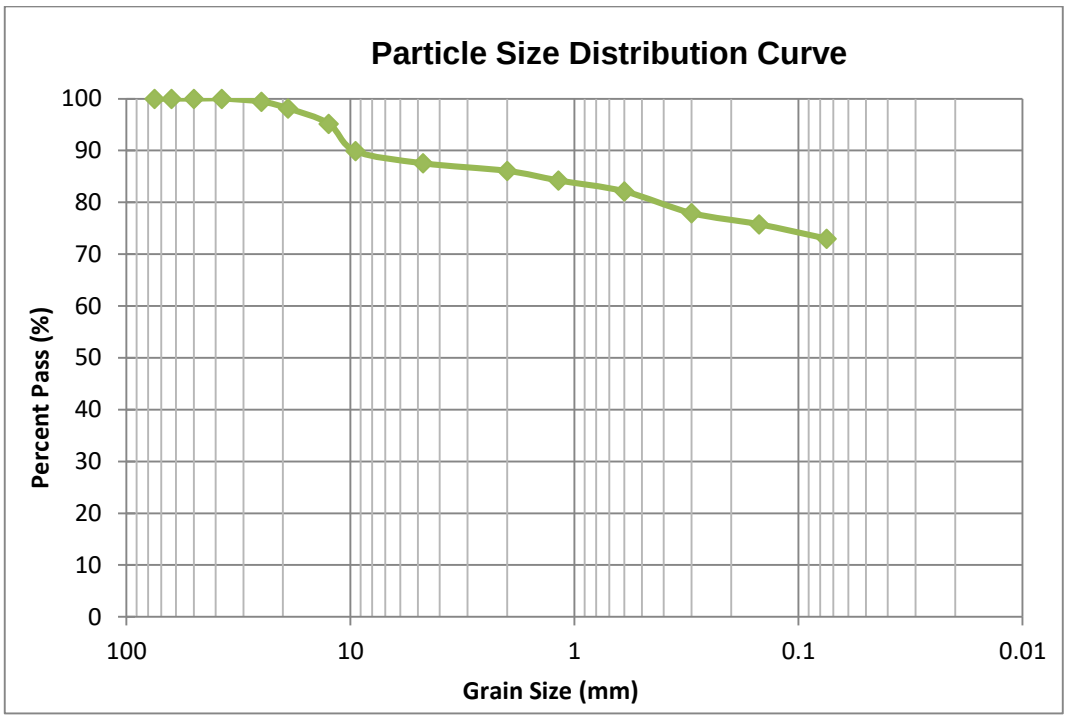

Figure A-1: Particle Size Distribution Curve of TP1-1

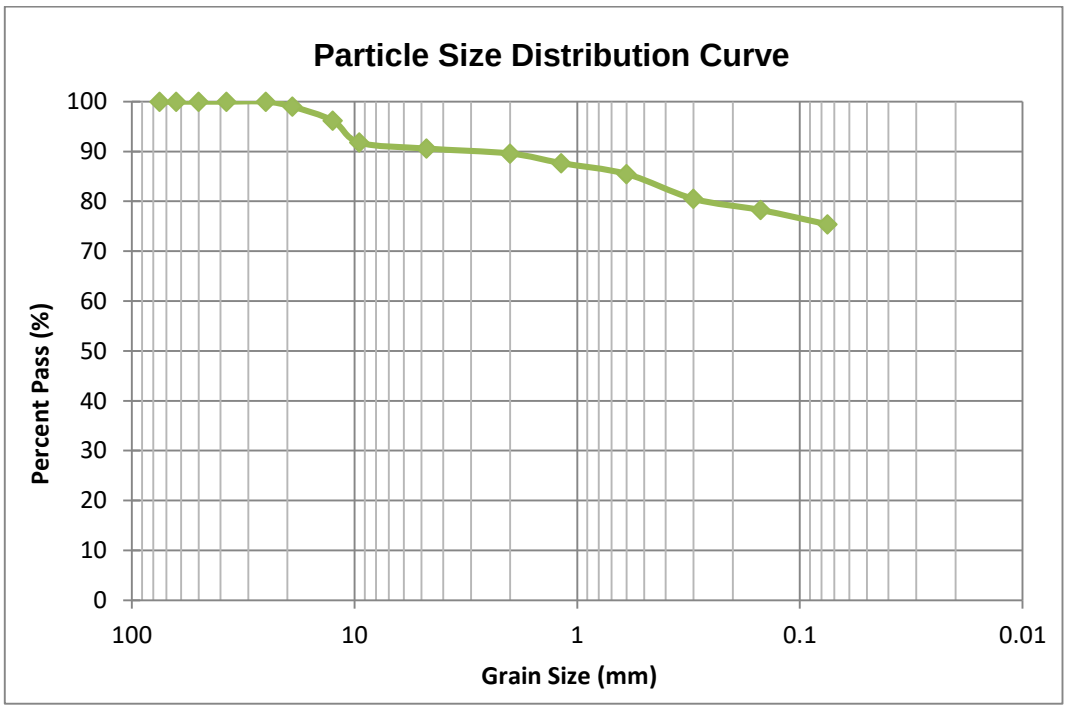

Figure A-2: Particle Size Distribution Curve of TP1-2

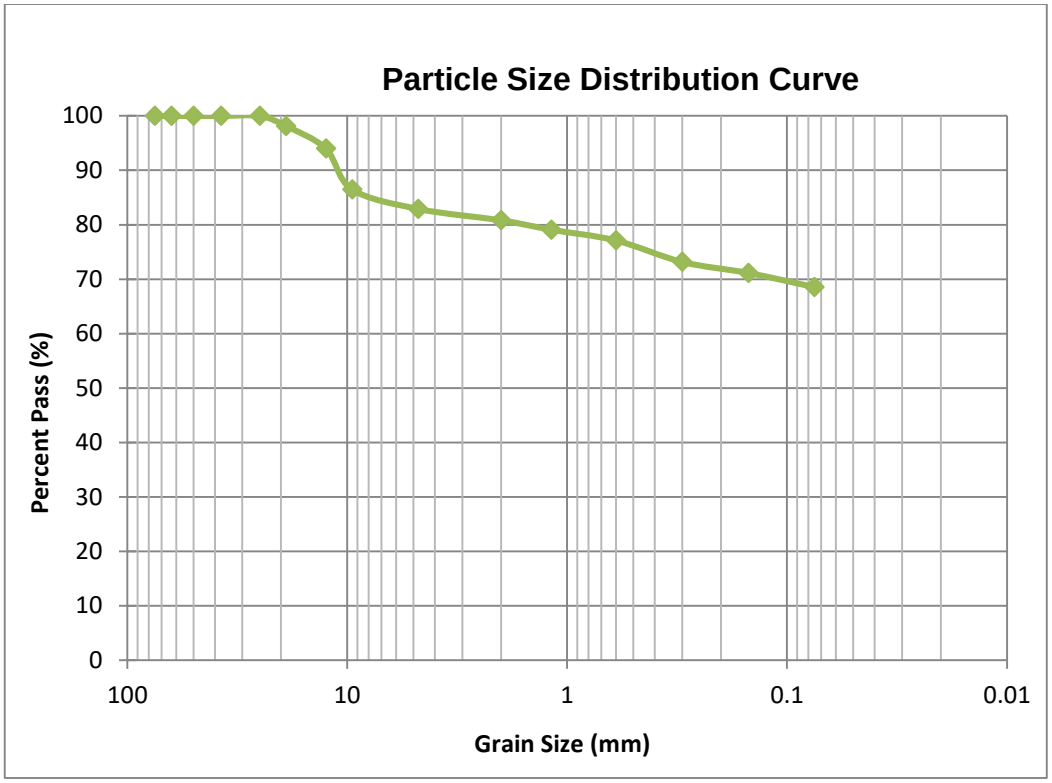

Figure A-3: Particle Size Distribution Curve of TP2-1

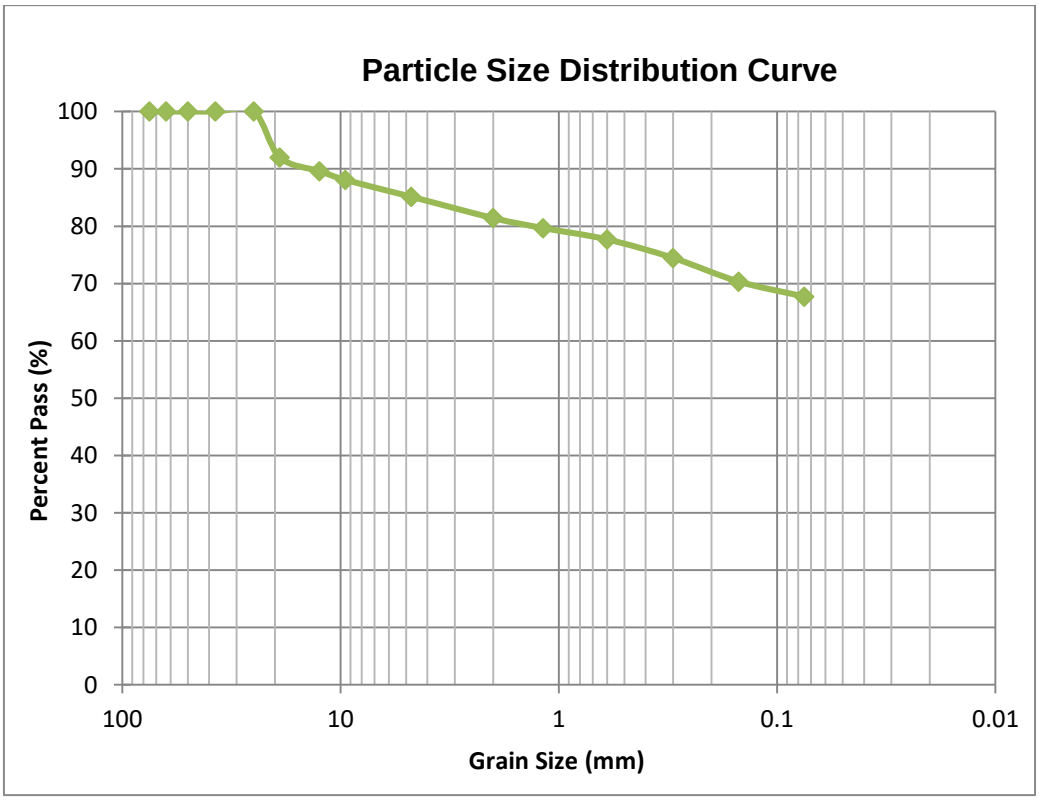

Figure A-4: Particle Size Distribution Curve of TP2-2

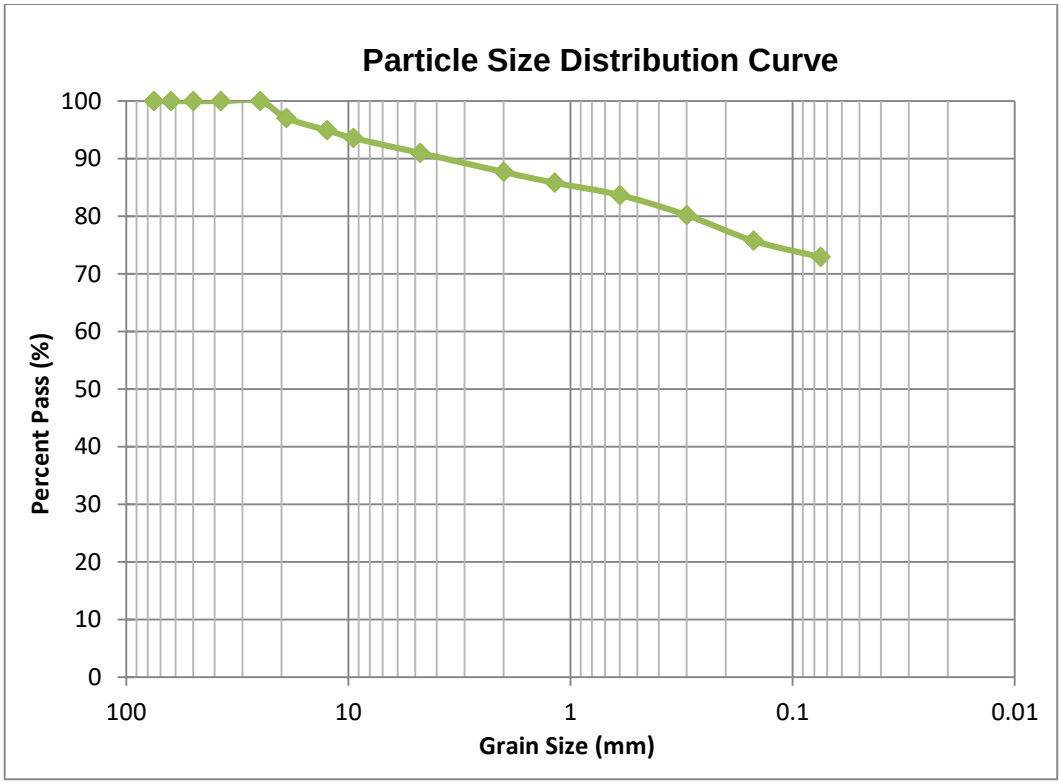

Figure A-5: Particle Size Distribution Curve of TP3-1

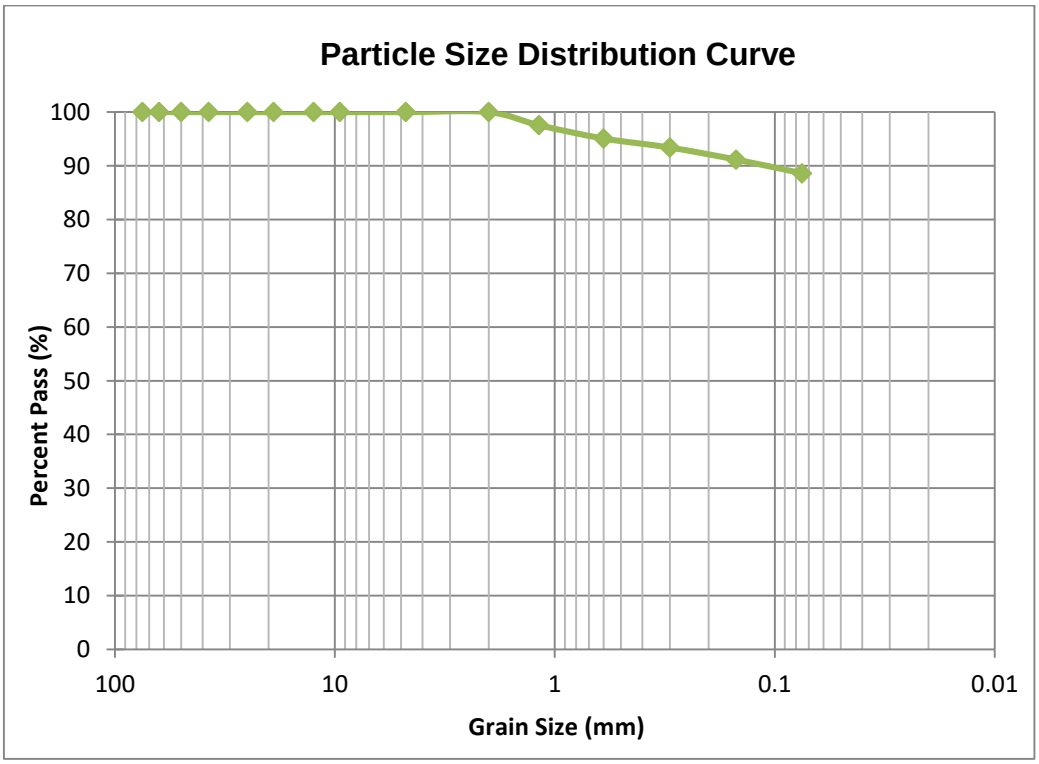

Figure A-6: Particle Size Distribution Curve of TP3-2

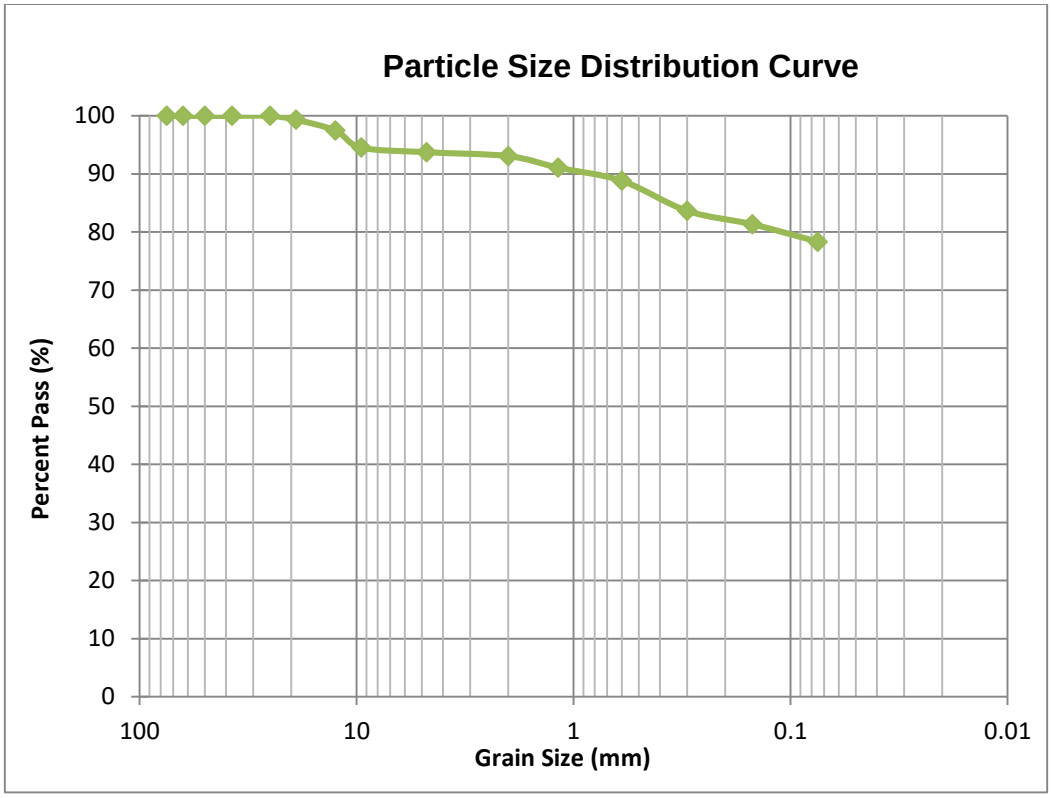

Figure A-7: Particle Size Distribution Curve of TP4-1

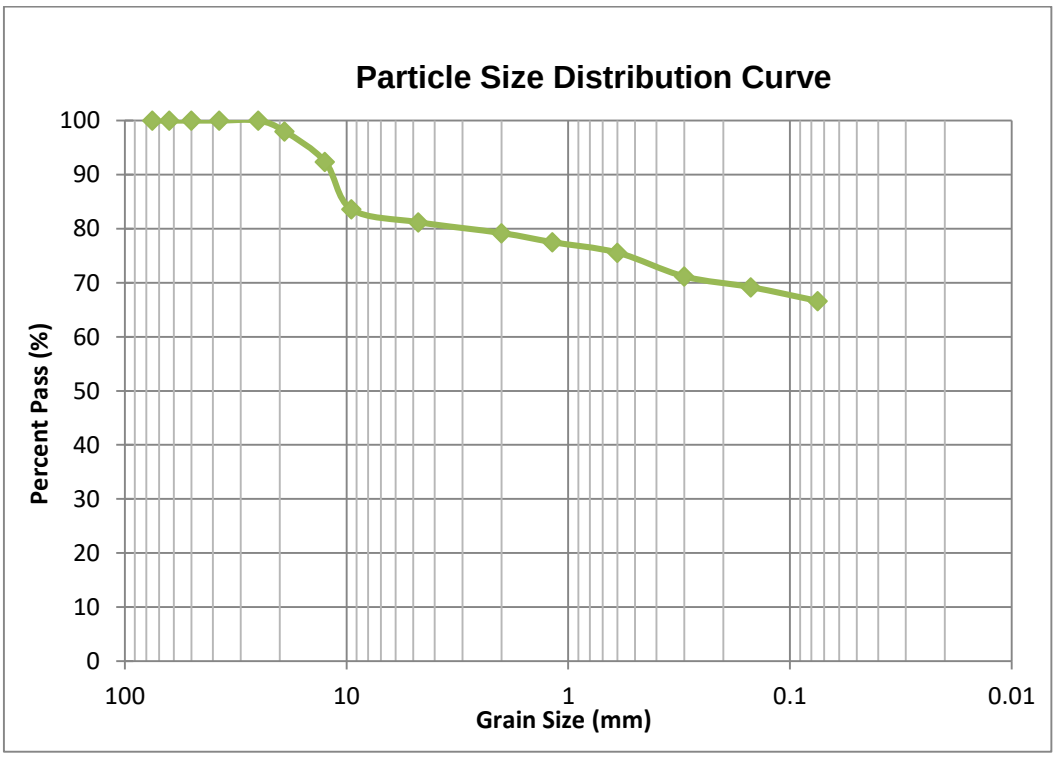

Figure A-8: Particle Size Distribution Curve of TP4-2

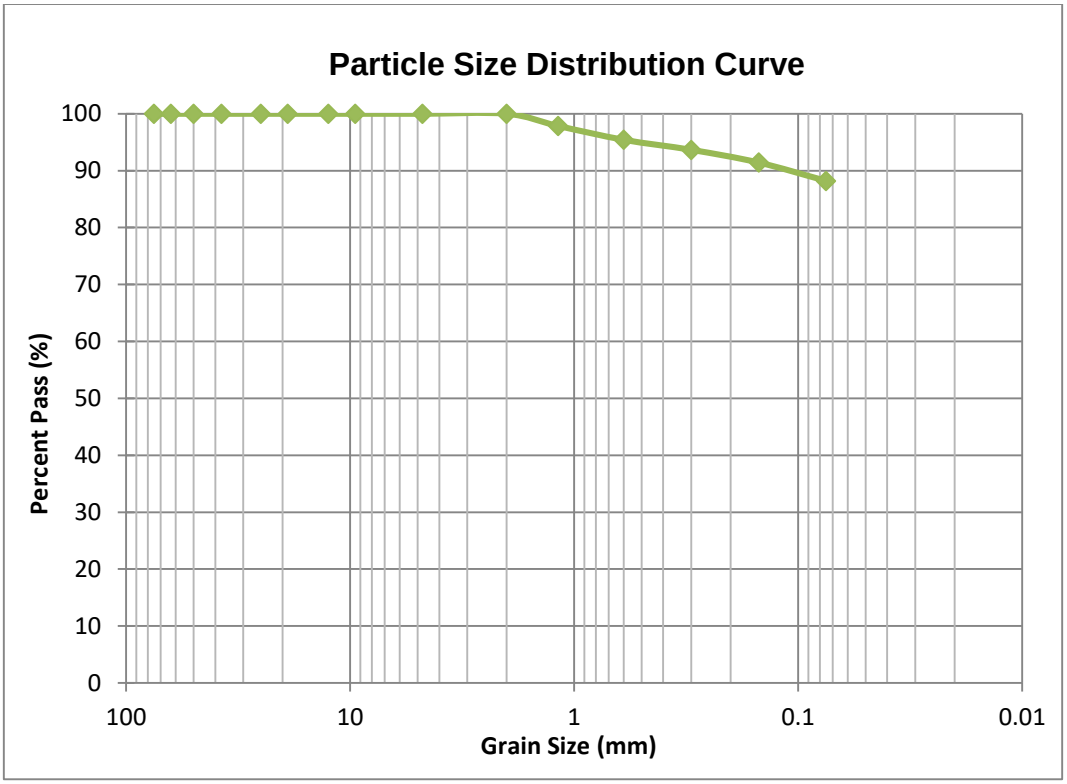

Figure A-9: Particle Size Distribution Curve of TP5-1

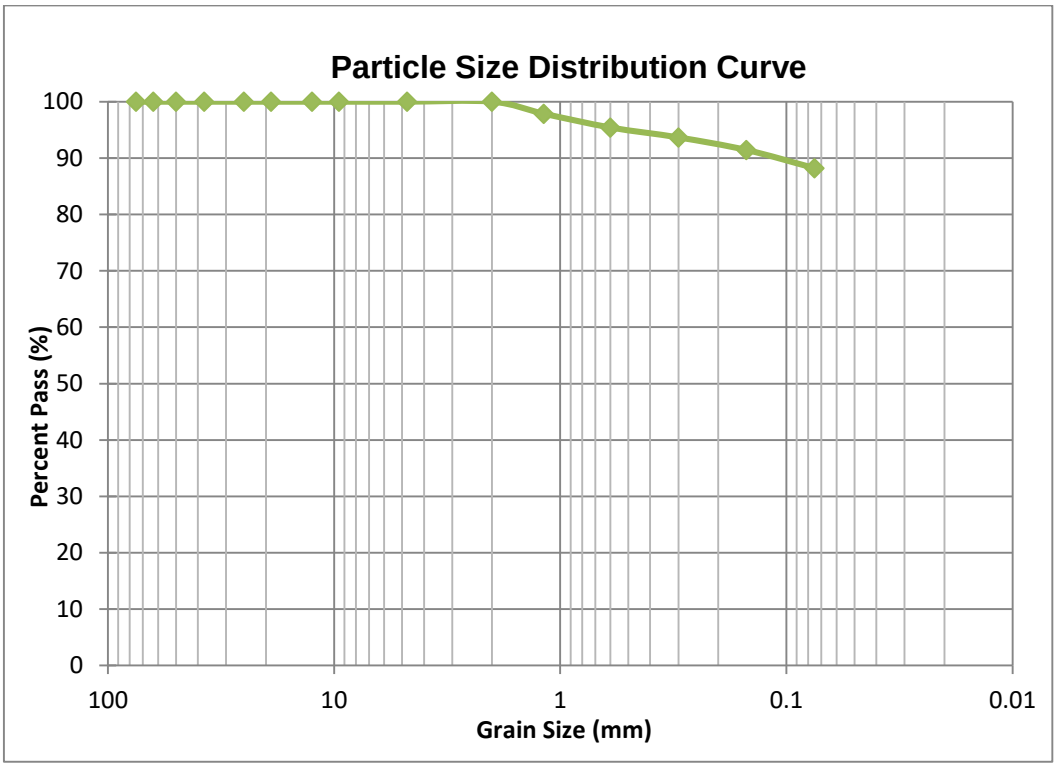

Figure A-10: Particle Size Distribution Curve of TP5-2

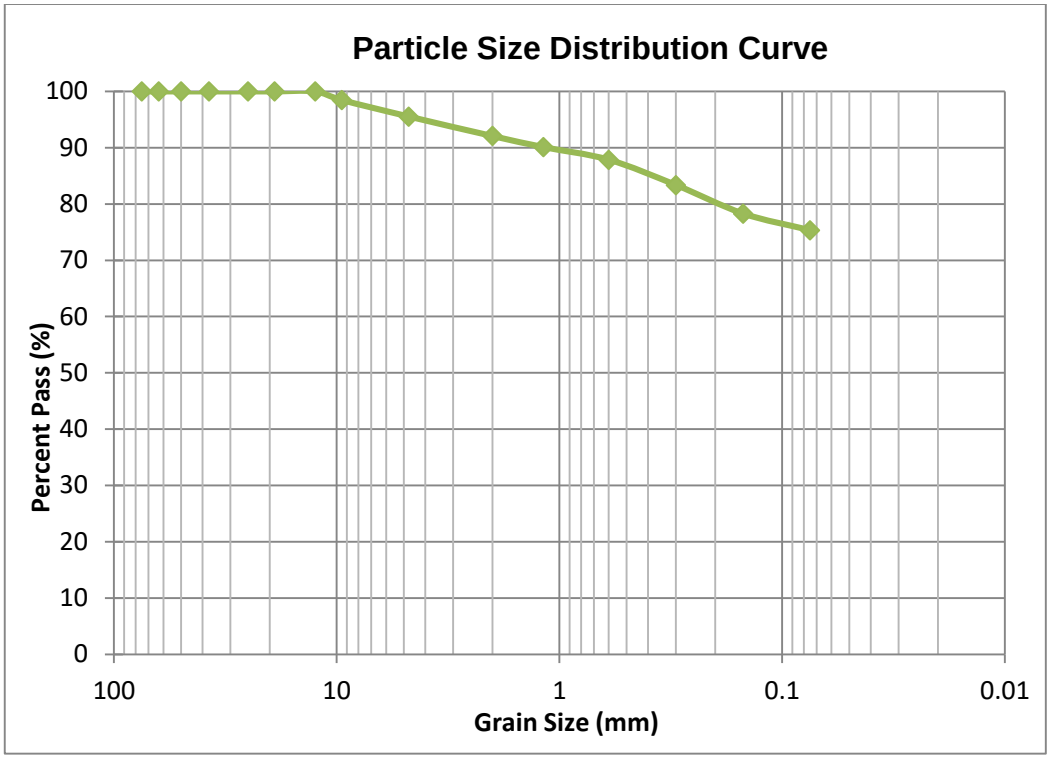

Figure A-11: Particle Size Distribution Curve of TP6-1

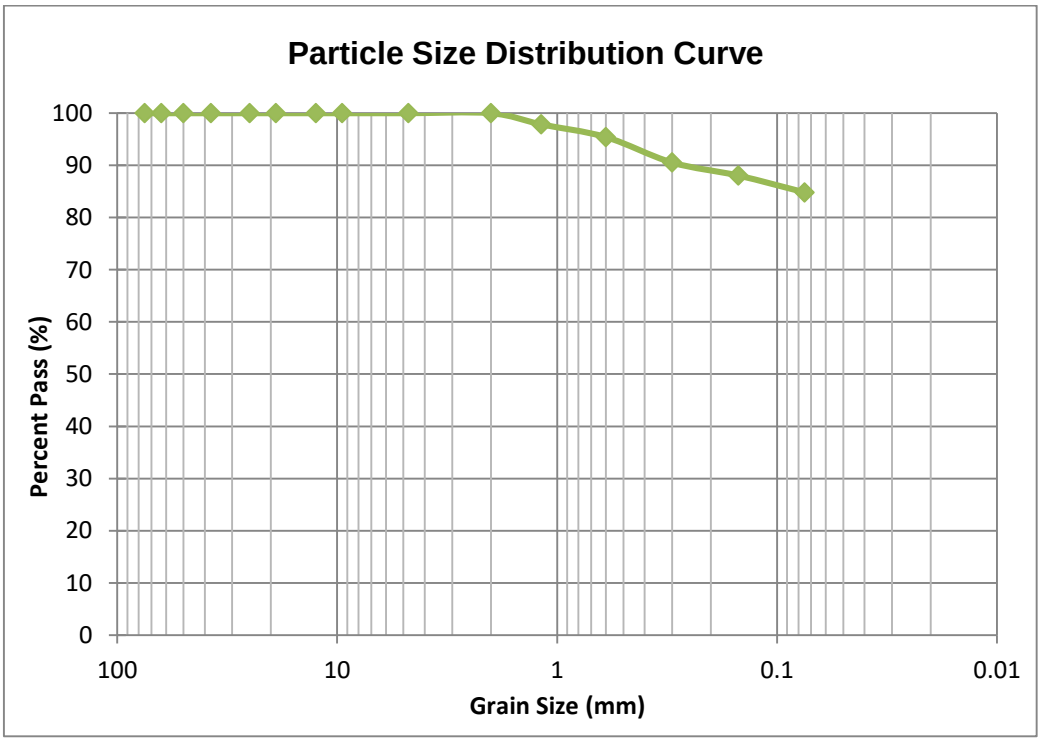

Figure A-12: Particle Size Distribution Curve of TP6-2

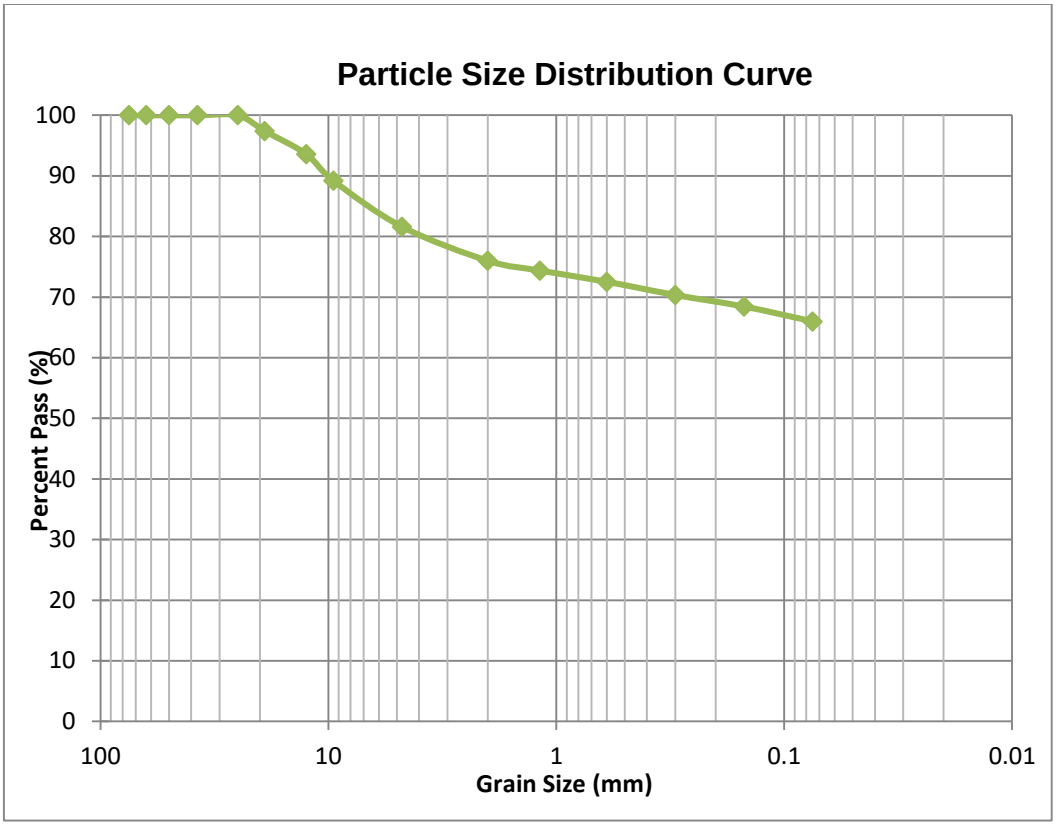

Figure A-13: Particle Size Distribution Curve of TP7-1

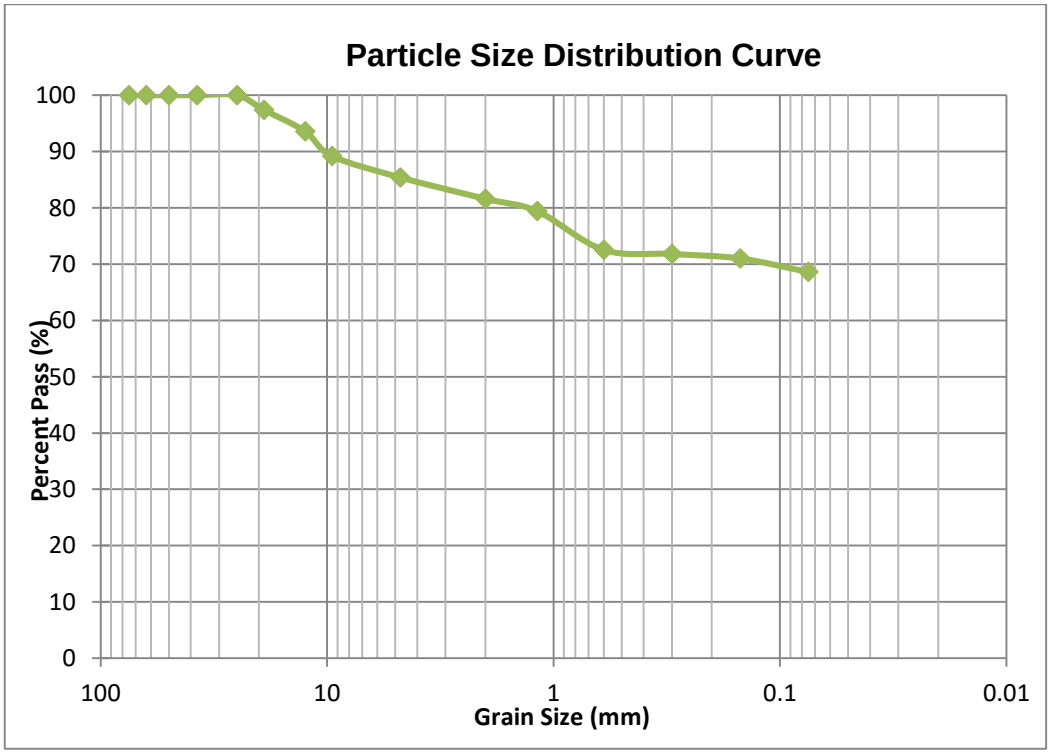

Figure A-14: Particle Size Distribution Curve of TP7-2

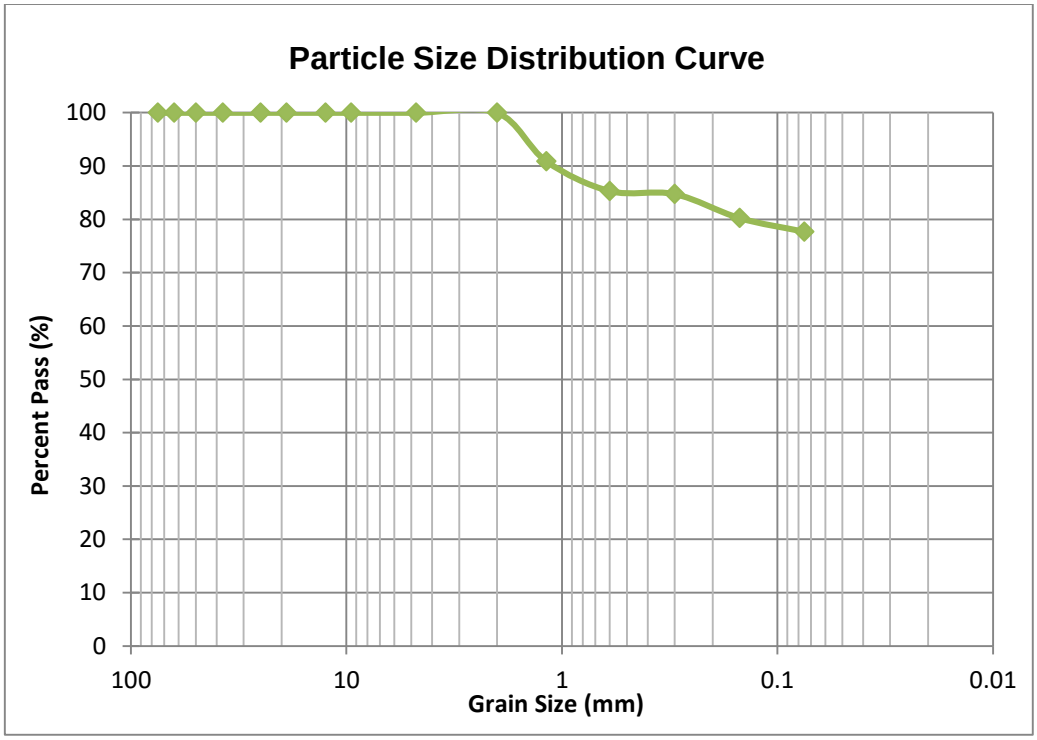

Figure A-15: Particle Size Distribution Curve of TP8

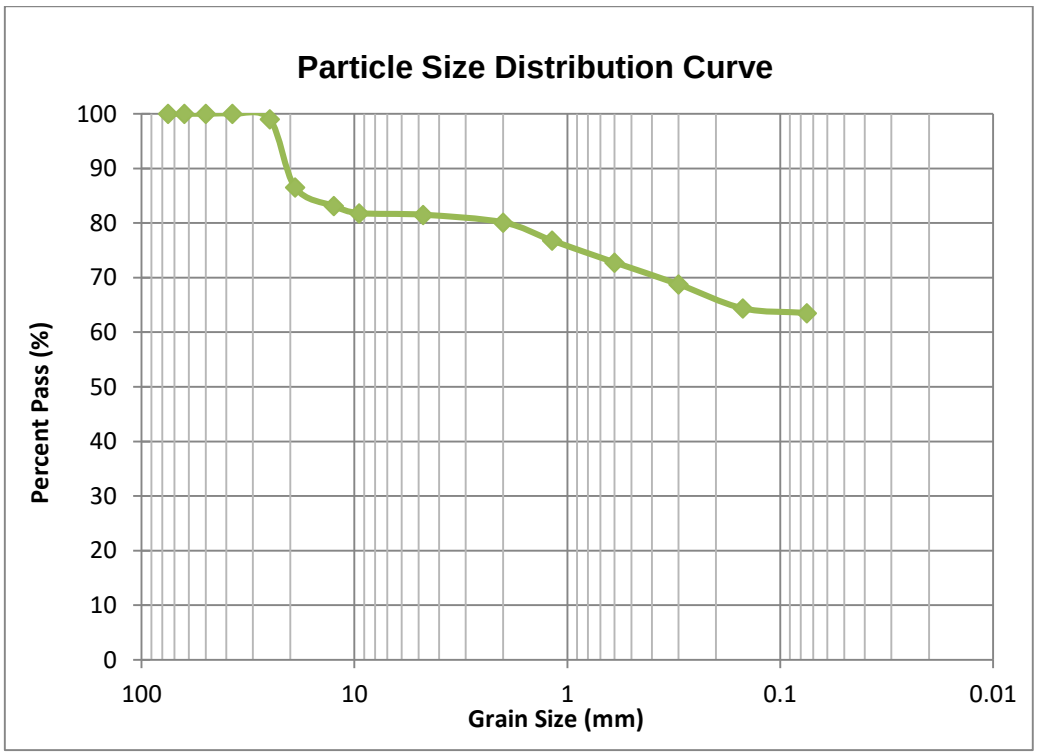

Figure A-16: Particle Size Distribution Curve of TP9-1

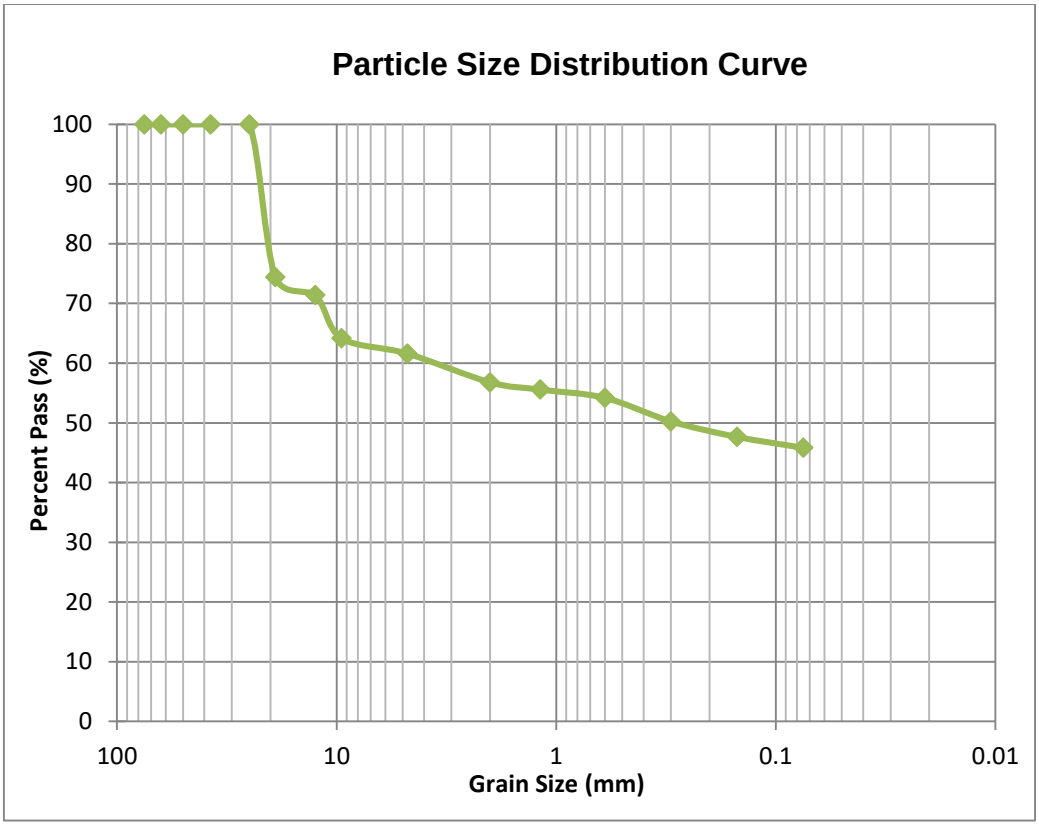

Figure A-17: Particle Size Distribution Curve of TP9-2

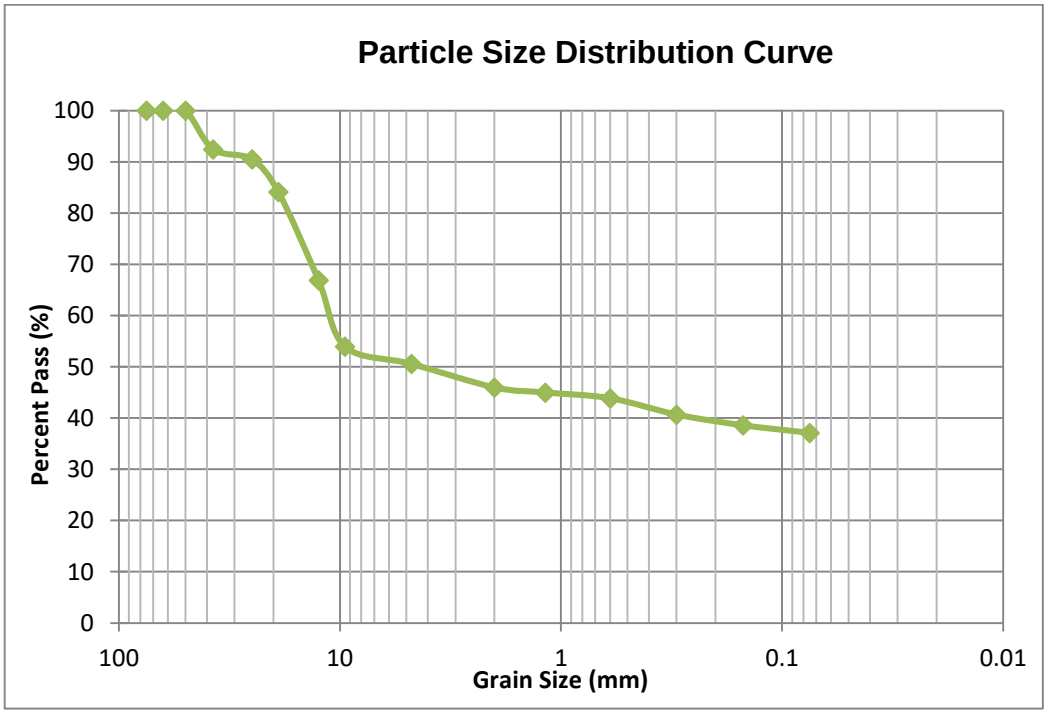

Figure A-18: Particle Size Distribution Curve of TP10

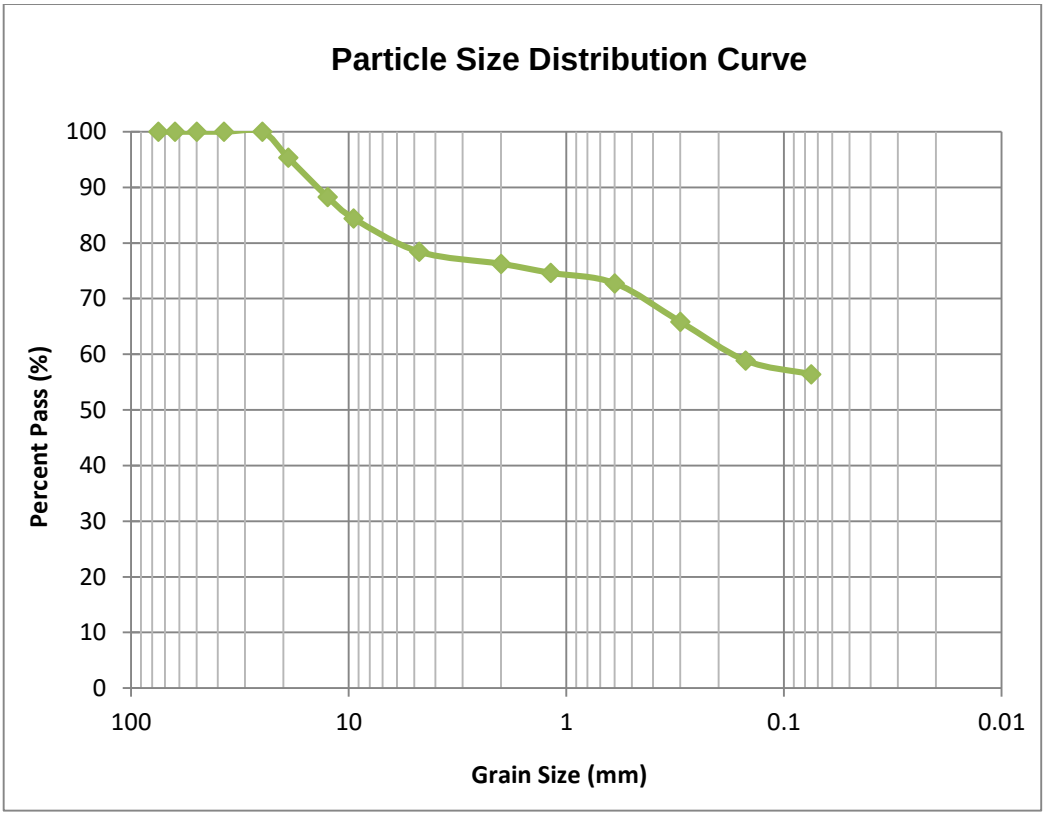

Figure A-19: Particle Size Distribution Curve of TP11-1

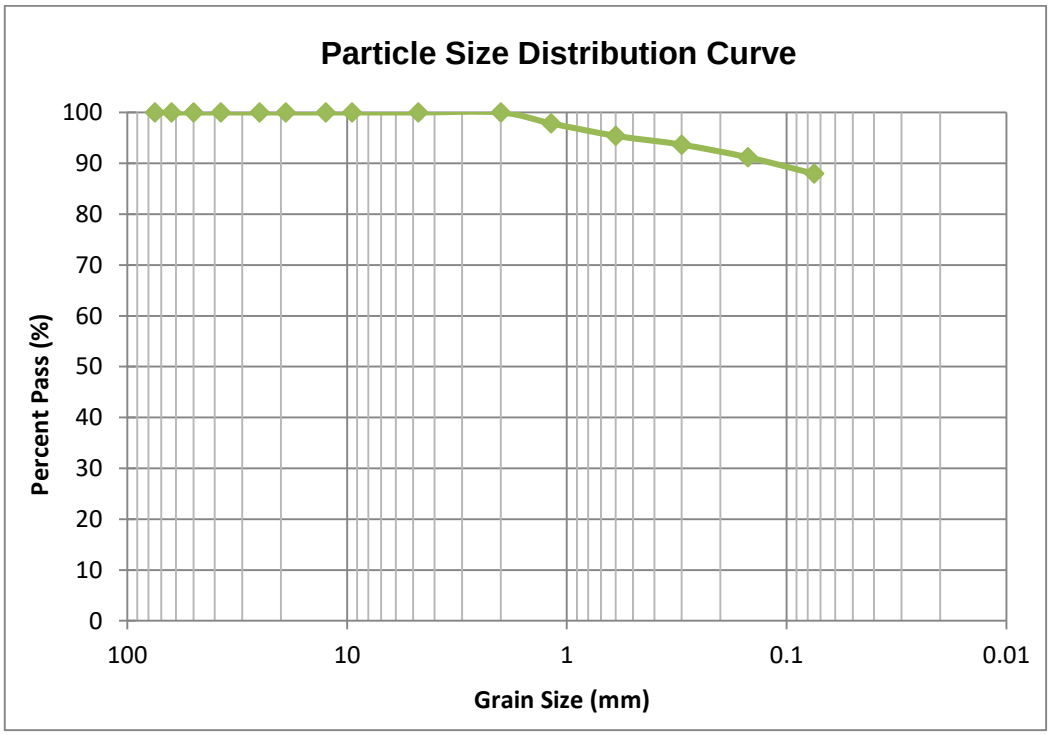

Figure A-20: Particle Size Distribution Curve of TP11-2

APPENDIX B: ATTERBERG LIMIT TEST RESULTS

TP1-1 Test Result

Table B-1: Atterberg Limits Analysis of TP1-1

	Liquid Limit			Plastic Limit	
No. Blows	33	27	17		
Wt.of cont. + wet soil (gm)	48.366	48.512	48.994	16.100	16.179
Wt.of cont. + dry soil (gm)	39.454	39.428	39.405	15.463	15.535
Wt. of water (gm)	8.91	9.08	9.59	0.64	0.37
Wt. container (gm)	21.715	21.932	21.789	14.167	14.217
Wt. dry soil (gm)	17.74	17.50	17.62	1.30	1.32
Water (%)	50.24	51.92	54.43	49.15	28.07
		LL= 52.4		**PL=38.6**	

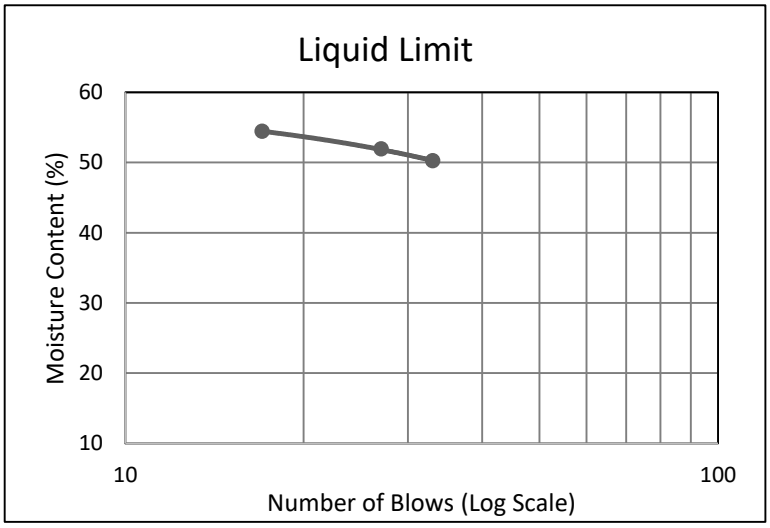

Figure B-1: Liquid Limit Chart of TP1-1

TP1-2 Test Result

Table B-2: Atterberg Limits Analysis of TP1-2

	Liquid Limit			Plastic Limit	
No. Blows	33	26	17		
Wt.of cont. + wet soil (gm)	49.070	49.200	49.480	16.660	16.570
Wt.of cont. + dry soil (gm)	40.950	40.840	40.750	15.980	15.930
Wt. of water (gm)	8.12	8.36	8.73	0.68	0.64
Wt. container (gm)	22.260	21.760	21.500	14.070	14.170
Wt. dry soil (gm)	18.69	19.08	19.25	1.91	1.76
Water (%)	43.45	43.82	45.35	35.60	36.36
		LL=43.9		**PL=35.9**	

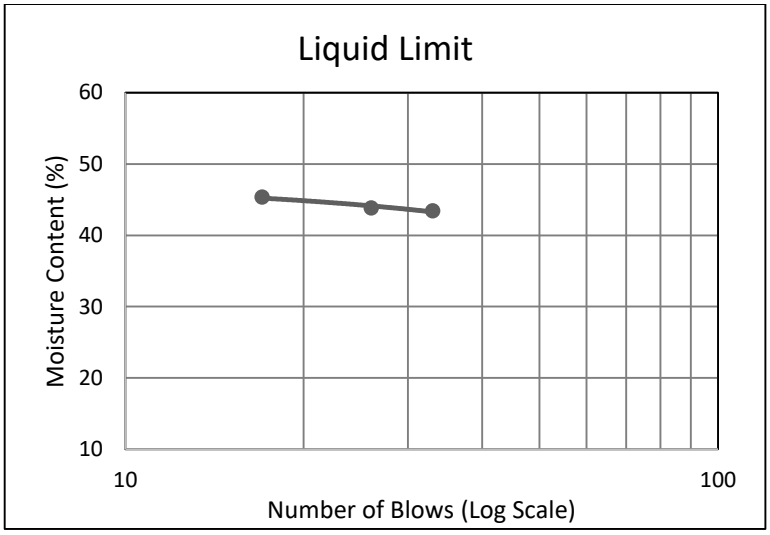

Figure B-2: Liquid Limit Chart of TP1-2

TP2-1 Test Result

Table B-3: Atterberg Limits Analysis of TP2-1

	Liquid Limit			Plastic Limit	
No. Blows	33	25	17		
Wt.of cont. + wet soil (gm)	47.259	47.534	47.691	16.780	16.680
Wt.of cont. + dry soil (gm)	39.000	38.881	38.915	15.990	15.930
Wt. of water (gm)	8.26	8.65	8.78	0.69	0.63
Wt. container (gm)	22.246	21.816	22.027	14.071	14.160
Wt. dry soil (gm)	16.75	17.07	16.89	1.91	1.76
Water (%)	49.30	50.71	51.97	35.70	36.30
		LL=50.5		**PL=36.0**	

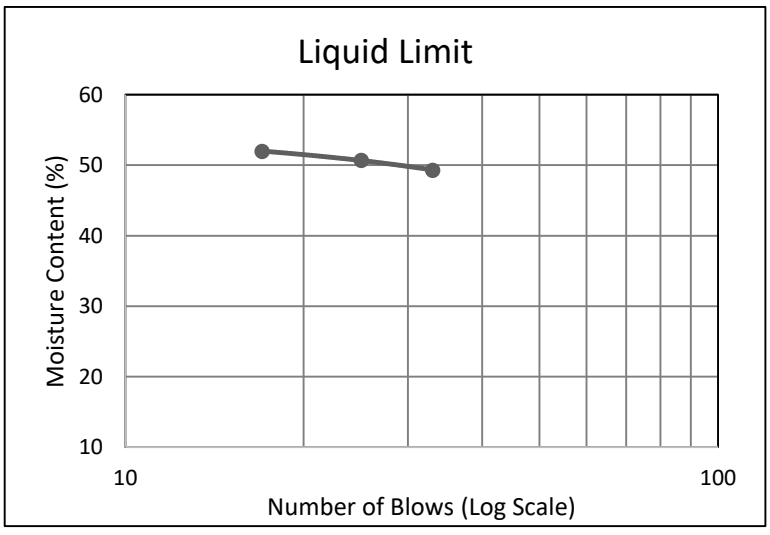

Figure B-3: Liquid Limit Chart of TP2-1

TP2-2 Test Result

Table B-4: Atterberg Limits Analysis of TP2-2

	Liquid Limit			Plastic Limit	
No. Blows	33	25	18		
Wt.of cont. + wet soil (gm)	48.163	48.489	48.721	16.110	16.189
Wt.of cont. + dry soil (gm)	39.745	39.757	39.894	15.473	15.585
Wt. of water (gm)	8.42	8.73	8.83	0.65	0.38
Wt. container (gm)	21.998	21.846	21.872	14.177	14.227
Wt. dry soil (gm)	17.75	17.91	18.02	1.30	1.32
Water (%)	47.43	48.75	48.98	49.15	28.07
		LL=48.4		**PL=38.6**	

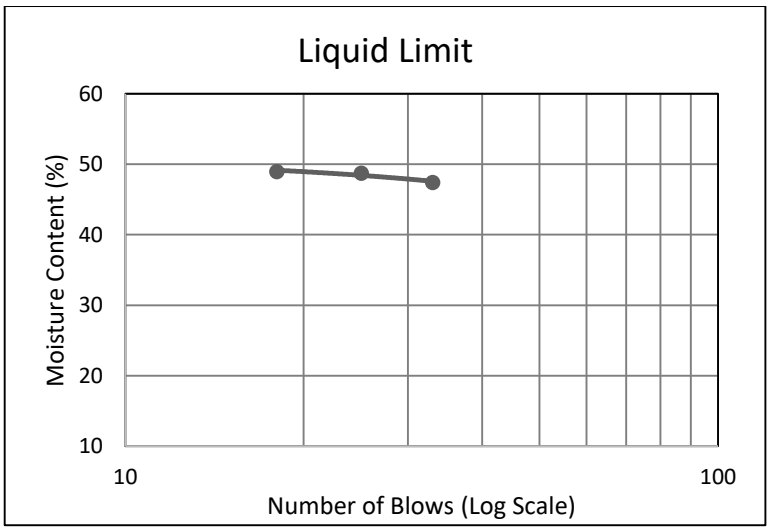

Figure B-4: Liquid Limit Chart of TP2-2

TP3-1 Test Result

Table B-5: Atterberg Limits Analysis of TP3-1

	Liquid Limit			Plastic Limit	
No. Blows	33	25	17		
Wt.of cont. + wet soil (gm)	48.350	48.661	48.927	16.220	16.313
Wt.of cont. + dry soil (gm)	39.728	39.587	39.696	15.661	15.828
Wt. of water (gm)	8.62	9.07	9.23	0.56	0.48
Wt. container (gm)	22.932	21.676	21.777	14.214	14.530
Wt. dry soil (gm)	16.80	17.91	17.92	1.45	1.30
Water (%)	51.33	50.66	51.52	38.63	37.37
		LL=51.0		**PL=38.0**	

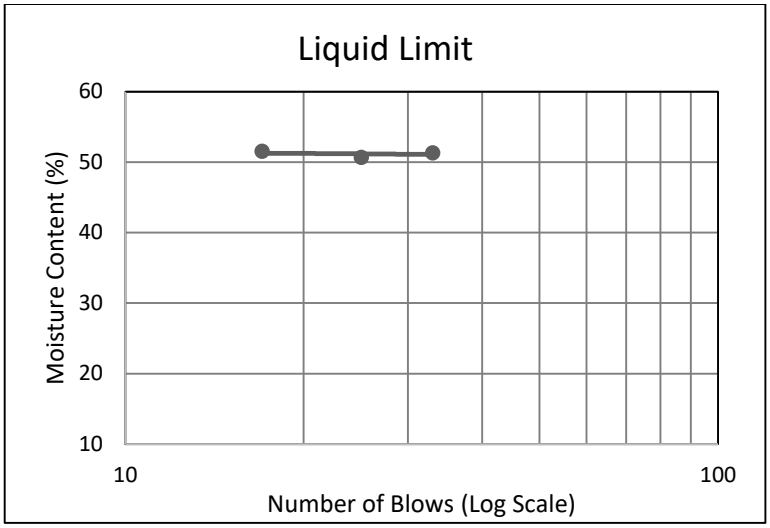

Figure B-5: Liquid Limit Chart of TP3-1

TP3-2 Test Result

Table B-6: Atterberg Limits Analysis of TP3-2

	Liquid Limit			Plastic Limit	
No. Blows	33	27	16		
Wt.of cont. + wet soil (gm)	46.180	46.630	46.997	16.332	16.270
Wt.of cont. + dry soil (gm)	38.153	38.107	38.009	15.627	15.741
Wt. of water (gm)	8.03	8.52	8.99	0.71	0.53
Wt. container (gm)	22.109	21.767	21.886	13.773	14.223
Wt. dry soil (gm)	16.04	16.34	16.12	1.85	1.52
Water (%)	50.03	52.16	55.75	38.03	34.85
		LL=52.7		**PL=36.4**	

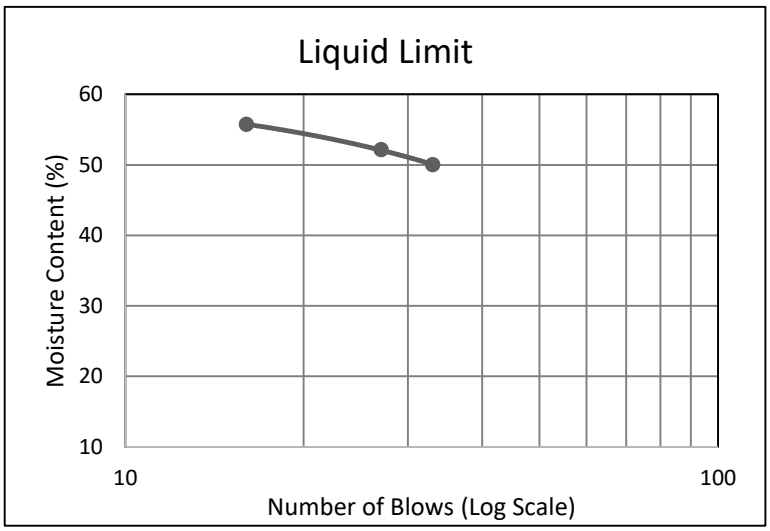

Figure B-6: Liquid Limit Chart of TP3-2

TP4-1 Test Result

Table B-7: Atterberg Limits Analysis of TP4-1

	Liquid Limit			Plastic Limit	
No. Blows	34	26	18		
Wt.of cont. + wet soil (gm)	49.234	49.561	49.837	16.230	16.030
Wt.of cont. + dry soil (gm)	39.814	39.629	39.750	15.730	15.530
Wt. of water (gm)	9.42	9.93	10.09	0.50	0.50
Wt. container (gm)	21.947	21.491	21.796	14.400	14.200
Wt. dry soil (gm)	17.87	18.14	17.95	1.33	1.33
Water (%)	52.72	54.76	56.18	37.59	37.59
		LL=55.6		**PL=37.6**	

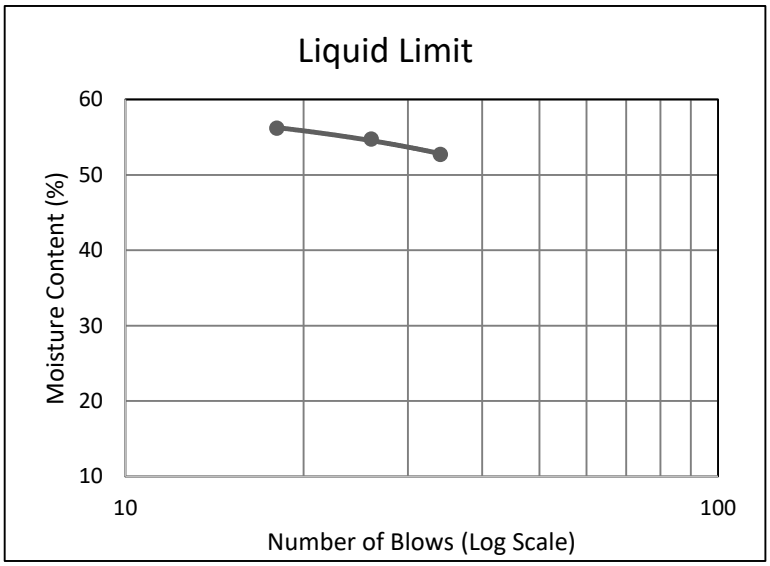

Figure B-7: Liquid Limit Chart of TP4-1

TP4-2 Test Result

Table B-8: Atterberg Limits Analysis of TP4-2

	Liquid Limit			Plastic Limit	
No. Blows	33	27	16		
Wt.of cont. + wet soil (gm)	47.369	47.426	47.733	16.850	16.950
Wt.of cont. + dry soil (gm)	38.777	38.657	38.849	16.170	16.190
Wt. of water (gm)	8.59	8.77	8.88	0.68	0.76
Wt. container (gm)	21.473	21.599	22.063	14.390	14.110
Wt. dry soil (gm)	17.30	17.06	16.79	1.78	2.08
Water (%)	49.65	51.41	52.93	38.20	36.54
		LL=51.5		**PL=37.4**	

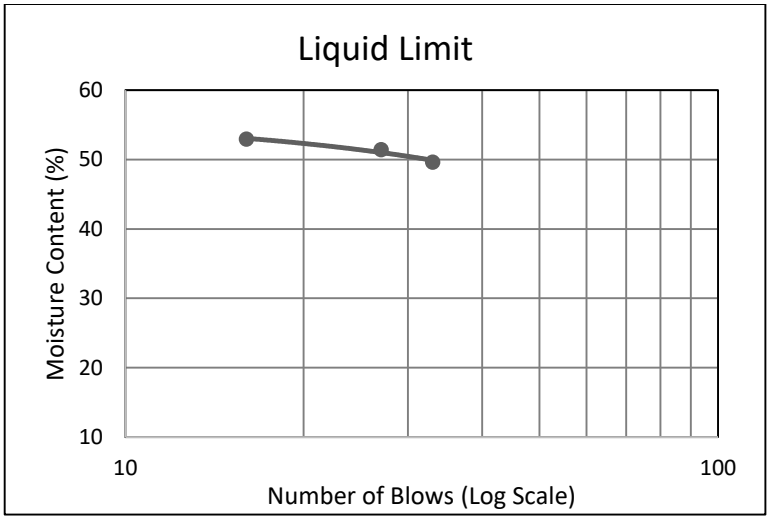

Figure B-8: Liquid Limit Chart of TP4-2

TP5-1 Test Result

Table B-9: Atterberg Limits Analysis of TP5-1

	Liquid Limit			**Plastic Limit**	
No. Blows	31	26	21		
Wt.of cont. + wet soil (gm)	45.42	45.38	45.15	16.332	16.495
Wt.of cont. + dry soil (gm)	37.22	38.01	37.61	15.693	15.846
Wt. of water (gm)	8.20	7.37	7.54	0.64	0.37
Wt. container (gm)	21.78	24.45	23.88	14.046	14.878
Wt. dry soil (gm)	15.43	13.56	13.73	1.65	0.97
Water (%)	53.12	54.33	54.95	38.80	38.22
		LL=54.2		**PL=38.5**	

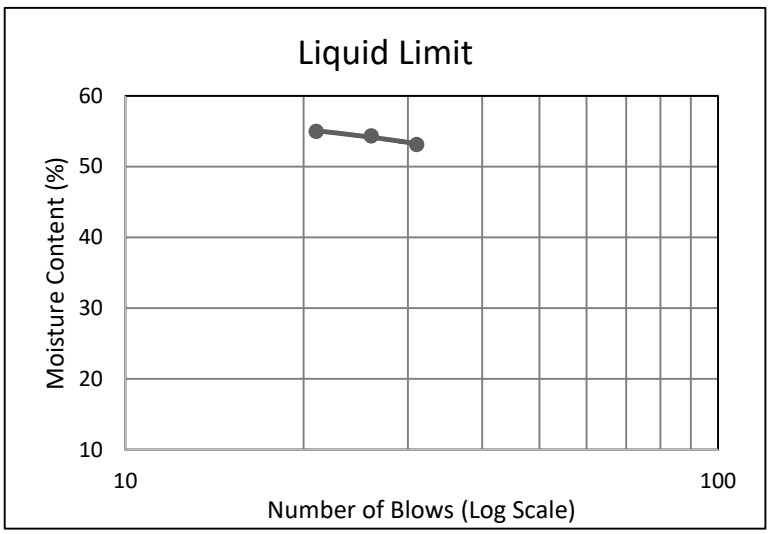

Figure B-9: Liquid Limit Chart of TP5-1

TP5-2 Test Result

Table B-10: Atterberg Limits Analysis of TP5-2

	Liquid Limit			Plastic Limit	
No. Blows	30	25	20		
Wt.of cont. + wet soil (gm)	43.40	43.80	43.87	16.340	16.481
Wt.of cont. + dry soil (gm)	35.64	35.83	35.87	15.693	15.846
Wt. of water (gm)	7.76	7.97	8.00	0.65	0.38
Wt. container (gm)	21.72	21.88	22.00	14.046	14.878
Wt. dry soil (gm)	13.92	13.95	13.87	1.65	0.97
Water (%)	55.76	57.11	57.68	38.80	38.20
	LL=56.2			**PL=38.4**	

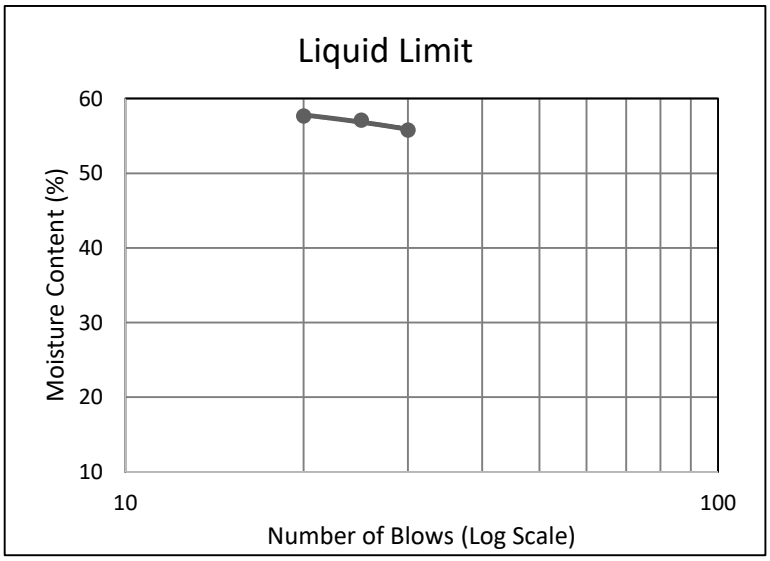

Figure B-10: Liquid Limit Chart of TP5-2

TP6-1 Test Result

Table B-11: Atterberg Limits Analysis of TP6-1

	Liquid Limit			Plastic Limit	
No. of blows	34	26	18		
Mass of cont. + wet soil (g)	49.07	49.49	49.68	16.20	15.94
Mass of cont. + dry soil (g)	39.85	39.99	39.88	15.63	15.29
Mass of water (g)	9.21	9.50	9.80	0.57	0.65
Mass of container (g)	21.66	21.84	21.97	14.11	13.52
Mass of dry soil (g)	18.20	18.15	17.92	1.52	1.77
Water Content (%)	50.64	52.36	54.71	37.50	36.72
	LL=53.7			**PL=37.1**	

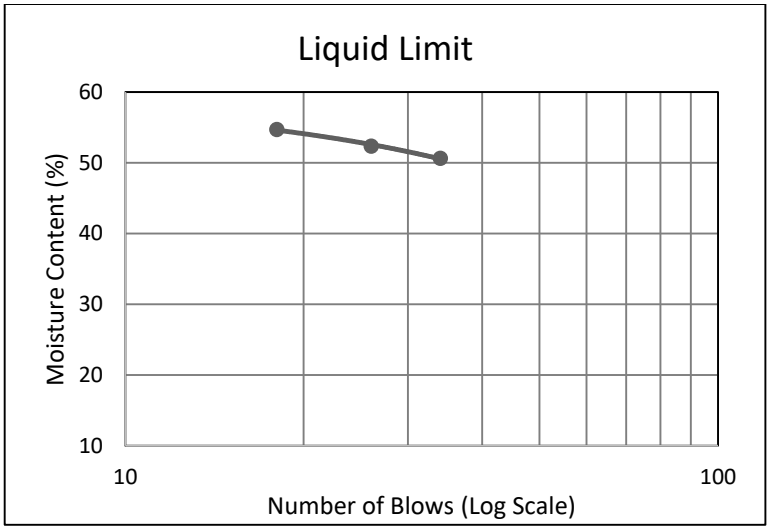

Figure B-11: Liquid Limit Chart of TP6-1

TP6-2 Test Result

Table B-12: Atterberg Limits Analysis of TP6-2

	Liquid Limit			Plastic Limit	
No. Blows	33	25	18		
Wt.of cont. + wet soil (gm)	48.163	48.489	48.721	16.560	16.470
Wt.of cont. + dry soil (gm)	39.745	39.757	39.894	15.880	15.830
Wt. of water (gm)	8.42	8.73	8.83	0.68	0.64
Wt. container (gm)	21.998	21.846	21.872	14.070	14.170
Wt. dry soil (gm)	17.75	17.91	18.02	1.91	1.76
Water (%)	47.43	48.75	48.98	35.60	36.36
	LL=48.3			**PL=36.0**	

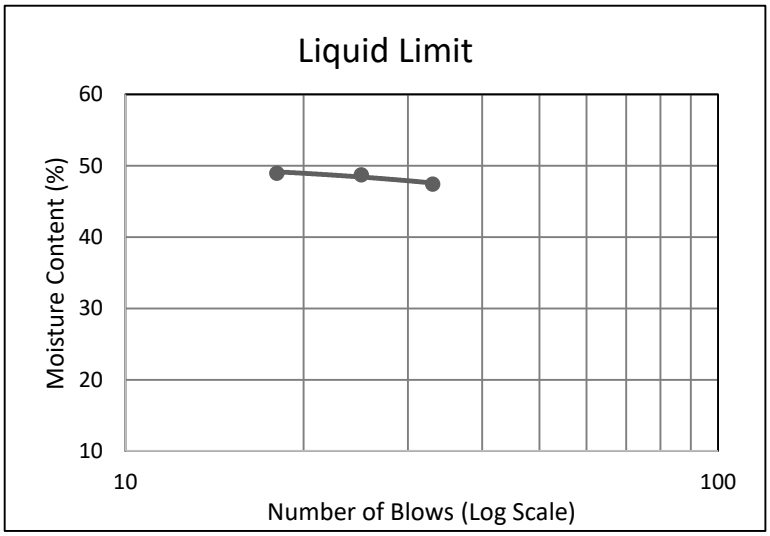

Figure B-12: Liquid Limit Chart of TP6-2

TP7-1 Test Result

Table B-13: Atterberg Limits Analysis of TP7-1

	Liquid Limit			Plastic Limit	
No. Blows	32	26	19		
Wt.of cont. + wet soil (gm)	44.020	44.253	44.478	16.503	16.773
Wt.of cont. + dry soil (gm)	37.454	37.583	37.396	15.929	16.199
Wt. of water (gm)	6.57	6.67	7.08	0.57	0.57
Wt. container (gm)	21.740	21.918	21.622	14.095	14.379
Wt. dry soil (gm)	15.71	15.67	15.77	1.83	1.82
Water (%)	41.78	42.58	44.90	31.30	31.54
	LL=42.9			**PL=31.4**	

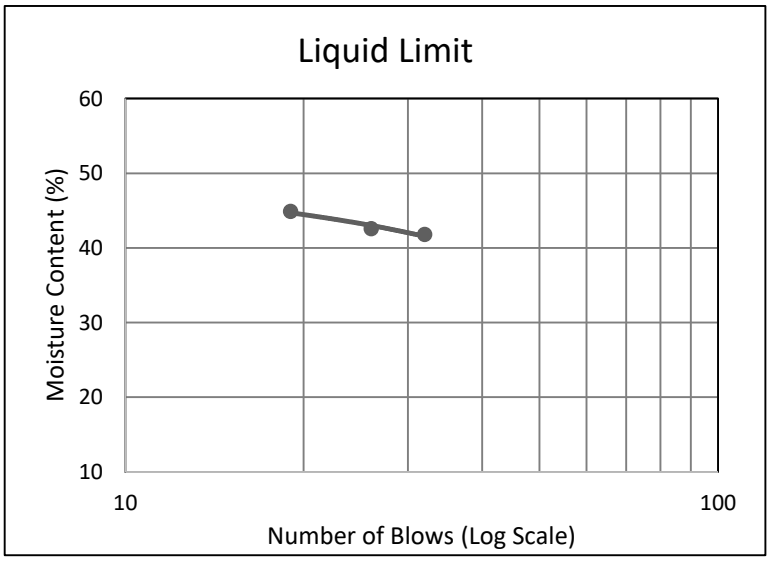

Figure B-13: Liquid Limit Chart of TP7-1

TP7-2 Test Result

Table B-14: Atterberg Limits Analysis of TP7-2

	Liquid Limit			Plastic Limit	
No. Blows	33	27	16		
Wt.of cont. + wet soil (gm)	48.330	48.540	48.900	16.800	16.770
Wt.of cont. + dry soil (gm)	41.040	40.930	40.890	16.090	16.090
Wt. of water (gm)	7.29	7.61	8.01	0.71	0.68
Wt. container (gm)	21.870	21.860	21.760	14.100	14.200
Wt. dry soil (gm)	19.17	19.07	19.13	1.99	1.89
Water (%)	38.03	39.91	41.87	35.68	35.98
	LL=40.3			**PL=35.8**	

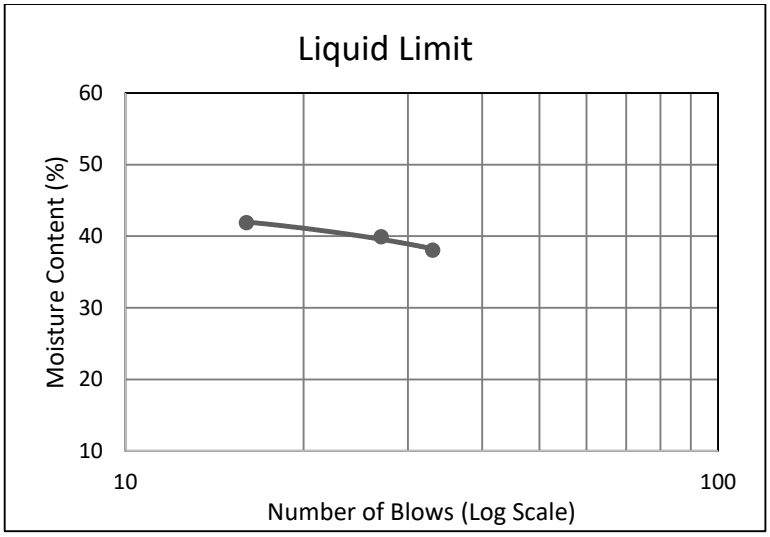

Figure B-14: Liquid Limit Chart of TP7-2

TP8 Test Result

Table B-15: Atterberg Limits Analysis of TP8

	Liquid Limit			**Plastic Limit**	
No. Blows	33	25	18		
Wt.of cont. + wet soil (gm)	49.290	49.310	49.280	16.332	16.495
Wt.of cont. + dry soil (gm)	39.500	39.160	38.820	15.693	15.846
Wt. of water (gm)	9.79	10.15	10.46	0.64	0.37
Wt. container (gm)	21.750	21.570	21.800	14.046	14.878
Wt. dry soil (gm)	17.75	17.59	17.02	1.65	0.97
Water (%)	55.15	57.70	61.46	38.80	38.22
	LL=57.9			**PL=38.4**	

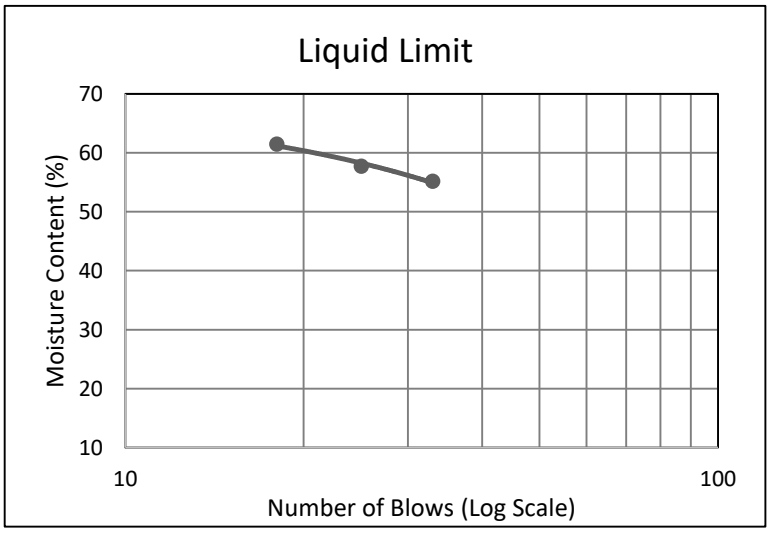

Figure B-15: Liquid Limit Chart of TP8

TP9-1 Test Result

Table B-16: Atterberg Limits Analysis of TP9-1

	Liquid Limit			Plastic Limit	
No. Blows	32	26	17		
Wt.of cont. + wet soil (gm)	46.358	46.608	46.829	16.230	16.030
Wt.of cont. + dry soil (gm)	38.157	37.985	38.013	15.730	15.530
Wt. of water (gm)	8.20	8.62	8.82	0.50	0.50
Wt. container (gm)	21.870	21.712	21.969	14.400	14.200
Wt. dry soil (gm)	16.29	16.27	16.04	1.33	1.33
Water (%)	50.35	52.99	54.95	37.59	37.59
	LL=52.7			**PL=37.6**	

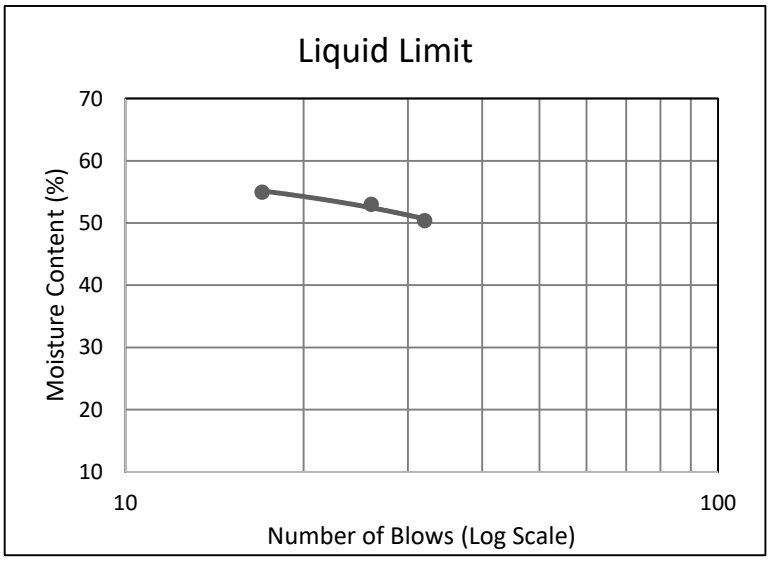

Figure B-16: Liquid Limit Chart of TP9-1

TP9-2 Test Result

Table B-17: Atterberg Limits Analysis of TP9-2

			Liquid Limit		Plastic Limit
No. Blows	32	27	22		
Wt.of cont. + wet soil (gm)	46.526	46.485	46.262	16.220	16.313
Wt.of cont. + dry soil (gm)	38.317	38.052	37.710	15.661	15.828
Wt. of water (gm)	8.21	8.43	8.55	0.56	0.48
Wt. container (gm)	21.898	21.710	21.511	14.214	14.530
Wt. dry soil (gm)	16.42	16.34	16.20	1.45	1.30
Water (%)	50.00	51.60	52.79	38.63	37.37
			LL=51.7		PL=38.0

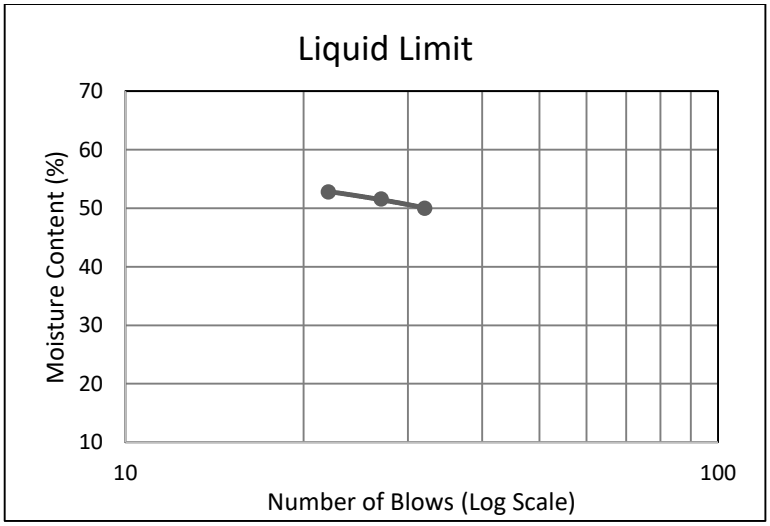

Figure B-17: Liquid Limit Chart of TP9-2

TP10 Test Result

Table B-18: Atterberg Limits Analysis of TP10

	Liquid Limit			**Plastic Limit**	
No. Blows	33	27	23		
Wt.of cont. + wet soil (gm)	44.96	44.60	44.77	16.198	16.586
Wt.of cont. + dry soil (gm)	36.85	36.46	36.58	15.655	15.913
Wt. of water (gm)	8.11	8.14	8.20	0.54	0.67
Wt. container (gm)	21.83	21.61	21.93	14.215	14.199
Wt. dry soil (gm)	15.03	14.85	14.65	1.44	1.71
Water (%)	53.95	54.83	55.95	37.71	39.26
	LL=56.2			**PL=38.4**	

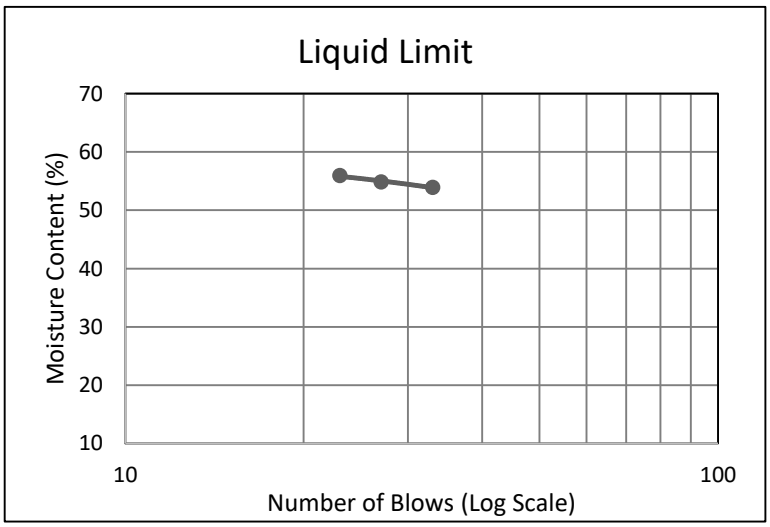

Figure B-18: Liquid Limit Chart of TP10

TP11-1 Test Result

Table B-19: Atterberg Limits Analysis of TP11-1

	Liquid Limit			Plastic Limit	
No. Blows	33	26	16		
Wt.of cont. + wet soil (gm)	48.470	48.610	48.850	16.857	16.739
Wt.of cont. + dry soil (gm)	41.190	40.760	40.450	16.138	16.067
Wt. of water (gm)	7.28	7.85	8.40	0.72	0.67
Wt. container (gm)	23.310	21.800	21.750	14.084	14.108
Wt. dry soil (gm)	17.88	18.96	18.70	2.05	1.96
Water (%)	40.72	41.40	44.92	35.00	34.30
	LL=42.5			**PL=34.7**	

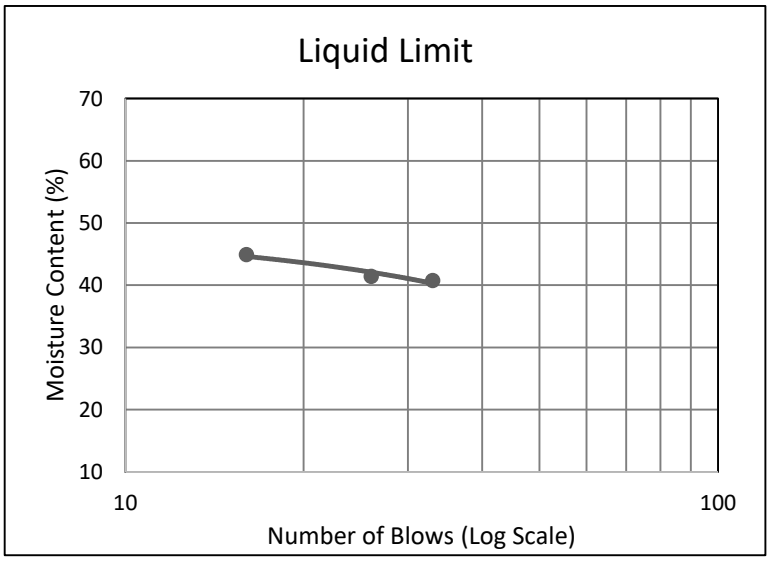

Figure B-19: Liquid Limit Chart of TP11-1

TP11-2 Test Result

Table B-20: Atterberg Limits Analysis of TP11-2

	Liquid Limit			Plastic Limit	
No. Blows	33	25	17		
Wt.of cont. + wet soil (gm)	47.387	47.397	47.603	16.617	16.853
Wt.of cont. + dry soil (gm)	37.989	37.939	37.911	15.960	16.097
Wt. of water (gm)	9.40	9.46	9.69	0.66	0.76
Wt. container (gm)	21.594	21.840	21.891	14.281	14.189
Wt. dry soil (gm)	16.40	16.10	16.02	1.68	1.91
Water (%)	57.32	58.75	60.50	39.13	39.62
	LL=59.0			**PL=39.4**	

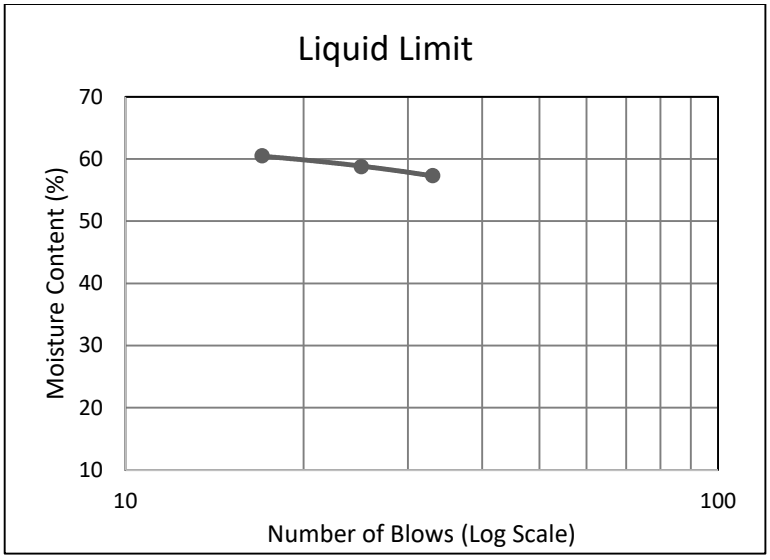

Figure B-20: Liquid Limit Chart of TP11-2

APPENDIX C: DIRECT SHEAR TEST GRAPHS

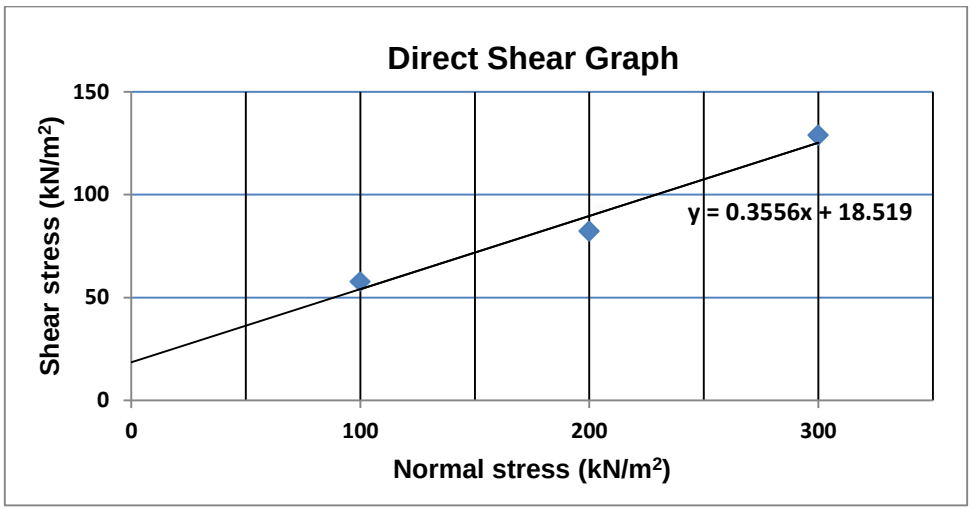

Figure C-1: Direct Shear Test Graph of TP1-1

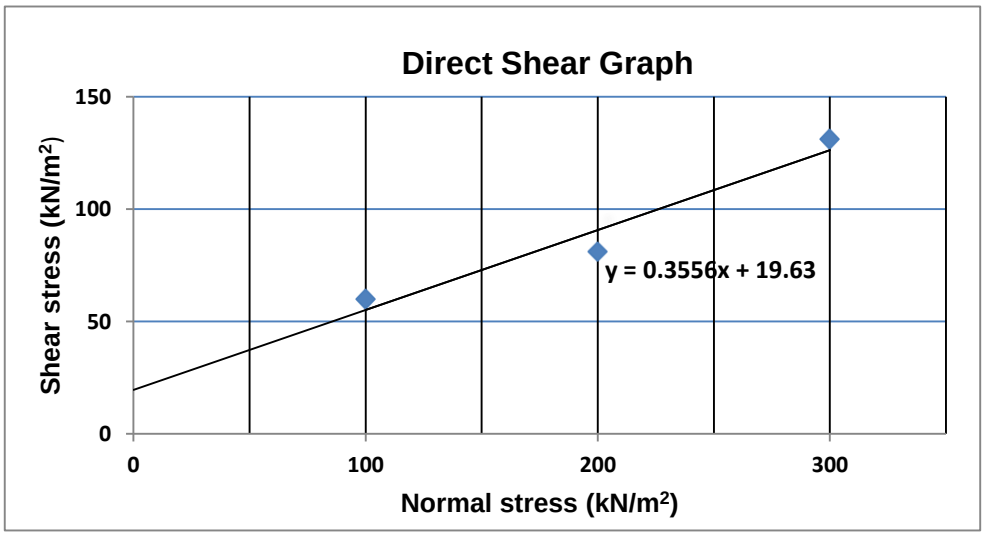

Figure C-2: Direct Shear Test Graph of TP1-2

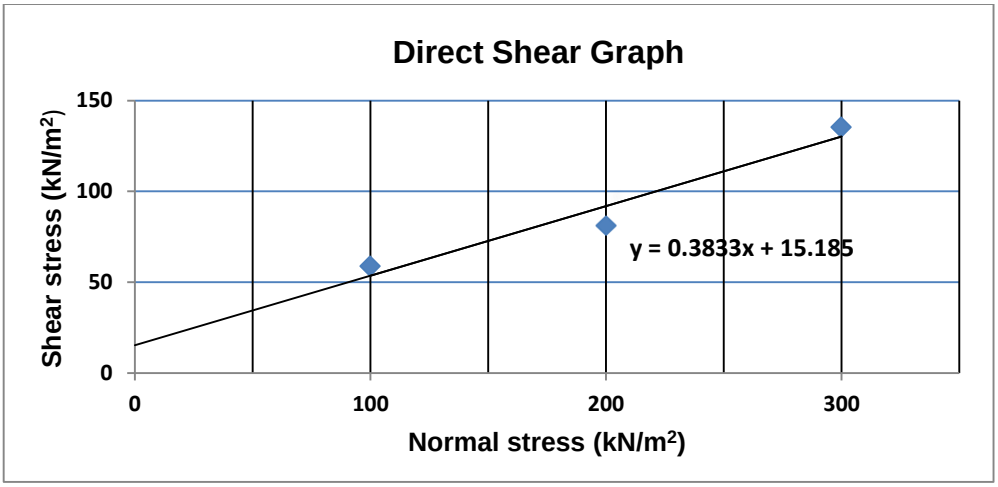

Figure C-3: Direct Shear Test Graph of TP2-1

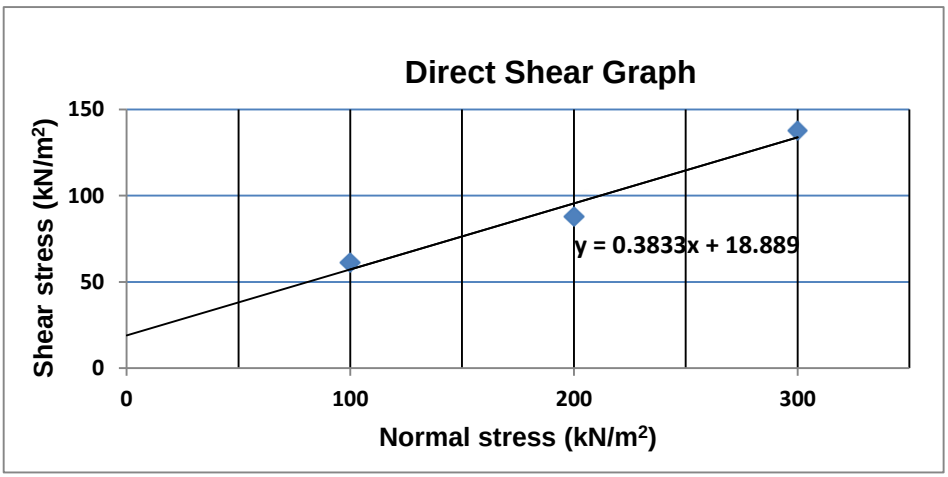

Figure C-4: Direct Shear Test Graph of TP2-2

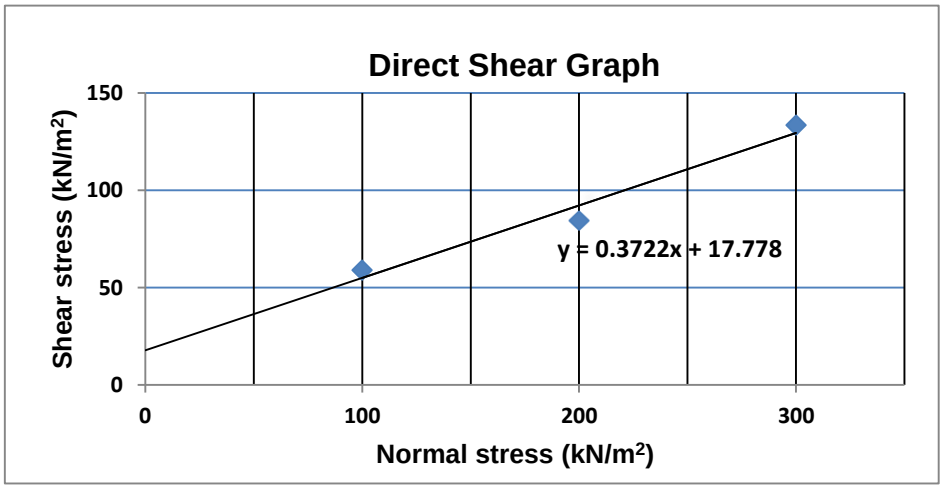

Figure C-5: Direct Shear Test Graph of TP3-1

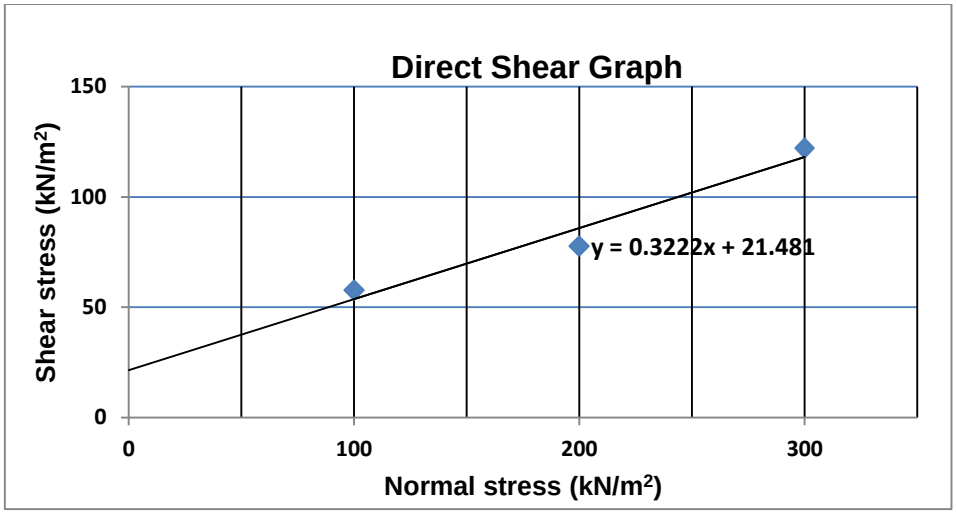

Figure C-6: Direct Shear Test Graph of TP3-2

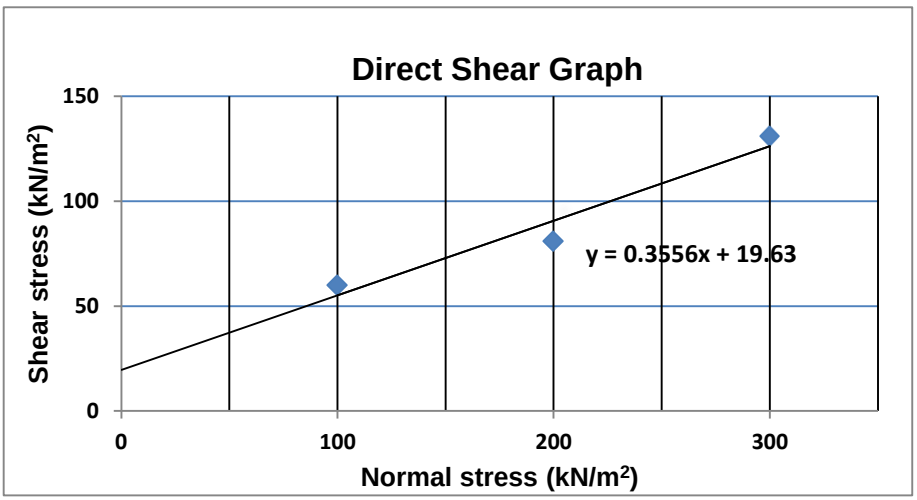

Figure C-7: Direct Shear Test Graph of TP4-1

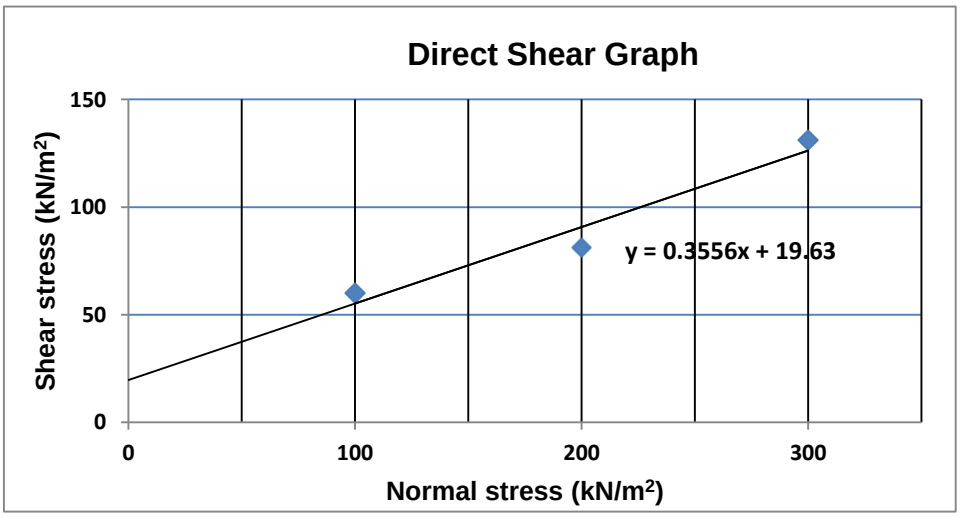

Figure C-8: Direct Shear Test Graph of TP4-2

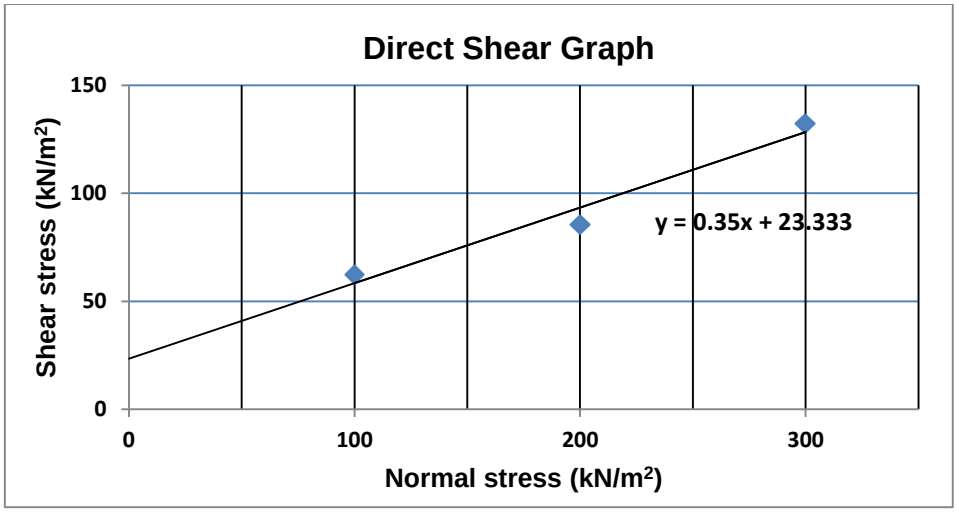

Figure C-9: Direct Shear Test Graph of TP5-1

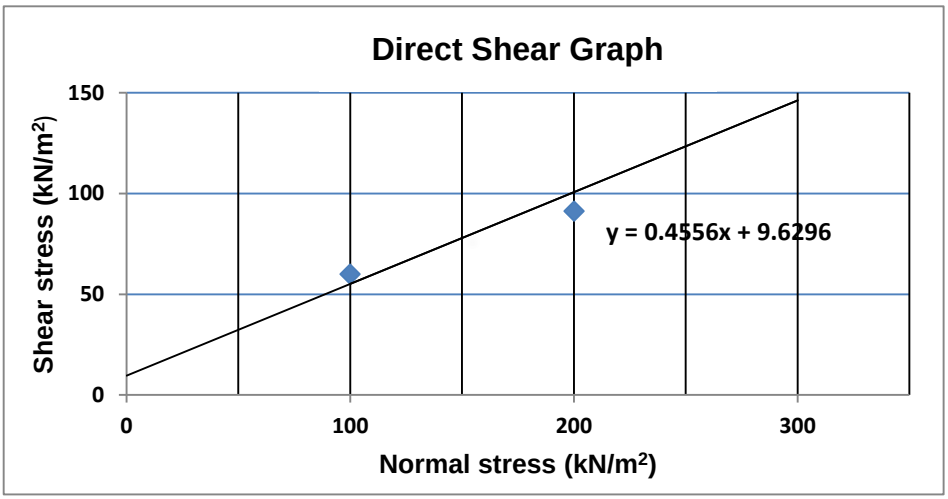

Figure C-10: Direct Shear Test Graph of TP5-2

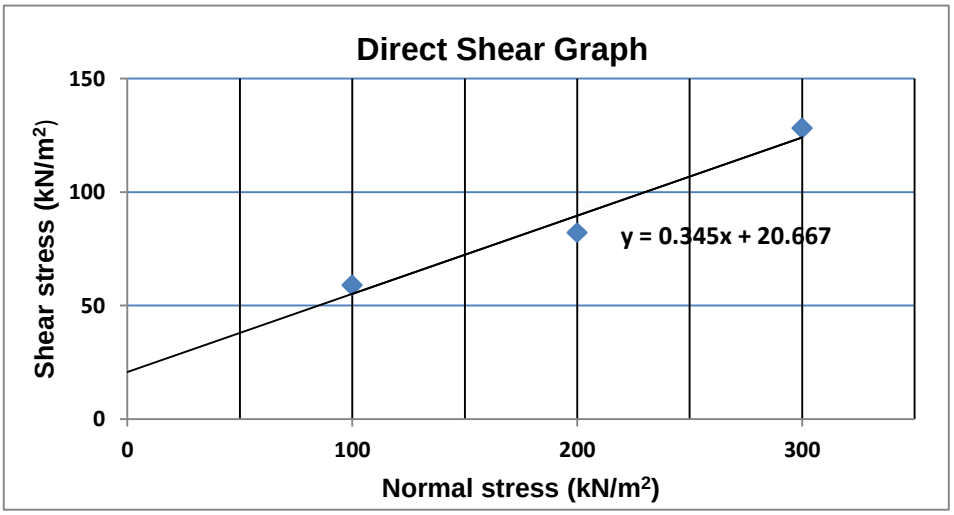

Figure C-11: Direct Shear Test Graph of TP6-1

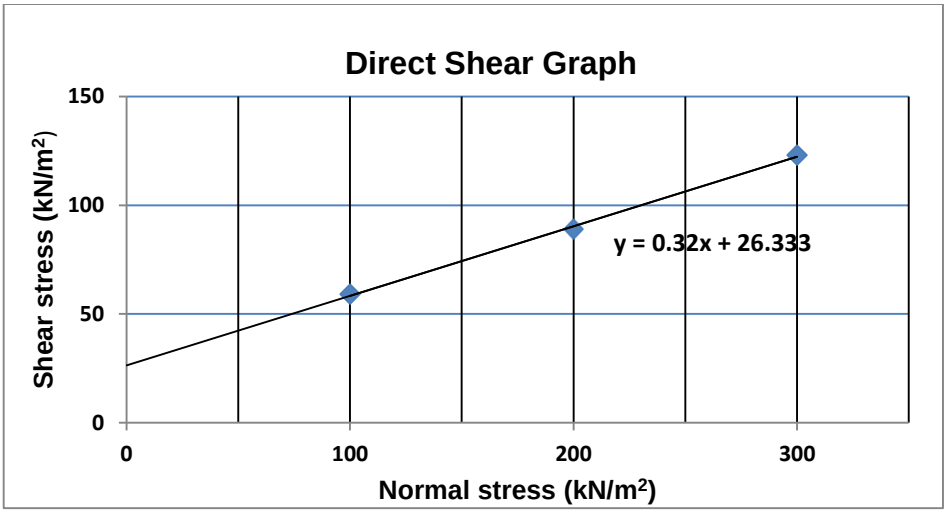

Figure C-12: Direct Shear Test Graph of TP6-2

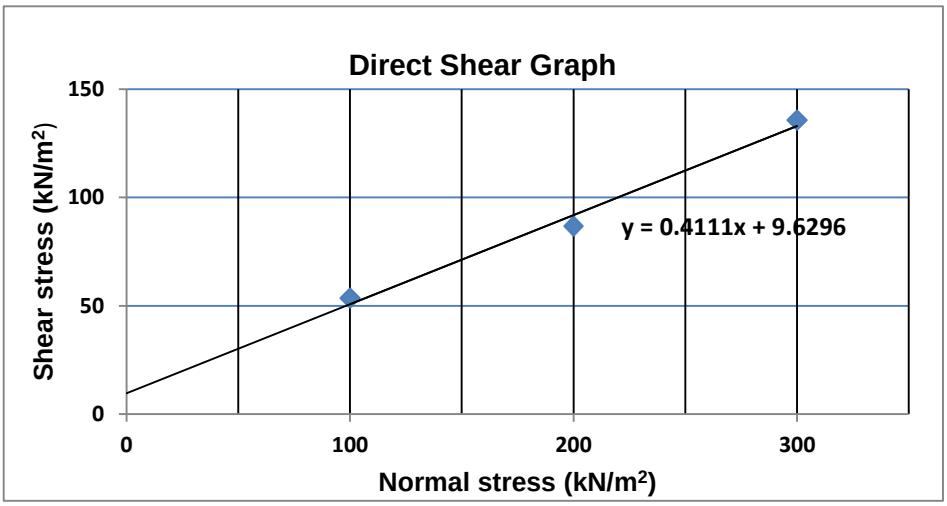

Figure C-13: Direct Shear Test Graph of TP7-1

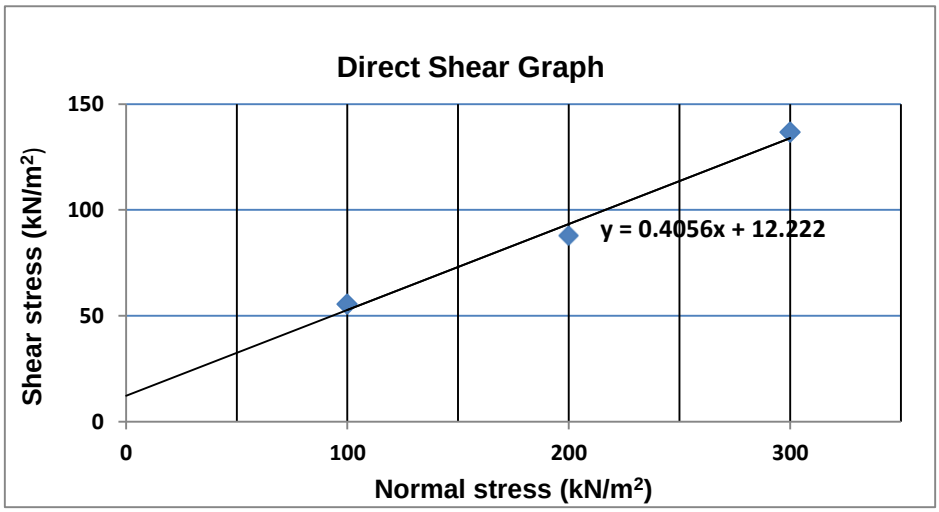

Figure C-14: Direct Shear Test Graph of TP7-2

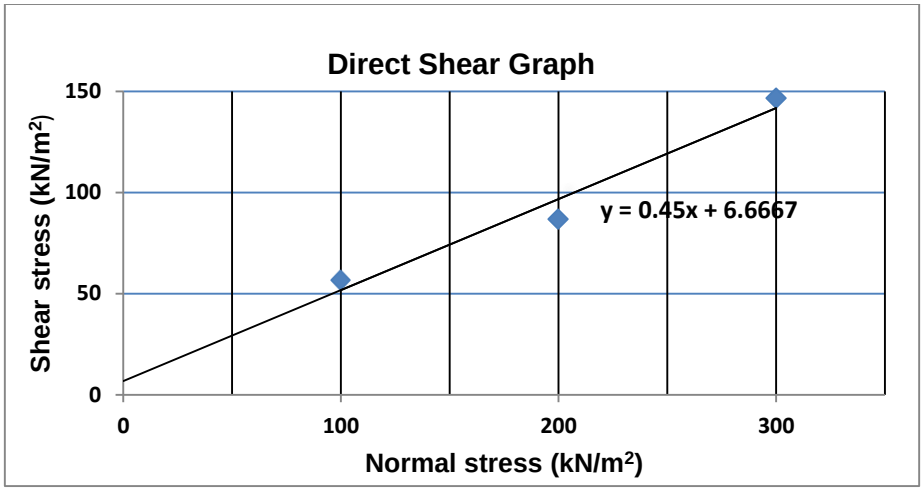

Figure C-15: Direct Shear Test Graph of TP8

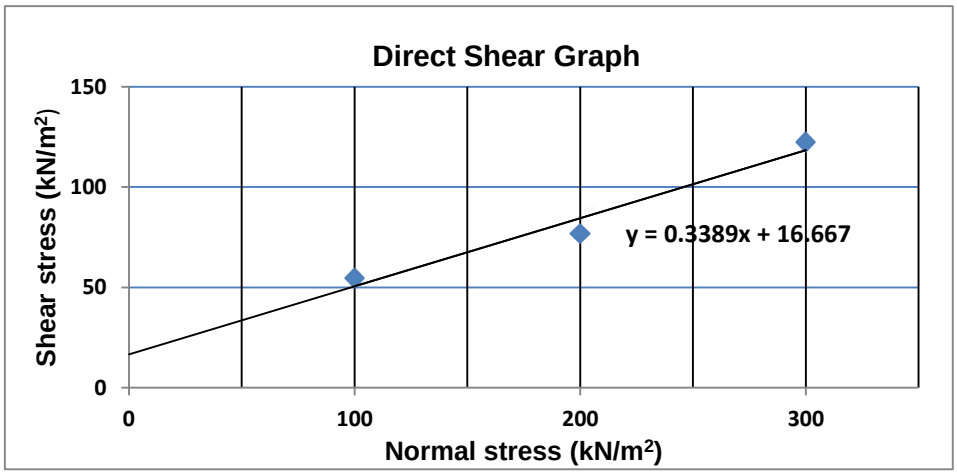

Figure C-16: Direct Shear Test Graph of TP9-1

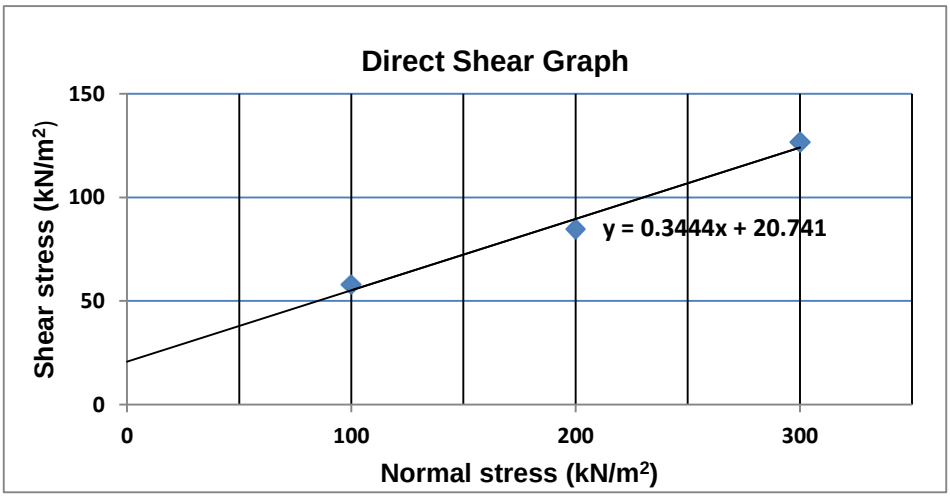

Figure C-17: Direct Shear Test Graph of TP9-2

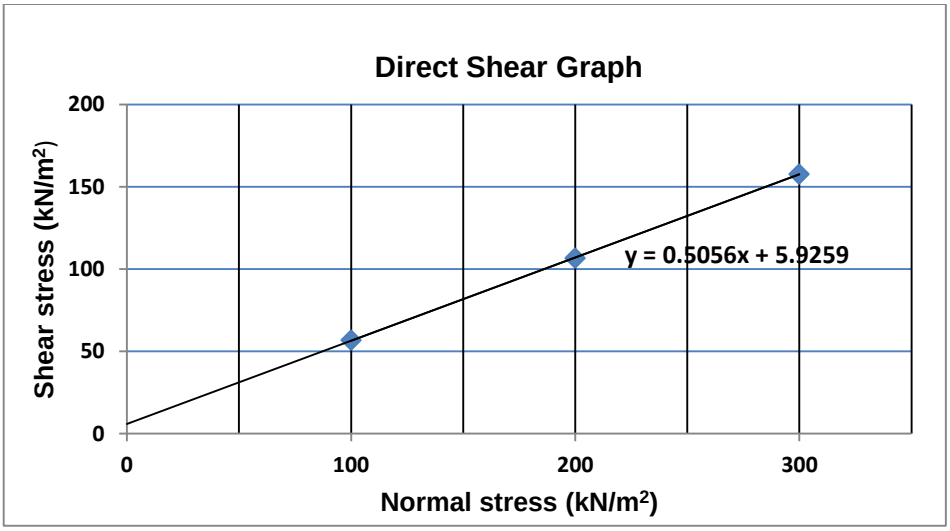

Figure C-18: Direct Shear Test Graph of TP10

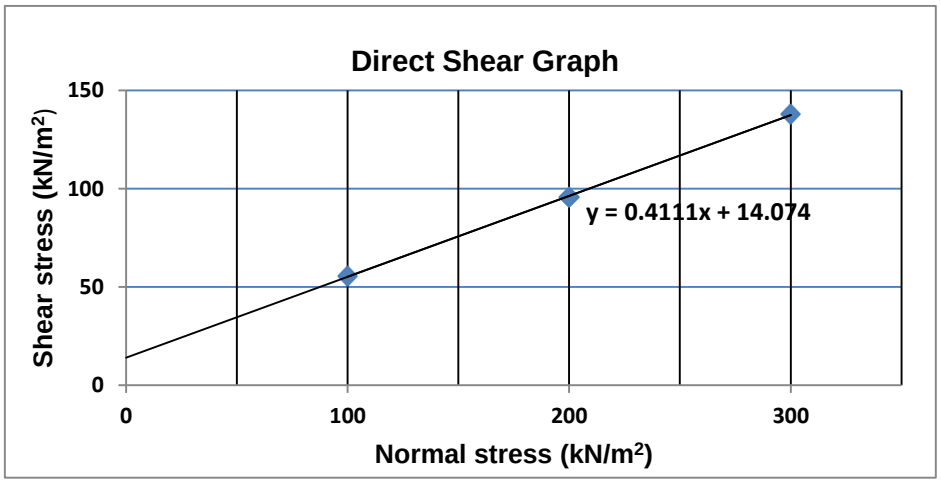

Figure C-19: Direct Shear Test Graph of TP11-1

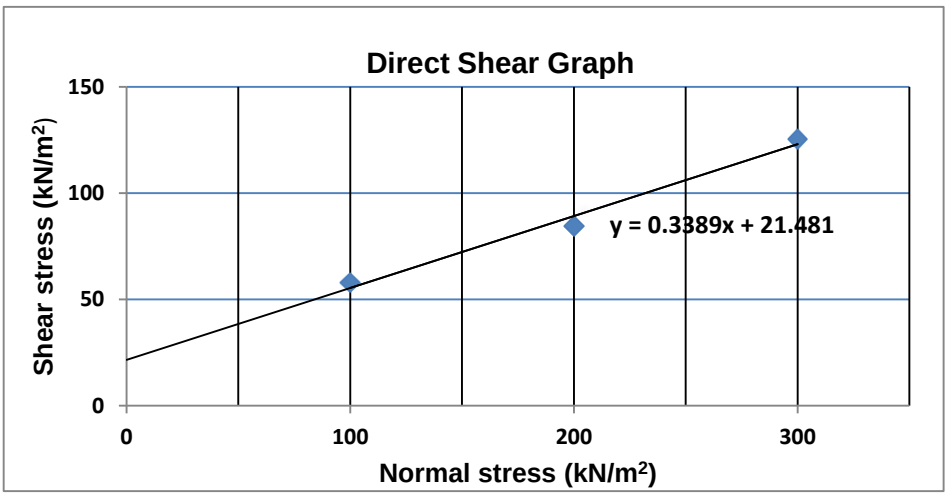

Figure C-20: Direct Shear Test Graph of TP11-2

APPENDIX D: SECONDARY DATA SUMMARY

Table D-1: Secondary data summary

No.	Grain size %		Atterberg Limit		NMC	BD (g/cm^3)	C (kPa)	ϕ (°)
	Sand %	Fine %	LL	PI				
1	13.0	87.0	58.0	23.3	17.5	1.821	12.0	18.0
2	34.0	66.0	53.5	20.6	16.3	1.833	15.0	16.0
3	26.0	74.0	54.4	19.7	17.7	1.846	13.0	16.0
4	15.0	85.0	46.5	12.7	16.8	1.851	13.0	20.0
5	9.0	91.0	47.0	15.7	18.5	1.811	18.0	19.0
6	10.0	90.0	57.0	25.4	16.3	1.829	14.0	21.0
7	13.0	87.0	42.0	16.4	14.7	1.825	16.0	16.0
8	22.0	78.0	41.4	12.8	16.5	1.834	18.0	15.0
9	16.0	84.0	51.2	15.7	18.6	1.841	16.0	19.0
10	24.0	76.0	57.5	21.1	17.4	1.866	15.0	18.0
11	21.0	79.0	41.1	13.7	13.6	1.832	11.0	19.0
12	16.0	84.0	61.2	25.4	19.9	1.848	23.0	19.0
13	21.0	79.0	71.4	29.1	22.6	1.855	21.0	19.0
14	18.0	82.0	68.6	29.0	19.3	1.858	17.0	20.0
15	29.0	71.0	62.4	27.5	18.7	1.846	21.0	19.0
16	31.0	61.0	63.1	27.0	17.6	1.846	12.0	21.0
17	28.0	72.0	64.5	29.3	18.6	1.858	17.0	19.0
18	27.0	73.0	65.2	28.2	19.9	1.864	16.0	20.0
19	17.0	83.0	65.4	29.1	21.1	1.839	14.0	20.0
20	29.0	71.0	50.2	21.7	17.6	1.842	17.0	18.0
21	19.0	81.0	43.9	13.4	13.7	1.841	14.0	18.0
22	21.0	79.0	51.7	12.7	18.5	1.847	17.0	18.0
23	17.0	83.0	61.2	23.8	19.5	1.822	16.0	19.0
24	12.0	53.0	60.8	26.6	18.8	1.849	13.0	19.0
25	20.0	80.0	51.3	20.5	13.7	1.835	12.0	20.0
26	16.0	84.0	43.3	17.0	14.4	1.843	14.0	22.0
27	13.0	87.0	56.4	23.7	19.0	1.798	18.0	20.0
28	16.0	84.0	60.0	28.9	20.2	1.768	14.0	16.0
29	20.0	80.0	42.0	12.7	16.7	1.811	14.0	20.0
30	18.0	82.0	36.4	12.1	14.4	1.821	17.0	20.0
31	23.0	77.0	42.9	14.4	17.4	1.846	17.0	20.0
32	21.0	79.0	64.1	29.0	16.6	1.839	15.0	21.0
33	32.0	68.0	42.0	14.2	13.7	1.840	15.0	21.0
34	23.0	77.0	41.9	14.7	15.4	1.871	11.0	22.0
35	25.0	75.0	53.5	15.5	17.8	1.847	13.0	20.0

36	28.0	72.0	53.7	21.7	17.0	1.825	18.0	20.0
37	29.0	71.0	48.6	13.1	15.6	1.836	9.0	19.0
38	33.0	67.0	67.6	26.4	20.0	1.846	16.0	21.0
39	12.0	88.0	67.3	25.7	21.5	1.871	21.0	19.0
40	16.0	56.0	46.6	9.2	16.9	1.842	21.0	20.0
41	9.0	91.0	54.7	14.8	15.6	1.844	31.0	13.0
42	20.0	80.0	56.3	18.8	16.8	1.851	23.0	18.0
43	17.0	85.0	59.3	18.9	17.3	1.892	19.0	20.0
44	15.0	85.0	51.2	14.0	18.6	1.876	29.0	15.0
45	20.0	80.0	53.3	15.6	21.0	1.851	27.0	18.0
46	20.0	60.0	50.2	12.8	18.3	1.868	20.0	20.0
47	18.0	82.0	51.3	13.4	17.6	1.826	14.0	22.0
48	12.0	88.0	52.7	16.5	21.3	1.865	24.0	18.0
49	21.0	60.0	53.7	15.9	15.7	1.802	14.0	22.0
50	28.0	72.0	52.7	15.6	17.9	1.824	21.0	18.0
51	13.0	87.0	59.0	19.8	20.4	1.742	25.0	14.0
52	9.0	71.0	48.5	11.1	18.6	1.886	14.0	22.0
53	17.0	83.0	57.7	19.4	18.7	1.884	21.0	19.0
54	14.0	58.0	46.2	9.8	16.6	1.854	21.0	18.0
55	19.0	81.0	54.4	16.9	23.5	1.851	24.0	18.0
56	9.0	66.0	46.2	11.7	18.7	1.872	12.0	22.0
57	21.0	79.0	57.7	18.3	19.4	1.884	21.0	19.0
58	16.0	83.0	55.4	16.2	18.4	1.871	18.0	21.0
59	16.0	62.0	46.3	8.8	18.2	1.872	21.0	21.0
60	15.0	85.0	58.3	20.1	13.9	1.844	20.0	18.0
61	11.0	59.0	56.6	17.8	19.5	1.824	21.0	18.0
62	20.0	80.0	62.4	23.1	14.6	1.864	11.0	28.0
63	12.0	78.0	43.7	9.0	14.6	1.874	22.0	18.0
64	20.0	80.0	53.6	15.3	21.5	1.816	27.0	14.0
65	15.0	61.0	51.2	12.7	16.4	1.872	12.0	22.0
66	11.0	69.0	61.4	22.0	19.4	1.861	10.0	22.0
67	21.0	53.0	45.3	7.0	22.4	1.786	20.0	20.0
68	9.0	64.0	45.3	8.6	18.0	1.879	20.0	20.0
69	9.0	68.0	51.4	12.9	19.4	1.864	16.0	21.0
70	15.0	85.0	63.3	23.0	22.6	1.874	26.0	18.0
71	20.0	80.0	55.3	16.9	22.6	1.874	26.0	18.0
72	20.0	80.0	56.3	18.8	16.8	1.851	23.0	18.0
73	13.0	87.0	62.6	23.3	20.4	1.854	23.0	19.0
74	11.0	89.0	52.7	14.1	20.4	1.854	23.0	19.0
75	19.0	81.0	59.7	22.4	21.4	1.874	24.0	20.0
76	12.0	71.0	55.4	17.8	21.4	1.874	24.0	20.0
77	14.0	76.0	46.6	11.4	20.4	1.868	21.0	20.0
78	10.0	90.0	56.3	16.9	19.4	1.816	27.0	14.0

79	12.0	76.0	59.0	19.5	22.6	1.882	23.0	14.0
80	20.0	80.0	53.6	14.3	19.7	1.839	22.0	19.0
81	14.0	76.0	58.7	21.5	19.7	1.839	22.0	19.0
82	11.0	89.0	55.4	16.9	20.7	1.881	17.0	21.0
83	23.0	57.0	56.9	17.7	19.4	1.894	16.0	24.0
84	13.0	70.0	56.4	17.9	16.9	1.864	19.0	20.0
85	9.0	64.0	50.2	13.1	16.9	1.864	19.0	20.0
86	12.0	64.0	51.7	13.2	20.4	1.864	21.0	20.0
87	15.0	73.0	52.5	14.0	19.4	1.862	16.0	22.0
88	16.0	62.0	47.7	10.1	20.4	1.872	21.0	21.0
89	12.0	88.0	59.6	20.2	20.4	1.872	21.0	21.0
90	9.0	51.0	51.3	13.8	19.4	1.862	21.0	19.0
91	19.0	61.0	46.2	9.8	16.6	1.854	6.0	30.0
92	12.0	88.0	55.9	17.8	16.6	1.854	21.0	18.0
93	15.0	66.0	52.7	15.5	18.4	1.872	12.0	22.0
94	12.0	88.0	51.7	13.7	21.0	1.862	21.0	19.0
95	9.0	51.0	58.6	21.1	21.6	1.857	23.0	19.0
96	20.0	59.0	53.6	16.1	17.4	1.855	17.0	19.0
97	21.0	53.0	47.9	11.7	19.7	1.869	10.0	25.0
98	12.0	88.0	59.5	19.8	19.0	1.852	21.0	19.0
99	12.0	88.0	48.6	11.3	18.4	1.852	28.0	18.0
100	11.0	89.0	63.6	22.3	23.5	1.861	24.0	19.0
101	13.0	87.0	52.7	16.3	23.5	1.861	24.0	19.0
102	14.0	71.0	51.7	13.5	20.3	1.862	23.0	19.0
103	9.0	66.0	45.4	9.1	16.4	1.872	12.0	22.0
104	18.0	82.0	51.3	12.6	15.9	1.842	10.0	25.0
105	12.0	88.0	56.2	17.8	12.6	1.872	6.0	30.0
106	18.0	82.0	57.4	17.9	17.4	1.864	18.0	20.0
107	15.0	65.0	49.7	12.2	18.4	1.884	16.0	21.0
108	18.0	82.0	43.6	7.0	18.4	1.884	16.0	21.0
109	21.0	79.0	46.6	9.1	19.4	1.842	10.0	25.0
110	19.0	81.0	53.6	16.1	20.3	1.824	21.0	18.0
111	15.0	65.0	43.6	7.0	16.4	1.884	16.0	21.0
112	19.0	81.0	53.6	16.1	20.3	1.824	21.0	18.0
113	12.0	66.0	43.6	7.7	16.6	1.824	8.0	22.0
114	12.0	88.0	58.7	19.3	15.7	1.888	10.0	23.0
115	11.0	57.0	40.4	3.2	15.7	1.888	10.0	23.0
116	20.0	80.0	52.7	15.3	19.7	1.824	21.0	18.0
117	25.0	75.0	50.7	13.2	21.5	1.864	18.0	19.0
118	7.0	93.0	57.5	20.1	21.2	1.850	21.0	18.0
119	15.0	85.0	52.4	15.3	18.5	1.872	18.0	21.0
120	17.0	83.0	55.4	17.7	17.4	1.872	18.0	21.0
121	11.0	69.0	49.4	10.8	21.4	1.861	10.0	22.0

122	15.0	66.0	52.7	15.5	20.5	1.872	12.0	22.0
123	15.0	85.0	53.7	16.1	23.6	1.824	21.0	18.0
124	25.0	55.0	44.7	9.5	17.4	1.886	13.0	23.0
125	18.0	82.0	59.7	20.2	23.6	1.882	21.0	20.0
126	14.0	86.0	60.4	19.7	17.7	1.876	20.0	20.0
127	22.0	78.0	50.3	13.8	18.4	1.824	21.0	18.0
128	26.0	56.0	50.4	12.8	17.7	1.876	20.0	20.0
129	9.0	51.0	53.4	15.9	16.8	1.862	21.0	19.0
130	11.0	89.0	56.2	16.8	15.7	1.851	16.0	21.0
131	18.0	82.0	54.3	16.9	23.6	1.864	23.0	18.0
132	14.0	82.0	52.2	16.0	16.4	1.852	28.0	18.0
133	16.0	84.0	52.6	14.0	17.7	1.861	19.0	20.0
134	17.0	83.0	54.7	16.4	21.4	1.884	22.0	20.0
135	13.0	87.0	53.6	17.1	20.4	1.881	20.0	20.0
136	16.0	84.0	48.5	11.1	18.4	1.842	21.0	20.0
137	12.0	66.0	51.4	14.0	16.6	1.824	8.0	22.0
138	15.0	85.0	58.7	22.3	12.4	1.820	13.0	21.0
139	13.0	87.0	50.3	12.9	23.5	1.861	24.0	19.0
140	15.0	85.0	52.3	13.8	17.2	1.872	18.0	20.0
141	14.0	55.0	45.7	8.4	19.7	1.869	10.0	25.0
142	16.0	61.0	48.4	11.9	20.3	1.871	20.0	20.0
143	13.0	62.0	52.7	15.4	18.3	1.887	15.0	21.0
144	17.0	68.0	48.6	11.3	17.2	1.842	21.0	20.0
145	15.0	77.0	52.2	14.8	19.4	1.867	21.0	20.0
146	12.0	88.0	51.3	12.6	15.9	1.842	10.0	25.0
147	20.0	80.0	53.9	16.5	23.6	1.864	22.0	18.0
148	13.0	87.0	55.7	17.5	21.2	1.822	22.0	20.0
149	15.0	79.0	55.4	17.1	21.4	1.844	20.0	19.0
150	14.0	73.0	53.3	13.8	18.2	1.882	20.0	20.0
151	19.0	81.0	51.3	14.7	19.4	1.824	21.0	18.0
152	13.0	87.0	58.7	19.5	18.6	1.854	23.0	19.0
153	16.0	79.0	50.9	13.4	20.9	1.882	20.0	20.0
154	15.0	71.0	51.3	15.1	23.5	1.824	10.0	22.0
155	11.0	89.0	56.4	18.9	23.4	1.840	25.0	18.0
156	19.0	81.0	54.4	16.9	21.7	1.851	23.0	18.0
157	6.0	94.0	45.7	8.5	19.4	1.824	22.0	18.0
158	19.0	66.0	45.2	9.6	20.4	1.854	23.0	19.0
159	10.0	64.0	54.4	16.2	14.4	1.872	14.0	22.0
160	11.0	89.0	56.4	18.9	18.4	1.840	25.0	18.0
161	19.0	81.0	54.4	16.9	18.4	1.851	23.0	18.0
162	12.0	88.0	57.7	19.2	17.7	1.884	12.0	23.0
163	23.0	54.0	48.7	12.1	17.7	1.884	12.0	23.0
164	14.0	86.0	62.4	22.0	19.5	1.862	23.0	19.0

165	15.0	85.0	52.7	14.4	17.7	1.810	23.0	17.0
166	12.0	88.0	59.5	19.8	19.0	1.852	21.0	19.0
167	11.0	89.0	58.6	19.4	19.4	1.816	31.0	14.0
168	12.0	88.0	60.4	21.1	23.5	1.851	24.0	18.0
169	14.0	86.0	59.5	21.0	20.4	1.882	16.0	22.0
170	20.0	80.0	53.7	15.8	17.4	1.824	24.0	18.0
171	9.0	66.0	48.3	14.8	18.5	1.861	10.0	22.0
172	17.0	83.0	55.4	17.1	20.4	1.884	21.0	19.0
173	16.0	83.0	55.4	16.2	18.4	1.871	18.0	21.0
174	11.0	89.0	56.2	16.8	15.7	1.851	16.0	21.0
175	13.0	72.0	51.3	12.8	14.9	1.872	14.0	21.0
176	14.0	66.0	45.7	9.5	19.4	1.879	20.0	20.0
177	9.0	66.0	42.7	8.1	16.4	1.872	12.0	22.0
178	5.0	95.0	56.2	18.0	21.6	1.810	18.0	21.0
179	23.0	77.0	52.7	15.1	16.6	1.822	27.0	16.0
180	20.0	80.0	51.4	12.5	19.4	1.824	24.0	18.0
181	15.0	85.0	51.2	14.0	18.6	1.876	29.0	15.0
182	9.0	51.0	48.5	11.1	21.6	1.857	23.0	19.0
183	15.0	61.0	51.2	12.7	21.4	1.861	10.0	22.0
184	11.0	69.0	54.7	17.5	16.4	1.872	12.0	22.0
185	9.0	66.0	51.2	12.7	16.4	1.872	12.0	22.0
186	12.0	88.0	62.4	22.2	21.4	1.851	24.0	18.0
187	19.0	81.0	55.7	16.7	21.4	1.851	24.0	18.0
188	21.0	79.0	55.7	17.4	15.6	1.876	21.0	19.0
189	10.0	90.0	56.4	18.1	21.6	1.824	24.0	18.0
190	16.0	84.0	48.3	11.1	15.7	1.861	19.0	20.0
191	14.0	72.0	47.7	10.5	18.4	1.833	20.0	20.0
192	15.0	85.0	55.7	18.1	19.3	1.864	26.0	18.0
193	19.0	70.0	60.4	21.8	21.6	1.882	21.0	20.0
194	19.0	81.0	63.6	24.1	20.3	1.824	21.0	18.0
195	10.0	80.0	51.2	13.1	19.6	1.882	16.0	22.0
196	15.0	85.0	62.4	21.1	16.6	1.742	25.0	14.0
197	11.0	58.0	48.2	11.8	16.4	1.849	22.0	20.0
198	13.0	87.0	58.7	19.5	16.4	1.854	23.0	19.0
199	17.0	83.0	46.6	8.3	16.4	1.824	17.0	19.0
200	17.0	83.0	49.4	11.2	14.6	1.855	17.0	19.0
201	11.0	89.0	63.3	23.0	18.5	1.872	20.0	22.0
202	20.0	58.0	54.6	15.4	18.5	1.872	20.0	22.0
203	11.0	58.0	50.4	14.0	18.7	1.849	22.0	20.0
204	18.0	82.0	49.7	12.2	16.9	1.842	21.0	20.0
205	15.0	65.0	43.6	7.0	21.7	1.884	16.0	21.0
206	10.0	80.0	50.4	12.0	19.6	1.889	16.0	22.0
207	13.0	87.0	55.7	18.1	16.5	1.822	27.0	16.0

208	20.0	80.0	60.4	21.2	20.6	1.876	20.0	19.0
209	20.0	80.0	59.4	21.9	21.4	1.870	17.0	20.0
210	15.0	73.0	49.4	12.9	20.4	1.833	20.0	20.0
211	14.0	73.0	52.7	14.2	23.6	1.821	18.0	21.0
212	9.0	66.0	47.4	13.1	17.9	1.861	10.0	22.0
213	13.0	87.0	53.7	16.5	24.4	1.886	27.0	17.0
214	15.0	85.0	56.4	18.2	20.3	1.862	23.0	19.0
215	22.0	78.0	51.3	13.1	15.2	1.884	10.0	22.0
216	21.0	79.0	55.7	17.1	19.3	1.879	31.0	15.0
217	13.0	87.0	52.6	15.7	19.7	1.861	24.0	19.0
218	15.0	55.0	49.7	12.2	14.6	1.824	10.0	22.0
219	14.0	86.0	62.4	22.0	19.5	1.862	23.0	19.0
220	14.0	71.0	50.4	11.7	19.5	1.862	23.0	19.0
221	20.0	80.0	52.2	14.8	16.2	1.862	20.0	18.0
222	15.0	85.0	52.7	16.5	20.7	1.862	20.0	20.0
223	13.0	87.0	53.7	15.4	24.7	1.876	24.0	19.0
224	17.0	83.0	58.4	19.0	23.6	1.884	29.0	18.0
225	14.0	68.0	47.3	10.0	22.4	1.858	19.0	21.0
226	15.0	73.0	50.5	11.2	23.5	1.862	16.0	22.0
227	11.0	59.0	55.7	18.3	12.5	1.889	16.0	22.0
228	21.0	53.0	42.7	4.4	19.7	1.786	20.0	20.0
229	15.0	85.0	57.6	16.9	16.9	1.844	20.0	18.0
230	12.0	88.0	60.4	20.9	20.4	1.864	21.0	20.0
231	13.0	85.1	65.5	32.4	19.3	1.837	18.0	20.0
232	20.9	73.8	54.5	27.7	16.6	1.819	19.0	20.0
233	9.3	89.1	50.4	24.0	38.1	1.862	24.0	6.3
234	22.2	72.9	59.0	36.0	54.2	1.814	17.5	22.1
235	25.4	68.7	49.3	22.0	54.2	1.692	52.6	6.3
236	24.8	75.1	50.0	21.0	28.3	1.835	66.5	23.5
237	1.4	98.6	62.0	32.0	28.6	1.947	65.4	41.1
238	8.7	91.3	51.2	29.0	31.0	1.937	51.1	9.6
239	4.3	95.7	64.2	29.0	55.4	1.825	31.3	19.7
240	18.3	81.8	57.0	25.0	48.5	1.784	33.0	23.2
241	5.3	94.7	54.5	16.0	54.6	1.947	25.8	23.0
242	13.9	86.1	80.0	41.0	56.9	1.570	9.6	21.6
243	11.0	88.9	53.0	25.0	34.3	1.906	42.3	8.4
244	12.2	87.8	84.0	49.0	63.9	1.743	28.4	8.7
245	10.4	89.6	64.5	35.0	43.4	1.733	64.8	15.2
246	12.6	87.3	55.0	27.0	53.6	2.151	25.6	15.1
247	1.3	98.7	77.5	35.0	41.8	1.741	25.1	8.0
248	23.2	76.3	49.0	23.0	31.0	1.725	25.2	9.1
249	29.7	68.8	37.0	14.0	35.5	1.732	29.8	8.5
250	3.5	93.0	70.0	36.0	51.5	1.751	25.8	12.4

251	1.1	98.9	57.0	26.0	48.3	1.734	26.1	7.4
252	1.2	98.6	71.5	39.0	48.7	1.741	27.0	7.4
253	2.8	97.3	58.0	33.0	33.4	1.575	16.3	11.3
254	6.2	93.8	42.0	22.0	30.5	1.693	16.2	17.2
255	3.9	96.2	59.0	37.0	47.3	1.677	17.0	16.7
256	3.0	97.0	37.5	22.0	49.3	1.541	18.6	15.6
257	2.6	95.5	45.0	23.0	43.8	1.695	17.0	11.9
258	21.9	75.8	48.0	28.0	57.9	1.525	14.3	11.3
259	8.5	91.5	41.0	24.0	46.9	1.697	19.6	17.7
260	25.2	74.8	61.0	22.0	40.6	1.434	62.5	9.1
261	19.0	81.0	52.6	12.9	19.4	1.824	25.3	18.4
262	17.0	83.0	53.4	14.6	18.6	1.876	28.7	15.3
263	6.8	93.2	57.0	30.0	39.0	1.865	124.7	13.4
264	5.2	94.8	61.7	28.0	37.0	1.865	103.3	10.4